

See discussions, stats, and author profiles for this publication at: <https://www.researchgate.net/publication/324747576>

Multiphoton excitation and its control in organic semiconductor molecules

Thesis · November 2010

DOI: 10.13140/RG.2.2.34703.28324

CITATIONS

0

READS

308

1 author:



M. Teich

SeeReal Technologies

32 PUBLICATIONS 212 CITATIONS

SEE PROFILE

Some of the authors of this publication are also working on these related projects:



Double-Helix-PTV [View project](#)



Reinhart Koselleck - Adaptive laser systems with wave front correction and phase conjugation for flow measurements distorted by refractive index effects [View project](#)

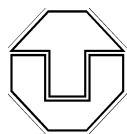
Institut für Angewandte Photophysik
Fachrichtung Physik
Fakultät Mathematik und Naturwissenschaften
Technische Universität Dresden

Multiphoton excitation and its control in organic semiconductor molecules

Diplomarbeit
zur Erlangung des akademischen Grades
Diplom-Physiker

vorgelegt von
Martin Teich
geboren am 28.03.1985 in Dresden

Dresden 30. November 2010



TECHNISCHE
UNIVERSITÄT
DRESDEN

Eingereicht am 30. November 2010

1. Gutachter: Prof. Dr. Karl Leo

2. Gutachter: Prof. Dr. Manfred Helm

Abstract

This work studies two-photon absorption in organic thin films made of Alq₃ or Alq₃:DCM that were evaporated on glass. Also, microcavities with Alq₃:DCM as the active layer were investigated. Several types of measurements were carried out in order to obtain information about the two-photon absorption of the DCM and Alq₃ molecules. Input-output measurements in a microcavity were performed to verify the two-photon absorption process in DCM molecules at 990 nm. A z-scan setup was built and modified for photoluminescence detection in order to characterize Alq₃ thin films and DCM doped layers. The two-photon absorption process in Alq₃ molecules at 800 nm excitation was verified by measuring photoluminescence during z-scan. The aspects of laser repetition rate and substrate influence on transmission measurements were taken into account and discussed. The two-photon absorption cross section of a Alq₃ thin film was estimated with a calibration measurement and confirmed by z-scan results.

Zusammenfassung

Diese Arbeit befasst sich mit der Zwei-Photonen-Absorption dünner organischer Schichten bestehend aus Alq₃ oder Alq₃:DCM, welche auf Glas gedampft wurden. Ebenso sind Mikrokavitäten mit Alq₃:DCM als aktive Schicht untersucht worden. Verschiedene Arten von Messungen sind realisiert worden, um Informationen über die Zwei-Photonen-Absorption von Alq₃ und DCM Molekülen zu erhalten.

Input-Output-Messungen wurden an Mikrokavitäten durchgeführt, um den Zwei-Photonen-Absorptionsprozess in DCM Molekülen bei einer Anregungswellenlänge von 990 nm zu verifizieren. Ein Z-Scan Setup wurde gebaut und für die Messung von Photolumineszenz modifiziert, um dünne Schichten von reinem Alq₃ sowie DCM dotierte Alq₃-Schichten zu charakterisieren. Der Zwei-Photonen-Absorptionsprozess von Alq₃ Molekülen wurde bei einer Anregungswellenlänge von 800 nm durch das Messen der Photolumineszenz mit Z-Scan nachgewiesen. Die Aspekte der Laser-Puls-Wiederholrate und der Einfluß des Substrates auf Transmissionsmessungen wurde berücksichtigt und diskutiert. Der Zwei-Photonen-Absorption Querschnitt von dünnen Alq₃-Schichten wurde mit einer Kalibrierungsmessung abgeschätzt und mit Hilfe von Z-Scan bestätigt.

Contents

1	Introduction	5
2	Theoretical background	7
2.1	Multi-photon processes	7
2.1.1	Linear optical properties of solids	7
2.1.2	Nonlinear optical characterization	9
2.2	Optical nonlinearities and limiting mechanisms	11
2.3	Structural and optical properties of Alq ₃ :DCM	16
2.3.1	Alq ₃ :DCM thin film	16
2.3.2	Molecular structure	20
2.3.3	Characteristic lifetimes	21
2.3.4	Förster transfer	23
2.4	Z-scan analysis	26
2.4.1	Gaussian beam profile	26
2.4.2	Nonlinear transmission and emission	30
2.4.3	Derivation of the z-scan transmittance formula	31
3	Experimental setups	37
3.1	Input-output measurement setup	37
3.2	Beam profiling setup	40
3.3	Z-scan technique	40
3.3.1	Open aperture z-scan	40
3.3.2	Closed aperture z-scan	42
3.4	Photoluminescence detection	44
3.4.1	On-axis detection of photoluminescence signal	44
3.4.2	Edge detection of photoluminescence signal	45
4	Results and discussion	47
4.1	Input-output measurements in microcavity	47
4.1.1	Lasing at 495 nm excitation	48
4.1.2	Two-photon optical pumping with 990 nm	49
4.1.3	Third harmonic generation for a wavelength of 1200 nm	51
4.2	Z-scan measurements in Alq ₃ :DCM thin film	52
4.2.1	Setup characterization	52
4.2.2	Photoluminescence measurements	55
4.2.3	Substrate	62
4.2.4	Transmission measurements	64
4.2.5	Estimation of the two-photon absorption coefficient	68
5	Conclusion and outlook	73

6	Appendix	75
----------	-----------------------	-----------

1 Introduction

This diploma thesis studies the nonlinear optical properties of organic molecules under femtosecond excitation. It gives an insight to mechanisms that occur at the high intensity irradiation that is reachable with ultra-short laser pulses. The main materials whose interaction characteristics are studied are the organic chromophores Alq₃ and DCM. Alq₃ was investigated in neat form as evaporated thin film but also in combination with DCM as a dopant. These organic molecules are known as very efficient emitters and, therefore, are used in light emitting devices. Especially, the combination of Alq₃:DCM was studied extensively in order to use it as an active layer in microcavities. The combination of highly reflective distributed Bragg reflectors (DBR) with the very broad absorption and emission spectra of DCM yields a promising organic laser with a low lasing threshold.

The aim of this work was to test the feasibility of two-photon excitation for an organic microcavity containing Alq₃:DCM. This is needed because DBRs are limiting the spectroscopic access to the microcavity. For single photon excitation, the DBRs hinder the use of short wavelengths as spectroscopic tool due to their strong absorption in the high energy side band. Via two-photon excitation one might circumvent this problem and gain access through the low energy side band in order to pump with twice longer wavelength than needed for molecular excitation. An important step in this investigation is to quantify the two-photon absorption cross section of the molecules. As π -electron systems are known to be fast reacting materials with large hyperpolarizabilities, efficient two-photon excitation is expected. In a microcavity, the field enhancement should account to an efficient excitation even for less probable two-photon events.

Before the experimental part of this thesis a compendium of theoretical background is placed which helps to understand and interpret multi-photon processes in materials especially organic molecular thin films. The first Chapter 2.1.2 is about the formal description of linear and nonlinear optics. After that, in Chapter 2.2, follows an overview of optical limiting mechanisms that lead to z-scan traces due to their absorptive and refractive character. A very important discussion about the molecular structure and the absorption behavior of Alq₃ and DCM closes the chapter.

First measurements were done in an organic microcavity with a femtosecond amplifier system and optical parametric amplifiers. The advantage of highest possible peak powers was used to prove the existence of two-photon absorption in the Alq₃:DCM system. Input-Output measurements served as the technique to reliably verify two-photon absorption in DCM molecules. The setup for these measurements is explained in Chapter 3.1, while the results can be found in Chapter 4.1. A second method was performed for further investigations concerning processes of higher order in Alq₃ and Alq₃:DCM. Nonlinear absorption and accompanying nonlinear refraction are investigated with the z-scan method. A detailed description of requirements and analysis is given in Chapter 2.4. The setup and an intuitive

explanation of focusing and defocusing effects and their influence on the z-scan trace can be found in Chapter 3.3. The results of z-scan measurements and their interpretation is outlined in Chapter 4.2.

Beside transmission measurements, photoluminescence was detected and evaluated with respect to two-photon absorption. Also, saturation processes in the one-photon excitation regime were investigated via photoluminescence in neat layer and organic microcavity.

2 Theoretical background

2.1 Multi-photon processes

This chapter is a short introduction to the theoretical background related to nonlinear processes in third order materials. At the beginning there is a short review of the general linear description for optical processes. After that the harmonic oscillator model is extended for higher order contributions. A short overview about two-photon absorption follows.

2.1.1 Linear optical properties of solids

Dipole approximation

In the so called dipole approximation one can describe the interaction of an external electric field with a molecule with the help of the induced dipole moment μ_{ind} that is expressed by the single electron charge e and the distance r between positive and negative charge balance point [1].

$$\mu_{ind} = -er \quad (2.1)$$

On the macroscopic scale one can say that the bulk response is N times μ_{ind} where N is the electron density that reacts on an external electric field, E .

$$P_{ind} = -Ner \quad (2.2)$$

Latter expression can be written in different form where the susceptibility of first order $\chi^{(1)}$ is introduced as a material constant. It describes the strength of the induced dipole moment created by the applied electric field E .

$$P_{ind}(E) = \chi^{(1)} E \quad (2.3)$$

With help of the susceptibility $\chi^{(1)}$ the dielectric constant ϵ can be written as:

$$\epsilon = 1 + 4\pi\chi^{(1)} \quad (2.4)$$

For comparison of materials and their optical response at certain frequencies one uses the refractive index $n(\omega)$ that is square root of the dielectric constant $\epsilon(\omega)$.

$$n(\omega) = \sqrt{\epsilon(\omega)} = \sqrt{1 + 4\pi\chi^{(1)}(\omega)} \quad (2.5)$$

The refractive index n is defined as a complex number which has by nature a real part n' and an imaginary part κ .

$$n = n' + i\kappa \quad (2.6)$$

While the real part n' corresponds to the dispersive nature of the material, the imaginary part κ corresponds to linear absorption.

In an experimental situation, these parameters are related to the phase velocity and Beer's Law, respectively. The refractive nature of a material does not change the frequency of a wave, but its wavelength. Therefore, the wavelength of an electromagnetic wave in a material is related to the vacuum wavelength by the following expression [2]:

$$\lambda = \lambda_0/n' \quad (2.7)$$

The phase velocity changes because it is the product of frequency ν and wavelength λ .

$$v_{phase} = c_0/n' \quad (2.8)$$

In case of absorption there is a decrease in intensity I observed that depends exponentially on the sample thickness L [2]:

$$I = I_0 \cdot \exp(-\alpha \cdot L) \quad (2.9)$$

The absorption coefficient is related to the imaginary part of the refractive index by $\alpha = 2k_0\kappa$ where k_0 is the vacuum wavenumber of an electromagnetic wave.

Harmonic oscillator model

The linear response of a dielectric medium can be described by a simple oscillator model where x is the elongation of a charge from its equilibrium state. The electric field $E(t) = 1/2E_0[\exp(-i\omega t) + \exp(+i\omega t)]$ is assumed to be sinusoidal and oscillates with frequency ω . The equation for the harmonic oscillator is written as:

$$\frac{d^2x}{dt^2} = 2\Gamma \frac{dx}{dt} + \omega_0^2 x = -\frac{e}{m} E(t). \quad (2.10)$$

Equation 2.10 describes a forced oscillator driven by an external field $E(t)$ at a frequency ω with damping factor Γ . The analytical solution of Equation 2.10 is the following:

$$x = -\frac{eE_0}{m} \frac{e^{i\omega t}}{\omega_0^2 - 2i\Gamma\omega - \omega^2} + c.c. \quad (2.11)$$

Combining the result with Equation(2.2), (2.3) and (2.5) one obtains the macroscopic parameters n' and κ of a dielectric medium:

$$n' = Re(n) = 1 - \frac{Ne^2}{m} \frac{2\pi(\omega^2 - \omega_0^2)}{(\omega^2 - \omega_0^2)^2 + (2\Gamma\omega)^2} \quad (2.12)$$

$$\kappa = Im(n) = \frac{Ne^2}{m} \frac{4\pi\Gamma\omega}{(\omega^2 - \omega_0^2)^2 + (2\Gamma\omega)^2}. \quad (2.13)$$

In these expressions the internal resonance ω_0 plays an significant role because the absorption has its maximum and the dispersion is at a turning point for $\omega = \omega_0$.

2.1.2 Nonlinear optical characterization

In the linear regime, the harmonic oscillator is a simplified description for small displacements of charges from their equilibrium state. When the external field and therefore the displacing force becomes stronger one must consider an-harmonic contributions to the potential in which the charge is situated. For external fields which attain comparable values like they exist within atoms or molecules one must modify the restoring term in Equation 2.10 by adding odd and even terms in x :

$$\frac{d^2x}{dt^2} = 2\Gamma \frac{dx}{dt} + \omega_0^2(x + ax^2 + bx^3 + \dots) = -\frac{e}{m}E. \quad (2.14)$$

If the an-harmonic contribution is still small compared to the linear reaction one can expand the macroscopic polarization to a power series in E :

$$P = \chi^{(1)}E + \chi^{(2)}E^2 + \chi^{(3)}E^3 + \dots. \quad (2.15)$$

The term proportional to E^3 in Equation (2.15) is responsible for nonlinear optical response of isotropic media. In general, every material shows in general 3rd order effects if it is excited with sufficient light intensity.

Important effects that belong to $\chi^{(3)}$ -processes are the optical Kerr effect (OKE), third harmonic generation (THG), four-wave mixing (FWM), E-field induced second harmonic generation and two-photon absorption (TPA). These effects usually happen at intensities in the order of 1-100 GW/cm² at any possible electronic transition in the material [1]. In case of exciting an internal resonance, there is an enhancement of nonlinearity because the medium dipoles oscillate coherently.

Two-photon absorption

Two-photon absorption occurs in two different ways. One is the stepwise absorption of two photons also called excited state absorption (ESA). It means there are two real absorptive states in the material that lead to a cascade of two one-photon absorption events.

The other one TPA, is an instantaneous event which was first considered theoretically by Goeppert-Mayer in 1931 [3]. It was found that Dirac dispersion theory describes the possibility of two-photon absorption. Selection rules can be different depending on the material. It is in principle even possible to excite transitions which are forbidden for one-photon excitation.

The instantaneous TPA event can be described by assuming a combined system of molecular transition and electric field in a quantum electrodynamic approach. This way of treatment leads to an intermediate state where residence time is infinitely short. From that fact follows the instantaneous nature of the TPA-process in comparison to the step-wise ESA where real states have finite lifetimes.

The nature of a two-photon absorption event is not easily identified. Time-resolved measurements like four-wave-mixing can clarify this question. Nonlinear transmission and fluorescence measurements are not capable of this.

If both photons have the same frequency, one talks about degenerate multi-photon absorption. Contrary to this stands the non-degenerate multi-photon absorption where photons possess different frequencies.

One can describe the exchange of energy between a molecule and electric field by time averaging the product of the applied electric field E and the first derivative in time of the macroscopic polarization \dot{P} [2]:

$$\frac{dW}{dt} = \left\langle E \cdot \dot{P} \right\rangle = \frac{1}{2} \omega \cdot \text{Im}(E \cdot P). \quad (2.16)$$

The susceptibility for two-photon absorption in case of two interacting fields with matched frequencies is $\chi^{(3)}(-\omega, -\omega, \omega, \omega)$. With the applied electric field $E(t) = 1/2 E_0 [\exp(-i\omega t) + \exp(+i\omega t)]$ the right side of Equation 2.16 becomes:

$$\frac{1}{2} P \cdot \exp(i\omega t) = \frac{1}{8} \chi^{(3)}(-\omega, -\omega, \omega, \omega) : E E E^* \cdot \exp(i\omega t). \quad (2.17)$$

The rate of energy absorbed in the process is [1]:

$$\frac{dW}{dt} = \frac{8\pi^2 h \nu^2}{n^2 c^2} I^2 \cdot \text{Im}(\chi^{(3)}). \quad (2.18)$$

The light intensity is defined as $I = E E^* n c / 8\pi$.

For the left side of Equation 2.16 one may write:

$$\frac{dW}{dt} = \left(\frac{dn_{\text{photon}}}{dt} \right) h \nu. \quad (2.19)$$

Assuming $dn_{\text{photon}}/dt = \sigma^{(2)} N F^2$ with $F = I/h\nu$ as the photon flux, one obtains an expression for the TPA cross-section, where N is the density of molecules:

$$\sigma^{(2)} = \frac{\pi^2 h \nu}{n^2 c^2 N} \cdot \text{Im}(\chi^{(3)}). \quad (2.20)$$

In an experimental situation, one observes an intensity change along the z' -direction in the sample:

$$\frac{dI}{dz'} = -(\alpha I + \beta I^2). \quad (2.21)$$

α is the loss factor due to linear absorption. β represents the two-photon absorption coefficient. It can be written as:

$$\beta = \frac{\sigma^{(2)} N}{h \omega}. \quad (2.22)$$

The two-photon absorption coefficient β is an experimental parameter related to the concentration of molecules, N . For comparison with other materials and experimental techniques, one refers to the material specific two-photon absorption cross section, $\sigma^{(2)}$. The solution of Equation 2.21 for negligible linear absorption α is:

$$I(z') = \frac{I_0}{(1 + \beta I_0 z')} \quad (2.23)$$

2.2 Optical nonlinearities and limiting mechanisms

This chapter is a review of all possible mechanisms that lead to a transmission change in a z-scan setup. There are mechanisms of absorptive nature like TPA, ESA and free-carrier absorption. Mechanisms of refractive nature like the bound electronic Kerr effect and induced scattering by free electrons also produce z-scan signals.

Instantaneous and cumulative nonlinearities

In general, one distinguishes between two groups of effects: instantaneous and cumulative nonlinearities. The former gives a polarization density resulting from an applied electric field that occurs instantaneously with the incoming electromagnetic wave.

As described in Chapter 2.1.2, the overall polarization of the medium can be expanded in a Taylor series in applied electric field, E . The first term represents the normal linear refraction and absorption. All following terms describe light-induced nonlinear effects. Here, the polarization density depends on the instantaneous electric field.

The most important term in all materials is the one of 3rd order in E , associated with $\chi^{(3)}$. It is the first possible nonlinear term which contributes to macroscopic polarization in any kind of isotropic, amorphous media. The 2nd order term in E associated with $\chi^{(2)}$ causes effects which can only arise in materials that are not centro-symmetric. Examples are frequency mixing, optical rectification and electro-optic effects.

In contrast to instantaneous nonlinearities, the cumulative effects have their origin in interactions with a memory [4]. Here, the polarization density reacts on a time scale comparable to or longer than the duration of excitation. Such interactions are normally dissipative and require an energy transfer from the field to the medium. The nonlinearity is initiated by this transfer and depends on the deposited energy instead of the instantaneous intensity. Examples are ESA, free-carrier absorption and refractive processes concomitant with them or with optically induced heating. Notably, the nonlinearity can become non-local, which means that the polarization density in one place depends on the electric field in another place in the medium. This may for example result from a temperature distribution created by different energy densities and thermal diffusion processes.

Cumulative nonlinearities depend on the fluence of incident pulse. As opposed to that instantaneous nonlinearities only depend on the intensity of a pulse. Hence, cumulative effects are insensitive to the pulse duration whereas instantaneous effects are affected by different pulse durations.

Reverse saturable absorption

Reverse saturable absorption (RSA) is observable in a molecular system if the excited state absorption cross section exceeds the ground state absorption cross section. The lifetime of T_1 and S_1 compared to the temporal pulse width is important for characterizing the way of absorption taking place at high peak intensities. A so called saturable absorber bleaches to transparency under intense illumination with laser light. The first dyes which did not bleach to transparency but instead started absorbing strongly at a certain intensity

were discovered in 1967 by Guiliano and Hess [5]. There are two different approaches to describe a system that shows RSA. The first uses a 3-level model for the situation that singlet states mainly absorb. The second approach is a 5-level model, which also accounts for participating triplet excitations (Figure 2.1(a)). This 5-level model is appropriate for nano- and picosecond pulsed excitation. It is obvious that 5-level systems are better reverse saturable absorbers because they include triplet excitations by inter-system crossing and, therefore, provide an excited state where population can be accumulated. For long pulse durations the triplet state T_1 can act as a metastable state that accumulates population during the time of one pulse and then leads to ESA.

The 3-level model applies for femtosecond pulsed excitation of organic molecules. When the first excited state S_1 becomes populated, two different situations may arise. If the absorption cross section σ_2 from S_1 to S_2 is smaller than the absorption cross section σ_1 from S_0 to S_1 , the total absorption cross section is dominated by the first transition from S_0 to S_1 , which may saturate like a two-level system (saturable absorber). But if σ_2 is larger than σ_1 total absorption is shifted to the second transition from S_1 to S_2 and total absorption increases with increasing input intensity (RSA). One can describe the situation for a certain wavelength with the following formula:

$$\frac{dI}{dz'} = -[N\sigma_1 + N_1(\sigma_2 - \sigma_1)] \cdot I \quad (2.24)$$

Where dz' is the infinite small element of the medium through which the light passes and N is the total number of active molecules per area in dz' . N_1 is the population of the first excited state and N_2 is negligible small. For $N_2 = 0$ the medium obeys Beer's law and

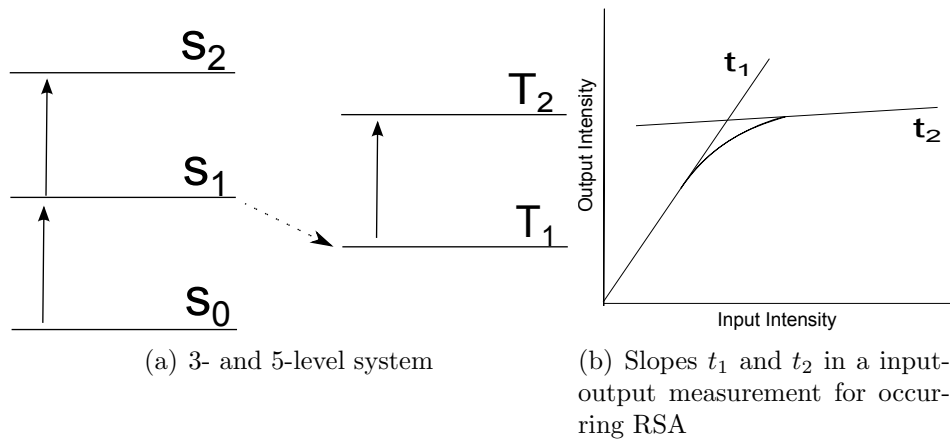


Figure 2.1: Schematics for the description of reverse saturable absorption. S_i are singlet and T_i are triplet states of an organic molecule. t_1 and t_2 are transmittances for the change from saturable absorption to reverse saturable absorption. [4]

the input-output curve obeys $t_1 = 10^{-\sigma_1 NL}$. As shown in Figure 2.1(b), the first excited singlet state can become significantly populated at high fluences and transmittance reaches a new constant value of $t_2 = 10^{-\sigma_2 NL}$. If the ratio σ_2/σ_1 is sufficiently large, the slope of the input-output plot is smaller than the one before.

Two-photon absorption

In contrast to ESA, TPA is an instantaneous process. The TPA coefficient (in SI units) is defined as follows [6]:

$$\beta = \frac{3\omega}{2\epsilon_0 c^2 n_0^2} \cdot \text{Im}[\chi^{(3)}] \quad (2.25)$$

It includes the excitation frequency ω and linear refractive index n . The time scale of the material response is of the order of one optical cycle and, therefore, independent of the optical pulse length for a fixed intensity. The scaling of β with the band gap energy in semiconductors was first discovered by Wherrett [7] and experimentally verified by Hutchings and Stryland [8].

$$\beta(\omega) = K \frac{\sqrt{E_p}}{n_0^2 E_g^3} \cdot F(x), \quad (2.26)$$

$$F(2x) = \frac{(2x - 1)^{3/2}}{(2x)^5},$$

$$x = \frac{2\hbar\omega}{E_g}$$

Equation 2.26 describes the fact that wide-band gap materials exhibit smaller TPA coefficients.

Nonlinear refraction

Nonlinear refraction occurs due to a nonzero real part of $\chi^{(3)}$ or upon charge-carrier generation by either linear or nonlinear absorption. Kaplan [9] described the external self-action in thin nonlinear media. A non-uniform beam profile within the sample leads to a generation of the spatially nonuniform refractive index which acts either as a positive or a negative lens causing the beam to either focus or defocus. For a Gaussian beam profile, the dependence of the refractive index on intensity results in a parabolic refractive index change near the beam axis.

$$\Delta n = \Delta n_0 \cdot \exp\left(-\frac{2r^2}{w_0^2}\right) \cong \Delta n_0 \left(1 - \frac{2r^2}{aw_0^2}\right) \quad (2.27)$$

Δn_0 is the index change on the beam axis. For a thin nonlinear medium of thickness L , the parabolic approximation yields a spherical lens with a focal length of:

$$f = \frac{aw_0^2}{4\Delta n L} \quad (2.28)$$

In this way, the focal length is inversely proportional to the refractive index change. The larger the induced refractive index change the shorter is the distance at which light is dispersed in a setup like z-scan. In most cases, $\text{Re}[\chi^{(3)}]$ and optical free-carrier generation

contribute to nonlinear refraction. This means that instantaneous and accumulative processes are interfering. Additionally, nonlinear absorption can also significantly alter this process. Under such conditions, the index change is not simply proportional to the input intensity. In this case, the precise energy deposited must be known as well as its redistribution due to recombination and diffusion processes.

In a TPA material, the bound electronic Kerr effect is present. The strength of the electronic Kerr effect is described by [6]:

$$\gamma = \left(\frac{\mu_0}{\epsilon_0} \right)^{1/2} \cdot \frac{3\text{Re} [\chi^{(3)}]}{4n_0^2}. \quad (2.29)$$

One relates $\gamma[SI]$ to $n_2[esu]$ by $n_2[esu] = (n_0 c / 40\pi) \cdot \gamma[SI]$.

The refractive index change due to Kerr-nonlinearity for a given peak intensity I_0 is expressed as:

$$\Delta n_{\text{Kerr}} = \gamma \cdot I_0. \quad (2.30)$$

For photon energies below $0.8E_g$, γ is predicted by a nonlinear Kramers-Kronig transformation of the TPA dispersion [10]. Here, γ peaks near the TPA absorption edge change their sign from positive to negative as the photon energy exceeds $0.7E_g$.

Self-defocussing associated with the TPA generation of free carriers may also occur. Nonlinear refraction associated with carrier generation depends on the carrier density. In Drude model, the refractive index change is directly proportional to the carrier density [4].

$$\Delta n_{\text{fc}} = n_{eh} \cdot N_c \quad (2.31)$$

$$\frac{\partial N_c}{\partial t} = \frac{\beta I^2}{2\hbar\omega} \quad (2.32)$$

Equation 2.32 shows that carrier generation becomes effectively a $\chi^{(5)}$ process when the TPA transition is saturated. For saturation, the β coefficient becomes intensity dependent and the carrier generation term is proportional to I^3 .

A model of two parabolic bands in a direct band gap semiconductor gives the refractive index change per photo-generated carrier pair

$$n_{eh} = -\frac{e^2}{2n_0\epsilon_0 m_{eh}} \cdot \left(\frac{1}{\omega^2} - \frac{1}{\omega^2 - \omega_g^2} \right). \quad (2.33)$$

The first term in Equation 2.33 represents the addition of a free electron-hole pair (intra-band contribution) and the second term is the removal of a bound electron resonant at ω_g (inter-band contribution). When ω is smaller than the band gap, the inter-band contribution is negative and enhances the intra-band effect. For ω larger than the band gap, it competes with the intra-band component. Thus n_{eh} is enhanced when laser frequency approaches the band edge from below. Free charge carrier related nonlinearity will dominate Kerr-nonlinearity above a certain fluence.

$$F_{\text{crit}} = \frac{\gamma}{n_{eh}} \cdot \frac{2\hbar\omega}{\beta} \quad (2.34)$$

Induced scattering

Nonlinear absorption and induced scattering can not be distinguished via z-scan.

When the wavelength is much smaller than particle size one talks about Rayleigh-scattering [11]. It distributes light uniformly in all directions around the particle. In case of a comparable or larger wavelength relatively to the particle size forward Mie-scattering is dominant [12]. In solids irreversible decomposition processes can lead to a degradation of the linear response. Scatterers may also work as grains that enhance nonlinear effects in their surrounding [13].

2.3 Structural and optical properties of Alq₃:DCM

The intrinsic properties of conjugated chromophores are discussed in this chapter. The focus lies on the structural properties which are connected to the π -electron system and their importance to high hyper-polarizabilities and its effective nonlinear response. Also the temporal excitation behavior is of interest to clarify possible excitation and relaxation paths. Saturation effects for a transition occur especially in case of ultrashort pulses because of their high excitation densities. Particularly π -electron systems react very efficiently to femtosecond pulses. They are well known for their fast and large 3rd order optical response [14]. In a π -conjugated system the role of many-body effects is substantial. For the calculation of π -orbital interactions one must keep in mind the interconnection between geometric and electronic structure.

2.3.1 Alq₃:DCM thin film

Linear optical absorption and refraction of Alq₃

Tris-(8-hydroxyquinoline)aluminum Alq₃ is a metal chelate with an excellent internal and external luminescence efficiency (Garbuzov [15]). The structural formula is shown in Figure 2.2. Alq₃ has a large Stokes shift of 0.4 - 0.7 eV between the green emission band and the

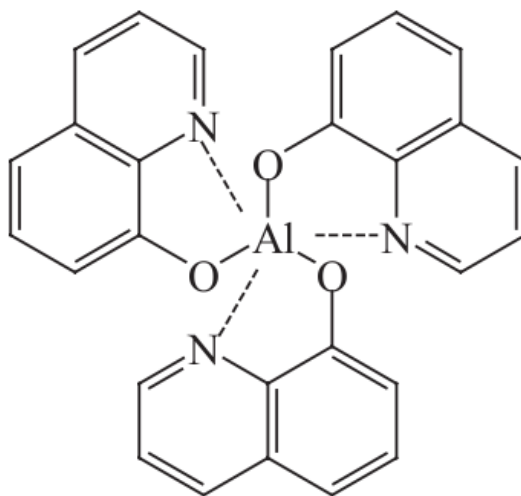


Figure 2.2: Molecular structure of Alq₃. The molecule consists of three side arms that are placed around one aluminum atom. [16]

lowest absorption band. The reasons for the large Stokes shift are low energy librations and rotations as they occur in a disordered thin film. Theoretical approaches exist, which describe these phenomena. [17]. As shown in Figure 2.3 there are two broad absorption bands [18]. One is situated around 390 nm (3.18 eV) and another at 270 nm (4.59 eV). The former corresponds to the S_0 - S_1 and the latter to the S_1 - S_n transition. The weaker feature at 390 nm is defined as the transition between the highest occupied molecular orbital (HOMO) and the lowest unoccupied molecular orbital (LUMO) calculated by Curioni [19]. The band at 270 nm exists due to transitions from the ground state to higher-energy molecular orbitals and has a complex asymmetric structure.

Comparing room temperature and liquid nitrogen measurements one can identify a lack

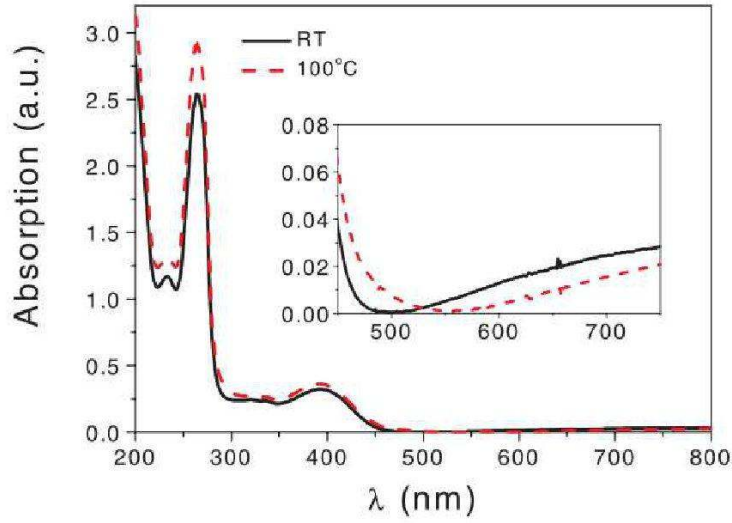


Figure 2.3: Absorption spectra of an Alq_3 thin film evaporated on a glass substrate. [18]

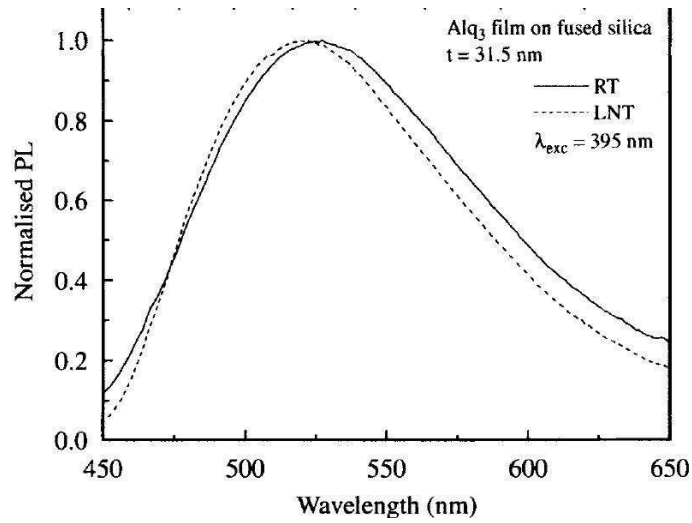


Figure 2.4: Photoluminescence spectra of Alq_3 at room and nitrogen temperature [18]

of strong molecular interaction [18]. It is a proof for the fact that main physical processes take place in one single molecular structure with little or no exchange between neighboring molecules. Phonon-assisted transitions are responsible for the broad luminescence spectrum which is plotted in Figure 2.4. Any exciting photon energy in the spectral range from 270 nm to 390 nm contributes to the broad green photoluminescence. This comes from fast non-radiative relaxations of the singlet states S_1 and S_n to their lowest vibrational states and a subsequent radiative recombination to the ground state. Internal conversion of equal multiplicity (singlet or triplet) occurs within 100 femtoseconds. In practice one can consider the lowest vibrational state as the level where radiative relaxation starts.

Inter-system crossing involves a transition between states of different multiplicity. Due to its spin forbiddance, it occurs at a lower rate compared to the radiative relaxation that has a

rate $10^8 s^{-1}$. Hence Alq_3 is a very efficient singlet emitter.

The refractive index for different wavelengths is shown in Figure 2.5. The linear refractive

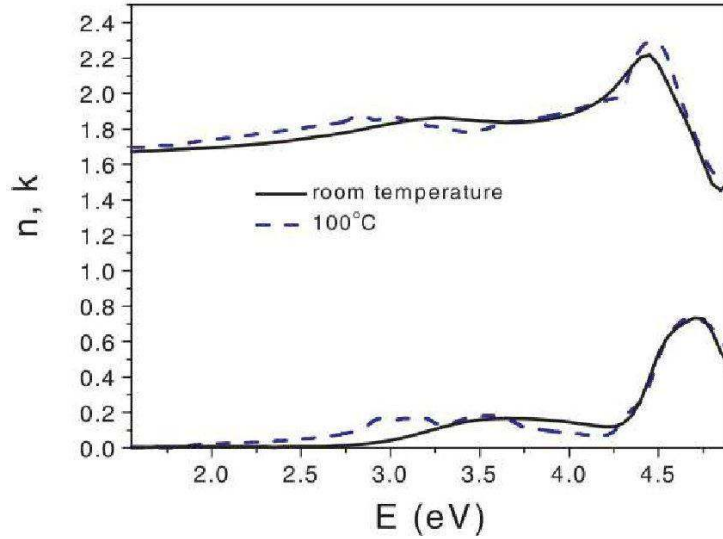


Figure 2.5: Refractive index n of an Alq_3 thin film at room temperature (upper part) [18]

index at 800 nm (1.55 eV) is 1.69. At a wavelength of 400nm (3.1 eV) linear refractive index is 1.72. In Figure 2.6 is shown an absorption measurement between 250 nm and $1.8 \mu m$ of

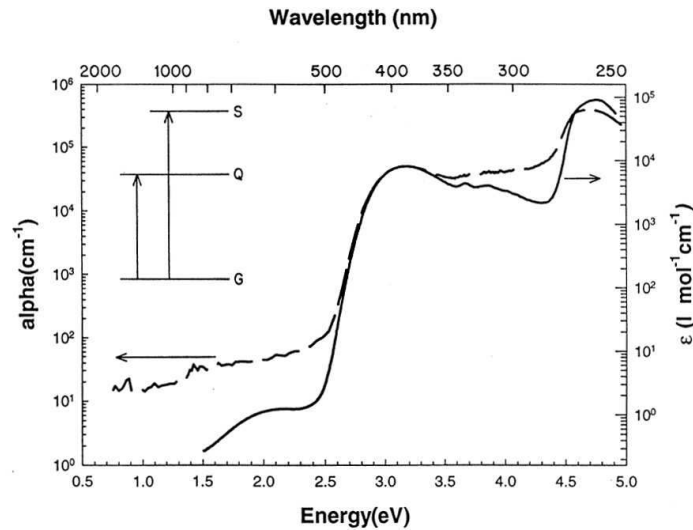


Figure 2.6: Linear absorption coefficient α for an Alq_3 thin film (dashed line) [16]

Alq_3 thin film on a glass substrate. The linear absorption coefficient at 800 nm (1.55 eV) is $2 \cdot 10^1 cm^{-1}$. At a wavelength of 400nm (3.1 eV) linear absorption is $4 \cdot 10^4 cm^{-1}$ [16]. Linear absorption at 400 nm is three orders of magnitude larger than at 800 nm wavelength.

Evaporated films of Alq_3 are of amorphous nature and exhibit short as well as long range potential fluctuations. It can be discussed how these structural properties influence the

electronic behavior in the material. Anderson's theorem gave a description of the localization of the electronic wave-function due to short range potential fluctuations [20]. The long range potential fluctuation yields a symmetric and an anti-symmetric Fourier component. The antisymmetric component can locally change the HOMO-LUMO band gap [21].

Non-linear optical absorption of DCM

4-(dicyanomethylene)-2-methyl-6-[p-(dimethylamino)styryl]-4H-pyran (DCM) is a commercial laser dye (Mukherjee [22], Jakabovic [23]) introduced by Tang as a highly fluorescent dopant in organic electroluminescent matrices at the end of 1980s. It attracted much

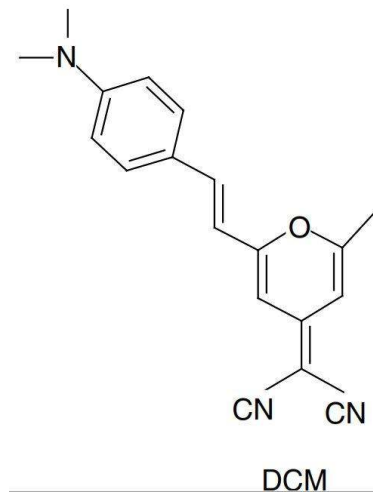


Figure 2.7: Chemical structure of the DCM molecule [24]

interest due to its strong emission in visible spectral region. DCM molecules possess a donor- π -acceptor structure (D- π -A). They show strong 3rd order nonlinear effects and were investigated with the z-scan technique. (Shao [25], Svetlichnyi [26])

The molecules exhibit strong intra-molecular charge transfer character (ICT). There are two excitable electronic states close to each other in energy which contribute in an additive manner to the hyper-polarizability (Zhou [24], Moylan [27]).

In this work the energy transfer from Alq₃ to DCM via Förster transfer is important for the DCM emission. As there is a low concentration of doping in the Alq:DCM blend, DCM should behave like a free undisturbed molecule in its absorption and emission behavior. A similar approach was carried out by Xia [28] who doped DCM into PMMA. PMMA only absorbs around 800 nm and does not disturb DCM molecules which had a concentration of $2 \cdot 10^{-4}$ to $1 \cdot 10^{-3}$ mol/l. The photoluminescence spectra that were measured by Xia [28] in PMMA:DCM are shown in Figure 2.8. They exhibit a red shift with increasing doping concentration. The photoluminescence of DCM for low concentrations in the matrix has its maximum at 555 nm and spreads from 525 nm to 700 nm. Xia [28] measured a β coefficient of 81 cm/GW for DCM doped PMMA excited by femtosecond pulses. The concentration of DCM molecules was 10^{-4} mol/l. This yields a TPA cross section of 33 GM. ($1\text{GM} = 10^{-50}\text{cm}^4\text{photon}^{-1}\text{molecule}^{-1}$)

Chunosova [29] measured $5.1 \cdot 10^{-3}$ GM for 10^{-2} M DCM in a 1-methyl,2-pyrrolidone solution.

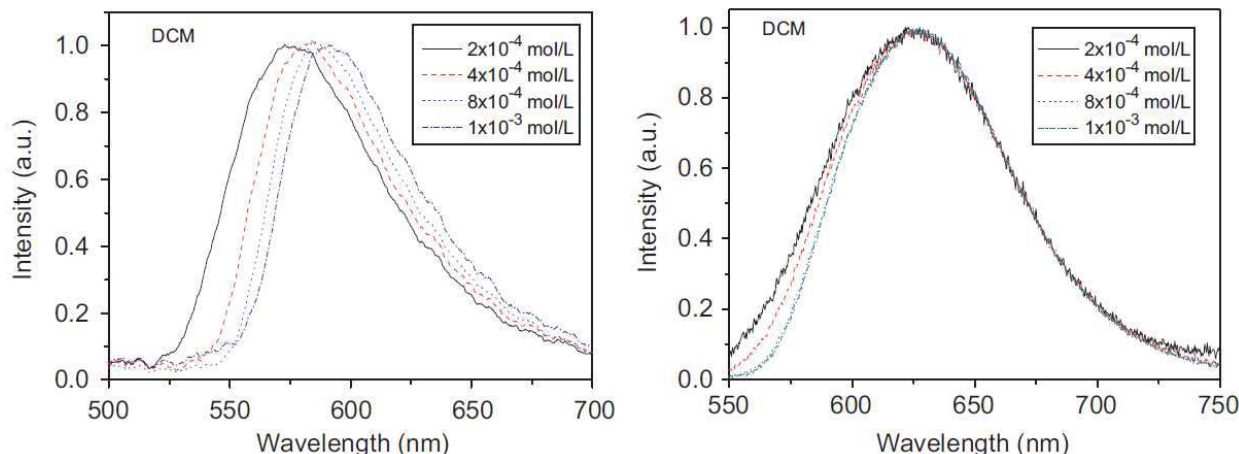


Figure 2.8: TPA excited photoluminescence of DCM molecules in a neutral PMMA matrix (left) and in a solution (right) [28]

2.3.2 Molecular structure

The cross section σ of a multi-photon event is mainly determined by the molecular structure [30]. Measuring the macroscopic parameter β , one obtains a statistic integral over all possible responses in the bulk. However, also unwanted effects like accumulation of heat or structural reorientation influence the bulk response β that only give a rough idea of processes occurring at molecular level. Nevertheless, it is useful to look at some facts which may significantly alter the bulk response due to spatial distribution of the π -electron systems that react most strongly on intense light irradiation. Most of the organic π -conjugated systems are very promising candidates for TPA in the near infrared spectral region where they are usually transparent. There exists a strong correlation between intra-molecular charge transfer and two-photon absorptivity. A permanent ground-state dipole moment can be a key factor to TPA [31]. In general third order optical nonlinearities are very sensitive to the length of π -electron conjugation paths [32]. The main structure of a two-dimensional chromophore consists of an electron-rich component (π -Donor) and an electron-withdrawing one (π -Acceptor). The intra-molecular charge transfer between these components is the driving force in higher order absorption and refraction. The spatial extend of these easily polarizable conjugated systems determines the strength of the nonlinear response. There are several configurations of states with an extended charge separation. In Figures 2.9 and 2.10 the categories are shown that exist for the structure of chromophores. DCM belongs to Type II which is an asymmetrical Donor-Bridge-Acceptor configuration. As a dipolar molecule DCM is a very effective TPA-chromophore [33]. Alq₃ is of Type III a 2-dimensional plane configuration with the exception that Alq₃ has tilted side arms which give the molecule a 3-dimensional spatial character. For Alq₃ multidimensional conjugation paths are possible between the Donor component in the middle and the Acceptor components in the side arms. Multi-polar transitions are possible due to the centro-symmetric structure of the Alq₃ molecules. The co-planarity in case of DCM enhances the intra-molecular charge transfer ability. Furthermore, DCM has a large dipole oscillator strength because of its non-symmetric structure (A-Bridge-D). A common TPA-engineering method in organic chemistry is to increase the number of conjugation paths or connecting several linear paths. The more extended the π -conjugated system the stronger the nonlinear response.

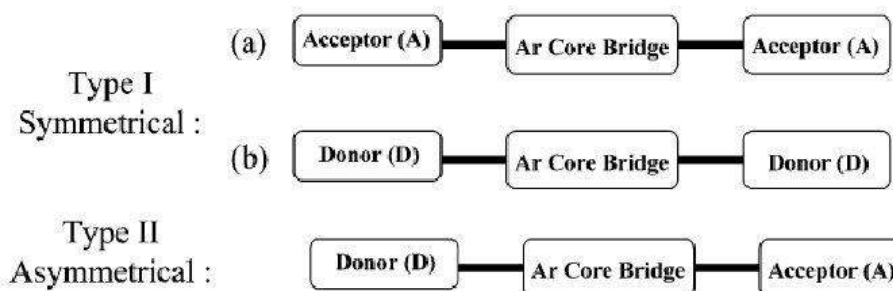


Figure 2.9: Linear spatial structure of a coplanar push-pull chromophores. There are three types of arranging donor, acceptor and bridge component. The symmetrical type I has two possibilities a) and b) whereas the asymmetrical type represents the third possibility [30].

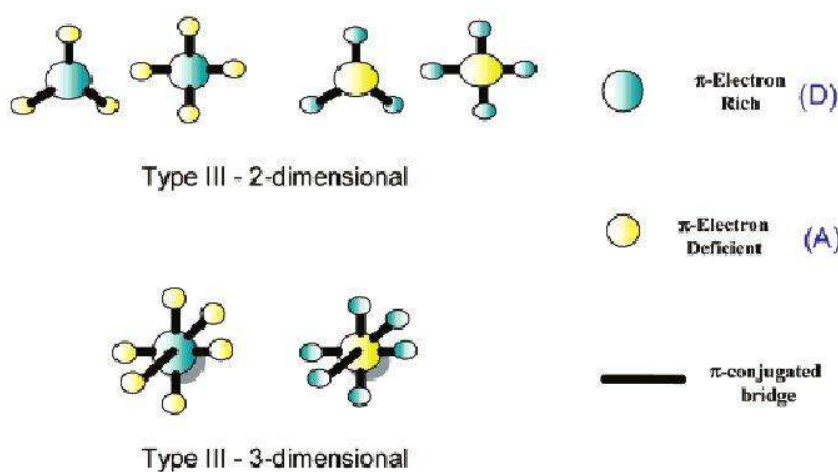


Figure 2.10: Centro-symmetric structure of a molecule with more than two bridges. Donor and acceptor groups are distributed in all directions of space (Type III) or in plane (Type II). [30]

2.3.3 Characteristic lifetimes

The temporal pulse width of excitation light source is an important parameter for the characterization of organic molecules concerning two-photon events. Measured β coefficients of organic compounds can be one or two orders of magnitude larger in the nanosecond regime than in the femtosecond regime [34]. This results mainly from the fact that the excitation of triplet states requires a relatively long time for ISC. The reason has its found in the characteristic relaxation times of each system. The question is how stable an excited state is and how likely it is to achieve an ESA within one pulse duration. This kind of multi-photon-induced excited state absorption leads to a much greater cross-section for longer pulse length and is therefore called effective cross-section [35].

The excitation from a singlet ground state S_0 to the first excited singlet state S_1 (or second singlet state S_2) through two-photon absorption (or three-photon absorption) is followed by internal conversion and vibrational relaxation to the lowest state of S_1 . (Figure 2.11) During transfer time of the pulse, relaxation process occurs inside the S_1 -band within 100 femtoseconds.

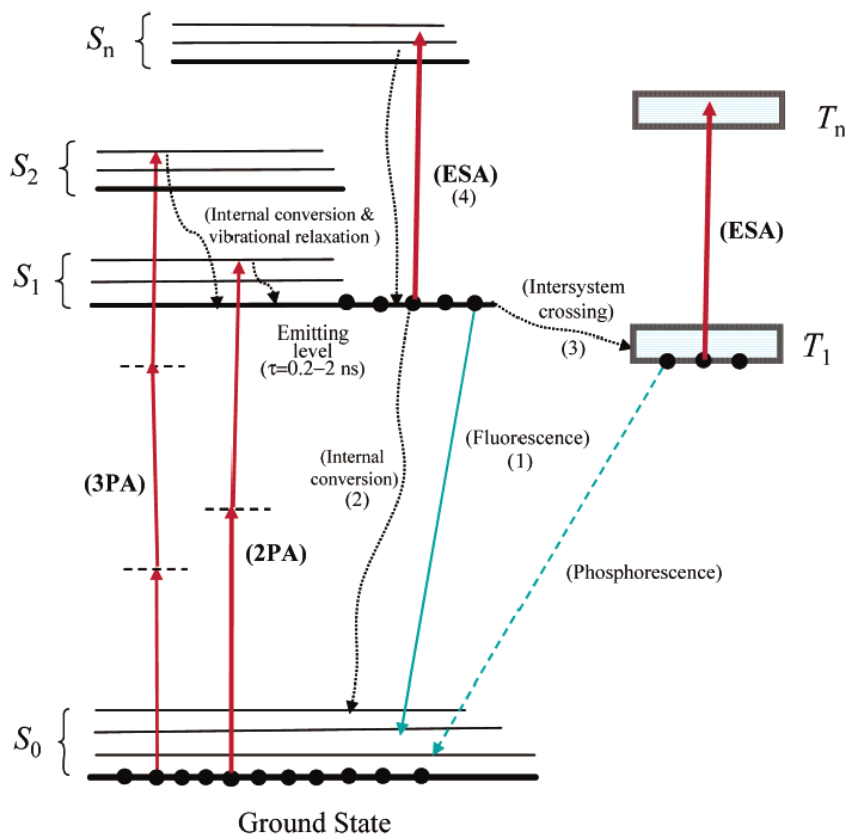


Figure 2.11: Energy level diagram of an organic molecule. Explained are instantaneous processes like three and two photon absorption but also cumulative ones like excited state absorption. All possible relaxation paths are indicated [30].

The population of the first triplet state T_1 can become very large within one nanosecond pulse. It makes ESA probable because one photon excitation can occur directly after multi-photon absorption by light of the same pulse. When the pulse duration is much shorter than the lifetime of S_1 and T_1 , there is no chance to induce a cascaded absorption event during one pulse. The triplet state T_1 has a much longer lifetime than S_1 [35]. Excited state absorption (ESA) is much more likely from T_1 to a higher lying T_n than from S_1 to S_n because during its long lifetime, the T_1 excitation will be exposed by light of the same pulse.

Saturation effects under sub-picosecond excitation

If no higher lying levels are accessible, then the saturation of a transition occurs as in a two-level system at high intensities. There is a chance to saturate a transition between two levels for example between the singlet states S_0 and S_1 . This happens when the excitation intensity is above a certain saturation intensity. Absorption then leads to a steady state behavior in the two-level system independent on number of photons which are absorbed instantaneously. The result is a 50-50 distribution where absorption and stimulated emission form an equilibrium.

The TPA coefficient β will decrease with increasing input intensity. Far below the saturation intensity, β is proportional to the molecular density N . When the depletion of the ground

states during pulse duration is not negligible anymore, the density of excited states ΔN becomes comparable to the total molecular density N .

$$\Delta N = N_0 - N_1 \quad \text{and} \quad N = N_0 + N_1$$

Where N_0 is the population density of the low energy state (e.g. S_0) and N_1 the population density of the high energy state (e.g. S_1). The rate equation for this two-level system in case of two-photon excitation is the following:

$$\frac{dN_1}{dt} = (N_0 - N_1) \cdot \frac{I^2}{h\nu} \cdot \sigma - \frac{N_1}{\tau} \quad (2.35)$$

The saturation intensity is defined as: $I_{\text{sat}} = h\nu/2\sigma\tau$ with a natural lifetime τ . The formulation of a rate equation in case of depletion is

$$\frac{d}{dt}(\Delta N) = - \left[\left(\frac{I}{I_{\text{sat}}} \right)^2 + 1 \right] \frac{\Delta N}{\tau} + \frac{N_0}{\tau}. \quad (2.36)$$

Equation 2.36 describes the fact that inversion is not possible in a two-level system.

ΔN decreases to a steady state value ΔN_{steady} for $t \rightarrow \infty$. ΔN_{steady} can approach zero for $I \gg I_{\text{sat}}$. It means that the maximum number of excited states is $N_0/2$. Without any excited state absorption in the system it is possible to imagine such a situation for two-photon absorption under femtosecond excitation of a small irradiated sample area. The TPA coefficient is defined as $\beta = \sigma \cdot \Delta N$. It approaches zero for $t \rightarrow \infty$ and $I \gg I_{\text{sat}}$.

$$\beta'(I) = \frac{\beta}{1 + \left(\frac{I}{I_{\text{sat}}} \right)^2} \quad (2.37)$$

By measuring at low and high intensities one can extract the true β coefficient and the saturation intensity I_{sat} .

2.3.4 Förster transfer

As the molecular doped system Alq₃:DCM is examined in this work, the main differences between the dopant (DCM) and the host (Alq₃) will be discussed. DCM is known as a very good laser dye with well separated absorption and emission bands. Alq₃ has good charge transfer properties but also an effective light conversion to photoluminescence. The doping concentration of DCM is only 2wt% which means that most of the light is absorbed by Alq₃ for a wavelength lying in the small overlap of absorption bands. The environment around the DCM molecules plays an important role. Alq₃ is a host which separates the DCM molecules spatially for 2wt% doping. Aggregation can be excluded at this doping concentration [36].

There is a small probability of DCM or Alq₃-aggregation due to the evaporation process. This would lead to an effective cross-section that is more sensitive to the surrounding polarity of the local environment than to the intrinsic TPA cross section of DCM and Alq₃, respectively. The combination of Alq₃ doped with DCM provides a suitable active layer for optical and electrical excitation in terms of organic laser development (Kozlov [37]).

Figure 2.12 shows the absorption and emission spectra of host and guest molecules in an

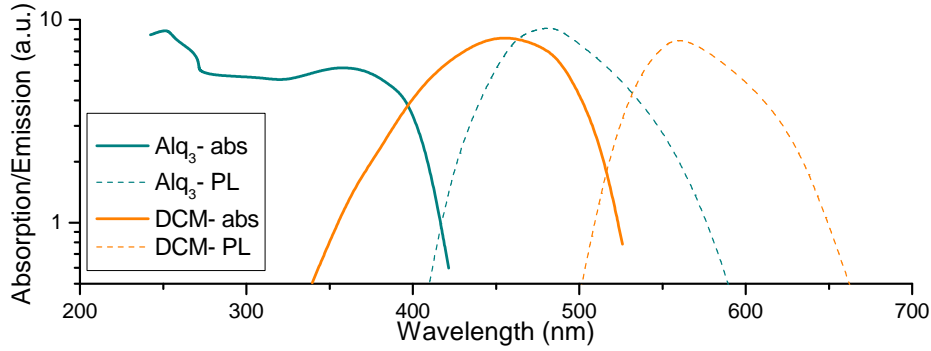


Figure 2.12: Absorption and Emission of Alq₃ and DCM in Alq₃:2wt%DCM

Alq₃:DCM thin film. As it is clearly visible, there is an overlap of the Alq₃ emission band and DCM absorption band. The energy transfer from the host to the guest molecule is called Förster transfer. This energy transport is a long range process compared to normal electron transport distances. It involves dipole-dipole coupling between $S_1^{\text{Alq}_3}$ state and S_0^{DCM} state. For a 2wt% doping concentration, a complete energy transfer is assumed (Kozlov [36]). There are no aggregation effects at this concentration. The energy transfer process from host to guest molecule is considered to be very efficient (Kozlov [38]). This implies that 80 MHz repetition rate lasers are still suitable for spectroscopy because accumulation of energy at the $S_1^{\text{Alq}_3}$ state is not expected within the temporal time distance of 12.5 ns between two pulses. The presence of the metal atom Al in Alq₃ can cause inter-system-crossing (ISC) to triplet states of Alq₃. Under femtosecond excitation this is negligible due to its long-lived timescale.

The nature of excitation in a π -conjugated system is the so-called Frenkel exciton. The deformation of a π -electron cloud by electrical fields leads to a dipole moment also described as a spin correlated electron-hole pair. The behavior of these excited states can significantly change in comparison to the single molecule due to aggregation of DCM. The vibrational dynamics are very different for clusters compared to isolated molecules, which means that the larger the aggregate the larger can be the extension of a π -electron cloud which then couples much less to vibrational states of a single molecule.

The organic layer of Alq₃:DCM is produced by a co-evaporation of both molecules in an ultra-high vacuum chamber. The inner structure and ordering in the layer depends on the intermolecular interaction in the vapor beam and on the substrate. A thin film of evaporated organic molecules is in principle a metastable kinetic form of aggregation. When the flux of hot-gas molecules impinges onto a colder substrate, condensation starts immediately before thermalization is achieved.

The properties of an organic layer are significantly influenced by intrinsic molecular properties as well as their interactions and kinetics during the growth of the layer. A very probable situation for Alq₃:DCM after evaporation is an amorphous layer with an increasing probability of aggregation for doping concentrations above 2wt%.

For optical purposes an ordered growth is not so crucial as for electrical transport. Especially 3rd order nonlinear processes have no phase-matching conditions which means that they occur in every isotropic medium regardless of symmetry. For Alq₃, a random orientation of the quasi-planar centro-symmetric molecules is expected. However, density variations are possible particularly when being co-evaporated with DCM molecules. This could somehow

alter the condensation geometry due to the linear shape of DCM and interactions between Alq₃ and DCM.

There are experimental experiences in evaporation on glass where extensive defects of structural, chemical and morphological nature occurred. These defects may enhance nonlinear optical responses due to their shape and boundaries where the strength of electric field is enhanced. This would result in a different absorption behavior of DCM especially for two-photon absorption which is very sensitive to any morphological change.

Humidity-induced crystallization of Alq₃

Aziz [39] showed that the humidity induces the formation of crystalline Alq₃ structures in initially amorphous films. Reactions occur with water and oxygen in an evaporated thin film of Alq₃ that is exposed to ambient atmosphere. Aziz [39] produced Alq₃ films of 30-60 nm thickness by vacuum deposition on glass. They were exposed to 100% relative humidity for 2 hours. The photoluminescence image in Figure 2.13 shows scattered bright sites of dense Alq₃ clusters surrounded by Alq₃-deficient regions appearing as dark halos. The clusters are protruding hemispherical lumps which can be several times thicker than the original film. Exposure to humidity for a longer period of time produces bigger aggregates of clusters ordered in concentric circular patterns. Microscopic IR absorption spectra (3800 - 700 cm⁻¹) show that the clusters are dense regions of Alq₃. They are collected by mass transfer and formed by surrounding areas leaving them deficient. The crystalline clusters have higher water content. It was proven by stronger water absorption bands.

Alq₃ hydration promotes a transformation from amorphous to crystalline phase. For [39] the crystallization seems to be independent of surface roughness and substrate. Even residual moisture in the organic layer from the production process could promote weak crystallization. On the other hand doping can improve stability of organic Alq₃ layer.

As it can be seen from Figure 2.13 the diameter of such a crystalline area in Alq₃ thin films varies from 10 to 100 μm [39]. Two-photon absorption is very sensitive to the molecular structure of organic thin films as discussed in Chapter 2.3.2.

In the Appendix of this work, measurements are shown that are supposed to indicate a long-term degradation process in a Alq₃:DCM sample stored in ambient atmosphere. Singular spots on such a sample show unusually strong nonlinear absorption measured with z-scan likely due to a crystalline phase of Alq₃. The size of such a spot was investigated by performing z-scan around the center of strongest absorption with an excitation beam focused to a beam waist of 20 μm.

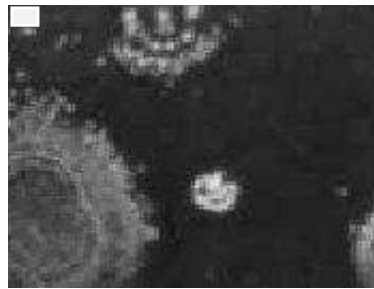


Figure 2.13: Photoluminescence image of an Alq₃ thin film sample that was stored in humid air. Hydration promotes a transformation from amorphous to crystalline phase. [39]

2.4 Z-scan analysis

2.4.1 Gaussian beam profile

Electric field

For the description of a laser beam one has to find a compromise between beam-optics and wave-optics [40]. A way using the mixture of both in order to derive the formalism for a Gaussian beam profile is shown in this section.

One obvious feature of a Laser beam is its directionality and collimation along the direction of propagation z , where the beam behaves very similar to a plane wave. The equation $E(z, t) = A_0 \cdot e^{-i(\omega t - kz)}$ is a solution of the following wave-equation in the vacuum:

$$\left(\nabla^2 - \frac{1}{c^2} \frac{\partial^2}{\partial t^2} \right) \vec{E}(\vec{r}, t) = 0. \quad (2.38)$$

In order to include a divergent part one introduces additionally to the plane wave behavior the character of a spherical wave: $\vec{E}(\vec{r}, t) = A_0 e^{-i(\omega t - \vec{k}\vec{r})} / |\vec{k}\vec{r}|$.

In the par-axial approach, one separates the beam into a longitudinal and a transversal component. The Fresnel-approximation (For $\rho \ll z, r \Rightarrow r = \sqrt{z^2 + \rho^2} \cong z + \rho^2/2z$) leads to a simplified expression for the electric field where ρ is the radius of the cylindrical coordinates.

$$E(\vec{r}) = \frac{A(\vec{r})}{|\vec{k}\vec{r}|} e^{i\vec{k}\vec{r}} \cong \frac{A(z, \rho)}{kz} \cdot \exp\left(i \frac{k\rho^2}{2z}\right) \cdot e^{ikz} \quad (2.39)$$

This has the form of a plane wave whose spatial phase is transversally modulated by the Fresnel factor $\exp\left(i \frac{k\rho^2}{2z}\right)$, which introduces a curvature of the wavefronts. The radius of the wavefront is defined as $R(z) = z - R_0$, being R_0 the center of the spherical wave solution. If one substitutes z by $q(z) = z - iz_0$ in Equation 2.39, the Gaussian TEM₀₀-mode profile follows.

$$E(z, \rho) = \frac{A_0}{k \cdot q(z)} \cdot \exp\left(i \frac{k\rho^2}{2q(z)}\right) \cdot e^{ikz} \quad (2.40)$$

It is useful to write $q(z)$ in the following form, and expand by $q^*(z) = z + iz_0$:

$$\frac{1}{q(z)} = \frac{1}{z - iz_0} = \frac{z + iz_0}{z^2 + iz_0^2} = \frac{1}{R(z)} + i \frac{2}{k \cdot w^2(z)} \quad (2.41)$$

New parameters are introduced:

$$w(z)^2 = w_0^2 \left(1 + \frac{z^2}{z_0^2}\right) \quad \text{the beam waist radius} \quad (2.42)$$

$$R(z) = z \left(1 + \frac{z^2}{z_0^2}\right) \quad \text{the curvature of the wavefronts} \quad (2.43)$$

$$z_0 = \frac{\pi w_0^2}{\lambda} \quad \text{the Rayleigh length (characteristic diffraction length)} \quad (2.44)$$

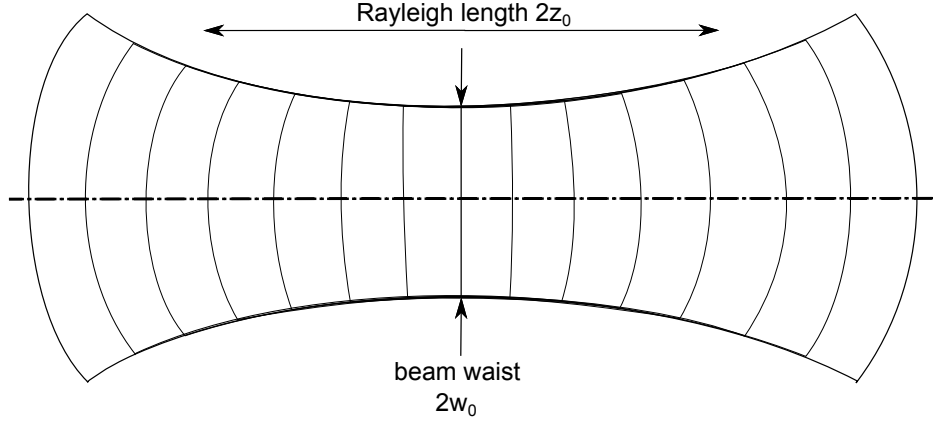


Figure 2.14: Caustic of a Gaussian TEM_{00} mode. The curved lines represent the wavefronts.

These parameters describe the dependence of the beam waist and the curvature of the wavefronts along propagation axis z . The Rayleigh range is defined as $2z_0$. It is for the identification of the near field ($z \ll z_0$) and the far field ($z \gg z_0$). The beam waist $2w_0$ ($w_0 = \sqrt{\lambda z_0 / \pi}$) describes the beam section thickness at $z=0$.

The above derivation of the Gaussian beam parameter yields the following formula for the electric field:

$$E(z, \rho, t) = E_0(t) \cdot \frac{w_0}{w(z)} \cdot \exp\left(-\frac{\rho^2}{w^2(z)} - \frac{ik\rho^2}{2R(z)}\right) \cdot e^{i(kz - \eta(z))} \quad (2.45)$$

Included are the following parameters:

$E_0(t)$ the temporal envelope

$\eta(z)$ the Gouy phase

The Gouy phase is needed to describe the additional curvature compared to a plane wave which the Gaussian wave adopts while passing a focus. The imaginary part of $q(z)$ sets the convention to find a real amplitude and a disappearing phase at $z=0$.

With the help of equation

$$a + ib = \sqrt{a^2 + b^2} \cdot e^{i \tan^{-1}(b/a)} \quad (2.46)$$

one may rewrite Equation 2.41:

$$\frac{i}{q(z)} = \frac{i}{z - iz_0} = \frac{-z_0 + iz}{z^2 + iz_0^2} = -\frac{1}{z_0} \frac{w_0}{w(z)} \cdot e^{-i \tan^{-1}(z/z_0)} \quad (2.47)$$

The function $-\pi/2 \leq \eta(z) \leq +\pi/2$ describes the small deviation from linear phase development (plane wave). This extra-phase is mainly collected in the inner half of the Rayleigh zone.

Intensity and energy flux density

The time averaged intensity distribution in a plane perpendicular to propagation can now be calculated and gives the familiar Gauss distribution [40].

$$\langle I(\rho, z) \rangle = \frac{c\epsilon_0}{2} E E^* = \frac{c\epsilon_0}{2} |E_0|^2 \left(\frac{w_0}{w(z)} \right)^2 \cdot e^{-2(\rho/w(z))^2} \quad (2.48)$$

The axial peak intensity is then

$$I(0, z) = \frac{c\epsilon_0}{2} |E_0|^2 \left(\frac{w_0}{w(z)} \right)^2. \quad (2.49)$$

Commonly, $2w(z)$ is given as the width where intensity has dropped to $1/e^2$ of the maximal on-axis value. This corresponds to 13% of the maximum intensity, i.e. inside the waist radius 87% of the total power is concentrated. Along the z-axis the intensity follows a Lorentzian profile. At $z = z_0$, half of the intensity is reached compared to

$$I(0, 0) = \frac{c\epsilon_0}{2} |E_0|^2 \quad (2.50)$$

For pulsed laser sources a time-dependence must be introduced to the intensity. The axial peak intensity for pulsed laser excitation is defined with the help of Equation 2.50:

$$I_0(t) = I(0, 0, t) = \frac{c\epsilon_0}{2} |E_0(t)|^2 \quad (2.51)$$

The time-dependent power for pulsed excitation in the common $1/e^2$ definition is then:

$$P(t) = \pi w_0^2 \cdot I_0(t) \quad (2.52)$$

Focusing law

A description of the optical beam propagation is given by the ABCD-law for normal beam optics [40], and its expansion for Gaussian optics.

In every place on the z-axis a Gaussian beam is described by the pair of parameters (w_0, z_0) or alternatively by the real and the imaginary part of $q(z)$. The ABCD-law then introduces a linear transformation of the beam parameters:

$$q_i = \frac{Aq_j + B}{Cq_j + D} \quad (2.53)$$

Now, a Gaussian beam shall be focused by a thin lens.

For a thin lens the matrix is written as: $\begin{pmatrix} A & B \\ C & D \end{pmatrix} = \begin{pmatrix} 1 & 0 \\ -1/f & 1 \end{pmatrix}$

Assuming a collimated beam the curvature of wavefronts is infinite ($R(z=0) = \infty$) at the front surface of the lens. It is known that the beam curvature is altered immediately after the lens but the beam diameter remains constant. The complex parameter q_2 at $z = 0$ directly behind the lens is now calculated using the above ABCD-law:

$$\frac{1}{q_2(z=0)} = -\frac{1}{f} + i\frac{1}{z_{01}} \quad (2.54)$$

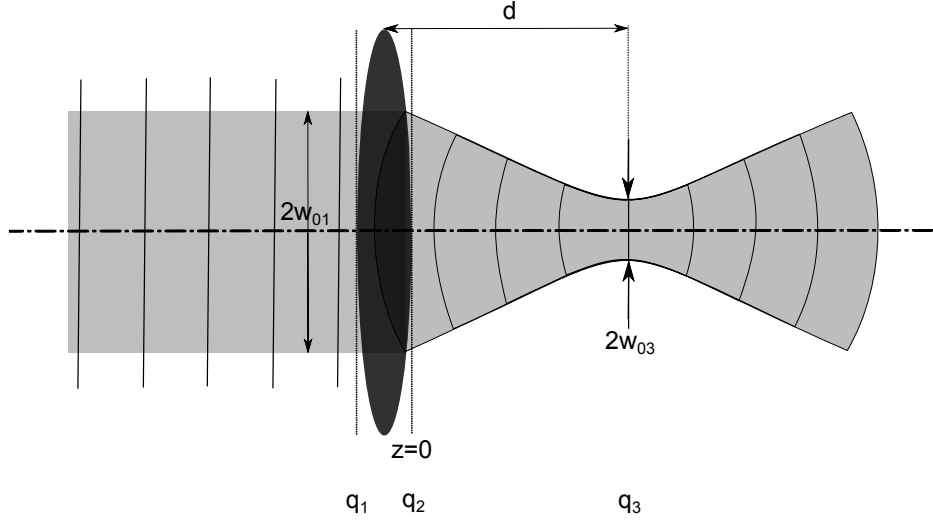


Figure 2.15: Gaussian beam focused by a thin lens. The collimated laser beam comes from the left to a focusing lens.

The finite curvature is now $1/R_2 = -1/f$ right behind the lens.

Then translation matrix for propagation to the focus conforms with: $\begin{pmatrix} A & B \\ C & D \end{pmatrix} = \begin{pmatrix} 1 & d \\ 0 & 1 \end{pmatrix}$.

This translation is described by $q_3(d) = q_2(0) + d$. (Compare Figure 2.15)

The distance d , where the focus is formed, is determined by a vanishing real part of q_3 . This means that the curvature is again infinite and the beam has a new waist radius w_{03} so that $q_3 = i \frac{\lambda}{\pi w_{03}^2}$. The calculated real and imaginary part of q_2 from Equation 2.54 is:

$$q_2 = \frac{-f}{1 + (f/z_{01})^2} \cdot \left(1 + i \frac{f}{z_{01}}\right) \quad (2.55)$$

At a distance of $d = \frac{f}{1 + (f/z_{01})^2}$, the real part is fully compensated, i.e the wavefronts are plane again. Beam optics would predict the focus at $d = f$. In case of a short focal length compared to the Rayleigh length this is still valid.

In order to calculate the beam waist, one must consider diffraction effects at the aperture of the lens. The common beam optics does not account for this.

If one writes the sum $q_3 = q_2 + d$ with the distance d from above one obtains q_3 and simply reads off z_{03} :

$$q_3 = -\frac{if^2}{z_{01}} \left[1 + \left(\frac{f}{z_{01}}\right)^2\right] \Rightarrow z_{03} \quad (2.56)$$

The reverse Rayleigh parameter at position 3 is thus:

$$\frac{1}{z_{03}} = \frac{1}{f} \cdot \frac{1 + (f/z_{01})^2}{f/z_{01}} \quad (2.57)$$

The ratio of the beam waist radii of the incident and the focused Gaussian beam is then:

$$\frac{w_{03}}{w_{01}} = \left(\frac{z_{03}}{z_{01}}\right)^{1/2} = \frac{f/z_{01}}{\sqrt{1 + (f/z_{01})^2}} \quad (2.58)$$

For $f \ll z_{01}$ one derives the Rayleigh criterion from diffraction theory.

$$w_{03} \cong \frac{\lambda f}{\pi w_{01}} \quad (2.59)$$

This approximation is a useful formula to determine the intensity at the focus of a lens for a Gaussian beam.

2.4.2 Nonlinear transmission and emission

If linear absorption in substrate and organic layer are negligible, one may write the transmittance of a sample with a thickness L for a given wavelength under two-photon excitation as [30]:

$$T(I) = \frac{1}{1 + \beta IL} \quad (2.60)$$

The main assumptions for this approach are:

- The incident light beam possesses a uniform transversal intensity distribution (e.g. a Gaussian beam profile)
- The beam cross-section remains unchanged inside the sample

Assuming a Gaussian beam profile Equation 2.60 is modified to:

$$T(I) = \frac{\ln(1 + \beta IL)}{\beta IL} \quad (2.61)$$

For a focused Gaussian beam, the variation of the beam size along the z-axis is a hyperbolic function. The effective focal depth or diffraction length z_0 is determined by the focal length f of the lens. The Rayleigh length z_0 should be comparable to or larger than the sample thickness, in terms of fulfilling second condition from above. On a length scale of several z_0 , the beam cross-section should remain unchanged inside the sample. This is important, for the above formula to be valid, because the absorptive region must be exposed only to a Gaussian beam distribution and not a disturbed profile.

One way to proceed is measuring $T(I)$ of different incident intensities and average β to obtain a reliable result. This is done with a fixed sample position. It is also possible to drive the sample through the focus and varying the intensity by variation of the irradiated area. This technique is called z-scan. It was first carried out by Sheik-Bahae [41]. The technique assumes a negligible dependence on the area size which is illuminated.

Important is the peak intensity I_0 in the focus that is not a directly measurable parameter. Therefore, I_0 is the largest error source in the measurement. One must know the beam waist radius w_0 in the focus and then calculate the intensity by:

$$I_0 = \frac{P_0}{\pi w_0^2} \quad (2.62)$$

where P_0 is the peak power of the laser beam. A peak power of 43 kW in a focus of $8.2 \mu\text{m}$ waist radius yields a peak intensity of 6.5 GW/cm^2 . The fact that w_0 is represented in a quadratic form gives a high sensitivity to the determination of the beam waist radius. Still,

also the measurement of P_0 may lead to notable errors.

It is also important to choose a large detector size and a position close to the sample. This avoids a signal change due to focusing or defocussing effects within the sample. It would lead to an asymmetric z-scan or a wrong intensity dependence in the fixed sample case.

Also, the repetition rate of the laser should not exceed a certain value depending on the excited material. Then energy is accumulated in the form of heat during the measurement and falsifies the absorption properties of the material due to possible temperature dependent behavior of absorption.

By measuring the emission, the number of photons absorbed by the material is easily identified. The slope of the emission signal plotted in log-log scale against incident intensity must be evaluated. In case of TPA, one expects a square dependence of the fluorescence signal:

$$\Delta I = I_0 - I(L) = \frac{I_0^2 \beta L}{1 + I_0 \beta L}. \quad (2.63)$$

The number of excited molecules ΔN is proportional to the intensity change ΔI if the absorption process is not dominated by a strong conversion to heat which would imply that a large part of the energy is thermally accumulated instead being emitted as fluorescence.

The following proportionality applies: $I_{\text{flu}} \propto \Delta N \propto \Delta I$. A very clean quadratic behavior is only absorbed in case of $I_0 \beta L \ll 1$. This condition is mostly fulfilled for a thin sample and an adequate intensity in the focus. The spectral and temporal behavior of the fluorescence is in general the same as in the case of one-photon excitation [30].

2.4.3 Derivation of the z-scan transmittance formula

The formulas below are taken from [41] and modified to the experimental conditions in this work. The electric field of a Gaussian spatial profile from a pulsed laser source is written as:

$$E(z, \rho, t) = E_0(t) \cdot \frac{w_0}{w(z)} \cdot \exp\left(-\frac{\rho^2}{w^2(z)} - \frac{ik\rho^2}{2R(z)}\right) \cdot \exp(-i\phi(z, t)) \quad (2.64)$$

When intense radiation impinges on the sample its refractive index is modified locally. This leads to self-phase modulation of the transmitted beam. The phase change corresponds to the Gouy-Phase $\eta(z, t)$ that was introduced in Equation 2.45. The transmittance formula is derived in the slowly varying envelope approximation (SVEA) and under the thin sample condition: $L \ll z_0$. For z-scan analysis the sample thickness L has to be much smaller than the ratio of Rayleigh length and maximal phase shift occurring.

$$L \ll \frac{z_0}{\Delta\phi(0)} \quad (2.65)$$

The change of refractive index due to the intensity variation during z-scan produces a phase shift along the propagation depth z' of the focused Gaussian beam inside the sample.

$$\frac{d(\Delta\phi)}{dz'} = \Delta n(I) \cdot k \quad (2.66)$$

The total refractive index of the medium is time-dependent during z-scan because of intensity changes during the impact of a laser pulse. Therefore, one must add a second term to the normal linear refractive index.

$$n(t) = n_0 + \Delta n(t) = n_0 + \gamma \cdot I(t) \quad (2.67)$$

The proportionality factor γ represents the strength of the refractive index change due to the high intensity $I(t)$. The accumulated phase shift at the exit surface of the sample is expressed as

$$\Delta\phi(z, r, t) = \Delta\phi_0(z, t) \cdot \exp\left(-\frac{2\rho^2}{w^2(z)}\right). \quad (2.68)$$

where the time-dependence is separated as follows

$$\Delta\phi_0(z, t) = \frac{\Delta\Phi_0(t)}{1 + z^2/z_0^2} \quad (2.69)$$

The on-axis phase shift with on-axis irradiation at the focus may be written as:

$$\Delta\Phi_0(t) = k \cdot \Delta n_0(t) \cdot L_{\text{eff}} \quad (2.70)$$

where the effective thickness is $L_{\text{eff}} = (1 - e^{-\alpha L}) / \alpha$ and the refractive index change is $\Delta n_0(t) = \gamma \cdot I_0(t)$. If one assumes linear absorption to be zero, then the electric field at the exit of the sample due to nonlinear refraction is:

$$E_{\text{exit}} = E(z, \rho, t) \cdot e^{i\Delta\phi(z, \rho, t)} \quad (2.71)$$

In order to obtain the far field pattern of the electric field one performs the Gaussian decomposition method (GD). One obtains an infinite sum for the radial distribution of the electric field at the aperture:

$$E_a(\rho, z, t) = E(z, t) \cdot$$

$$\sum_{m=0}^{\infty} \left\{ \frac{[i\Delta\phi_0(z, t)]^m}{m!} \prod_{n=1}^m \left[1 + i(2n-1) \frac{\beta}{2k\gamma} \right] \cdot \frac{w_{0m}}{w_m} \cdot \exp\left(-\frac{\rho^2}{w_m^2} - \frac{ik\rho^2}{2R_m} + i\eta_m\right) \right\} \quad (2.72)$$

with the Gouy-Phase η . For z-scan, only the first terms contribute. The propagation distance d from the sample exit to the aperture is included in the following parameters:

$$g = 1 + \frac{d}{R(z)} \quad w_{0m}^2 = \frac{w^2(z)}{2m+1}$$

$$d_m = k \cdot \frac{w_{0m}^2}{2} \quad w_m^2 = w_{0m}^2 \left(g^2 + \frac{d^2}{d_m^2} \right)$$

$$R_m = d \left(1 - \frac{g}{g^2 + d^2/d_m^2} \right)^{-1} \quad \eta_m = \tan^{-1} \left(\frac{d/d_m}{g} \right)$$

For $\beta IL_{\text{eff}} < 1$, the sum in Equation 2.72 converges. The intensity at the aperture is $I_a(\rho, t) = \frac{c\epsilon_0}{2} \cdot E_a(\rho, t) E_a^*(\rho, t)$. One determines the phase-shift dependent power transmitted through the aperture by the following integral.

$$P_a[\Delta\Phi_0(t)] = \frac{c\epsilon_0}{2} \int_0^{\rho_a} d\rho |E_a(\rho, t)|^2 \cdot \rho \quad (2.73)$$

The amount of light transmitted through the aperture in the linear regime is defined by:

$$S = 1 - \exp\left(-2\frac{\rho_a^2}{w_a^2}\right) \quad (2.74)$$

w_a is the beam waist radius at the aperture in the linear transmission regime. $P_i(t)$ is the incident power as defined in Equation 2.52. In order to get a normalized z-scan transmittance, one calculates the ratio of time integrations over transmitted and incident power, respectively.

$$T(z) = \frac{\int_{-\infty}^{+\infty} dt P_a[\Delta\Phi_0(t)]}{S \cdot \int_{-\infty}^{+\infty} dt P_i(t)} \quad (2.75)$$

For a given phase change $\Delta\Phi_0$, the magnitude and the shape of $T(z)$ are independent of wavelength and geometry if the far-field condition ($d \gg z_0$) is fulfilled. In the limit of small nonlinear phase changes $|\Delta\Phi_0| \ll 1$ Equation 2.75 is simplified to:

$$T(z) = 1 - \frac{4\Delta\Phi_0 x}{(x^2 + 9)(x^2 + 1)} \quad (2.76)$$

Where $x = z/z_0$.

The numerical solution of Equation 2.75 for the maximal expected transmittance change ΔT_{p-v} is (for $|\Delta\Phi_0| \leq \pi$):

$$\Delta T_{p-v} \cong 0.406 \cdot (1 - S)^{1/4} \cdot |\Delta\Phi_0| \quad \text{for a } \chi^{(3)}\text{-process} \quad (2.77)$$

$$\Delta T_{p-v} \cong 0.21 \cdot (1 - S)^{1/4} \cdot |\Delta\Phi_0| \quad \text{for a } \chi^{(5)}\text{-process} \quad (2.78)$$

The peak-valley distance in z-scan traces results in:

$$\Delta z_{p-v} = 1.72 \cdot z_0 \quad \text{for } \chi^{(3)}\text{-process} \quad (2.79)$$

$$\Delta z_{p-v} = 1.2 \cdot z_0 \quad \text{for } \chi^{(5)}\text{-process} \quad (2.80)$$

In case of negligible linear absorption the refractive index change is calculated from the phase change measured in z-scan as:

$$\Delta n_0(t) = \frac{\Delta\Phi_0(t)}{kL}. \quad (2.81)$$

k is the vacuum wavenumber for the excitation wavelength and L is the sample thickness. For pulsed excitation and an instantaneous sample response relative to temporal pulse width the time-averaged refractive index change is

$$\langle \Delta n_0(t) \rangle = \frac{\Delta n_0}{\sqrt{2}}. \quad (2.82)$$

Including two-photon absorption

If there is a contribution from the imaginary part of $\chi^{(3)}$, one writes the intensity along the propagation path through the sample as:

$$\frac{dI}{dz'} = -\alpha(I) \cdot I \quad \text{with} \quad \alpha(I) = \alpha + \beta I. \quad (2.83)$$

$$\frac{d\Delta\phi}{dz'} = \gamma I k \quad (2.84)$$

Solving these equations yields the field behind the sample:

$$E_{\text{exit}} = E(z, \rho, t) \frac{e^{-\alpha L/2}}{(1+q)^{1/2}} \exp\left(i \frac{k\gamma}{\beta} \ln[1+q]\right) \quad (2.85)$$

Notes the phase shift $\Delta\phi_{\text{exit}}(z, \rho, t) = \frac{k\gamma}{\beta} \cdot \ln[1+q(z, \rho, t)]$ in the exponent. The parameter q contains the two-photon absorption coefficient β :

$$q(z, \rho, t) = \beta \cdot I(z, \rho, t) \cdot L_{\text{eff}} \quad (2.86)$$

The electric field at the exit of the sample is now written as:

$$E_{\text{exit}} = E(z, \rho, t) \cdot e^{-\alpha L/2} \cdot (1+q)^{(ik\gamma/\beta-1/2)} \quad (2.87)$$

Where $\beta/2k\gamma$ is the the figure of merit.

A zero-order Hankel transformation leads to the field distribution at the aperture E_a . The transmittance $T(z)$ is calculated using Equation 2.73 and 2.75:

$$T(z, S=1) = \sum_{m=0}^{\infty} \frac{[-q_0(z, 0)]^m}{(m+1)^{3/2}} \quad (2.88)$$

The sum is convergent for $|q_0(z, 0)| = \left| \beta I_0(t) \cdot L_{\text{eff}} \cdot \frac{1}{1+(z/z_0)^2} \right| < 1$

Thermo-optical effects using high repetition rate lasers

Falconieri [42] analyzed thermo-optical effects that occur when high repetition rate lasers are used. When the temporal pulse spacing is much shorter than the thermal diffusion time, the sample does not return to its equilibrium state between two pulses. Energy is deposited in a cumulative way and a thermal lens is formed inside the sample. This effect is most strongest for a wide-band gap material where all the energy absorbed is thermalized and which have a negligible fluorescence quantum yield. Cumulative heating takes place due to absorption. The order of absorption may also be higher than linear such as two or three photon absorption. Even extremely low, non-resonant linear or nonlinear absorption coefficients cause large z-scan signals.

The detailed analysis in [42] gives the following transmittance changes and peak-valley distances. They differ from those derived for instantaneous nonlinearity in [41]:

$$\Delta T_{p-v} \cong 0.63 \cdot (1 - S)^{1/4} \cdot |\Delta \Phi_0| \quad \text{for a } \chi^{(3)}\text{-process} \quad (2.89)$$

$$\Delta T_{p-v} \cong 0.50 \cdot (1 - S)^{1/4} \cdot |\Delta \Phi_0| \quad \text{for a } \chi^{(5)}\text{-process} \quad (2.90)$$

$$\Delta z_{p-v} = 1.45 \cdot z_0 \quad \text{for a } \chi^{(3)}\text{-process} \quad (2.91)$$

$$\Delta z_{p-v} = 1.02 \cdot z_0 \quad \text{for a } \chi^{(5)}\text{-process} \quad (2.92)$$

The maximum transmittance change is larger for cumulative than for instantaneous effects and the peak-valley distance becomes shorter.

3 Experimental setups

In this chapter all setups used are explained. At first the setup for input-output measurements is described, followed by the z-scan setups. The latter include a beam profiling setup for spatial beam characterization. After that z-scan is explained qualitatively with its open and closed aperture method. Then two different methods for photoluminescence detection are shown. The z-scan setup was completely constructed by the author. Also, programming had to be done in Lab View for the different kinds of measurement.

3.1 Input-output measurement setup

Figure 3.1 shows a sketch of a setup that was built in order to measure the input-output characteristics of an organic microcavity. A Ti:Sa oscillator is used which produces 120 fs pulses at a wavelength of 800 nm with 80 MHz repetition rate. The laser beam passes a regenerative amplifier. To generate other wavelengths, the beam was guided through an optical parametric amplifier (OPA), which can produce a broad range of wavelengths. In the current work, wavelengths of 495 nm, 900 nm and 1200 nm were used. The incident

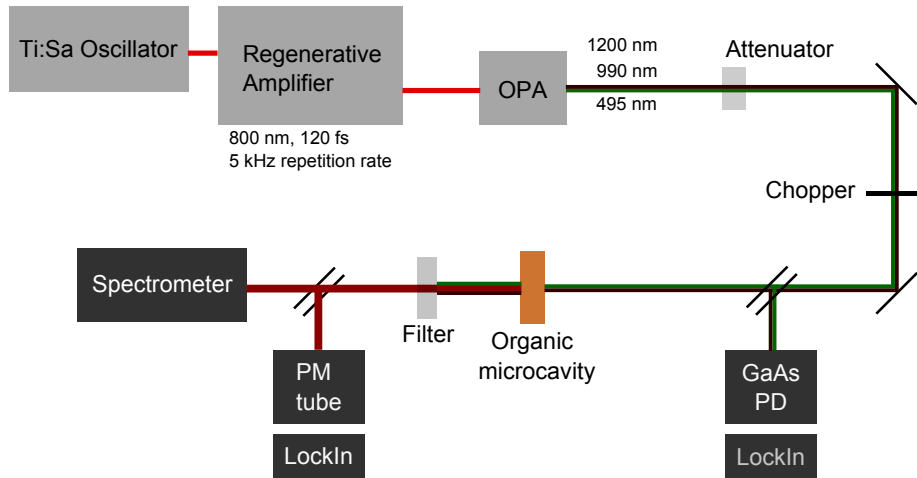


Figure 3.1: Schematics of the input-output setup. Photoluminescence from a microcavity was detected dependent on incident intensity. Excitation wavelength was filtered out in front of the spectrometer and photomultiplier (PM) tube.

intensity change was detected by a GaAs-photodiode placed in the reflected part of a beam splitter and then evaluated using a lock-in amplifier which obtained its reference signal from a beam chopper. There was also the possibility of attenuating the incident beam continuously by the combination of a $\lambda/2$ plate and a selective polarizing cube.

The excitation beam was focused onto a microcavity sample. Behind the sample, the pump wavelength was blocked. The output intensity change was detected in the reflected part of a second beam splitter using photomultiplier tube and evaluated by a second lock-in amplifier

triggered at the chopping frequency. For the input-output measurements programming was done in Lab View in order to simultaneously record data from the detectors. There was also the possibility to resolve the photoluminescence spectrally via a spectrometer consisting of a monochromator and a highly sensitive CCD camera. An important step

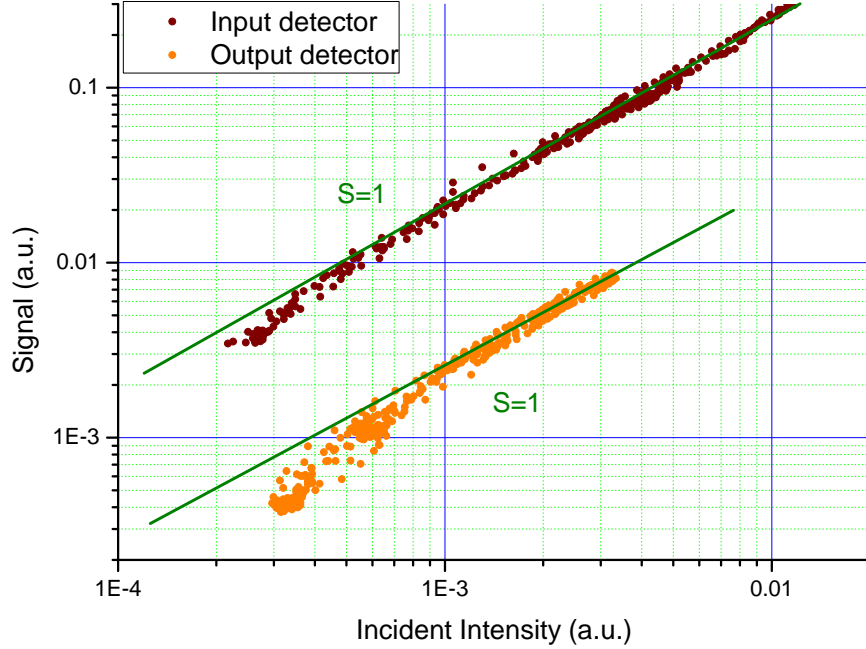


Figure 3.2: Check of detectors linearity. Both detectors show linear behavior without sample in the setup. The input intensity was changed over two orders of magnitude.

before measurement was to test the linearity of the detectors. Therefore, I made sure that no nonlinearities were introduced through the measurement technique. In Figure 3.2, the test result is shown. The input detector signal from the GaAs-photodiode is plotted against the output detector signal from the photomultiplier tube without any sample in the beam path. With the help of this measurement it became clear that any deviation from linearity must come from the sample when introduced to the setup. In Figure 3.3 is shown

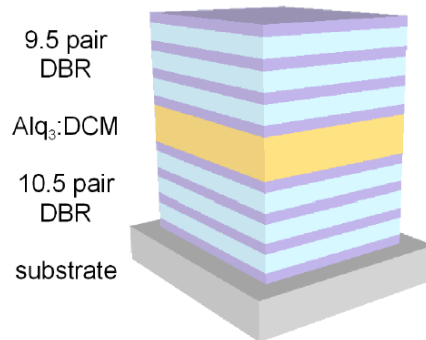


Figure 3.3: Organic microcavity that has an Alq₃:DCM active layer placed between two DBRs that consist of alternating SiO₂ and TiO₂ layers.

the structure of an organic microcavity. It consists of an Alq₃:DCM active layer placed

between two DBRs. These dielectric mirrors are alternating layers of SiO_2 and TiO_2 . The reflection of light through the DBRs creates a spectrally broad stopband where the cavity modes depending on the active layer thickness arise. On the high and low energy side of the stopband affiliate the so-called side bands, where a strong transmission through the microcavity is possible. A transmission spectrum of the above microcavity was simulated

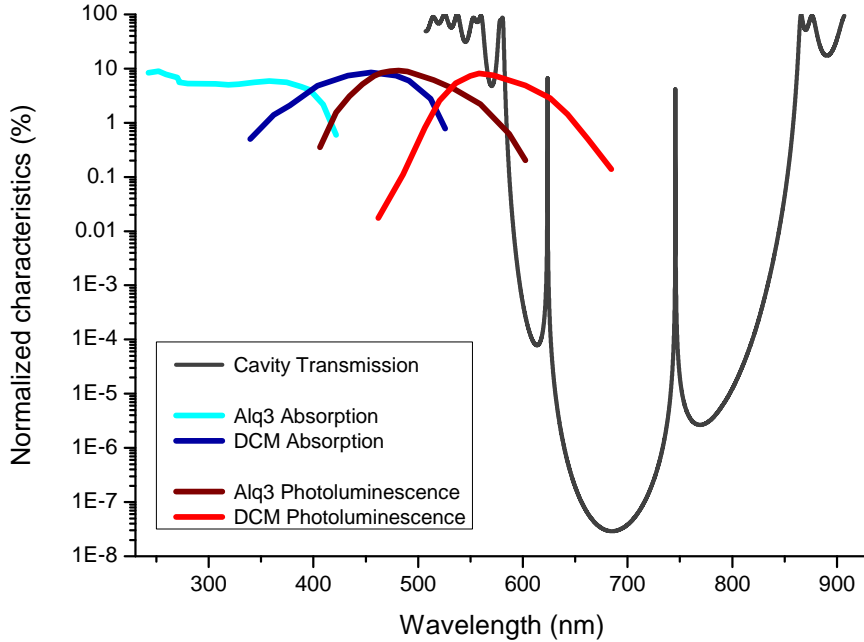


Figure 3.4: Film Wizard simulation of a microcavity transmission spectrum. Absorption and emission spectra of Alq_3 and DCM molecules for a Alq_3 :DCM thin film are plotted by the colored lines.

with Film Wizard and is shown in Figure 3.4. Obvious from Figure 3.4, the absorption bands of Alq_3 and DCM are situated in the high energy transmission side band of the microcavity. Two-photon excitation was accomplished through the low energy side band with a 990 nm beam. In this way, the resonance of the DCM absorption at 495 nm could be excited. At this excitation wavelength no absorption of Alq_3 molecules is present. DCM then directly emits into the cavity modes via its broad emission band which is extended from 500 nm to 650 nm. The sample was also excited with 1200 nm wavelength where two-photon excitation of Alq_3 and DCM molecules is not possible. At this wavelength third-harmonic generation can be observed. This wave-mixing process is commonly used for the determination of $\chi^{(3)}$ in thin samples [10].

3.2 Beam profiling setup

The spatial beam profile is measured using a μm -slit. The shape of a Gaussian TEM00 mode is measurable perpendicular to the direction of beam propagation by changing the slit position along the profile. At each position the transmission was detected with a Si-photodiode. A lock-in amplifier integrated the signal triggered by the chopper frequency. The beam profile was recorded in front of the z-scan lens as well as symmetrically around the focus.

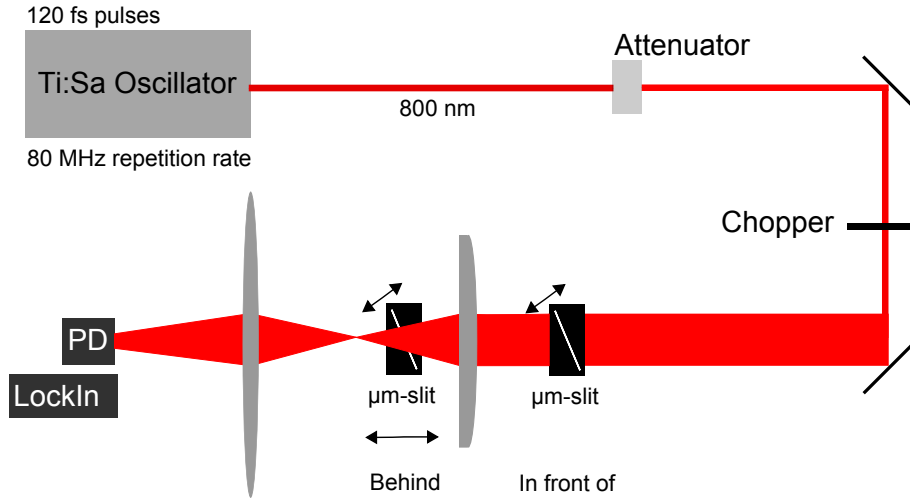


Figure 3.5: Setup for spatial beam profile characterization. The beam profile was measured in front of and behind the focusing lens of z-scan setup. A combination of photodiode, chopped beam and lock-in served to detect the transmitted light through a μm -slit.

3.3 Z-scan technique

In Figure 4.15 is sketched a simple z-scan setup with its main components. There is needed a focusing lens which narrows the Gaussian beam waist to a certain value that defines irradiated area on the sample. A common beam waist radius is formed between 10 and 30 μm from a spot size of 3 mm before the lens depending on focal length. The sample is placed on a translation stage which can be moved by with sub-micrometer precision. The focused beam hits the sample perpendicular to its surface and passes an aperture in the far field of the sample backside. There is the possibility to move the sample in plane perpendicular to the laser propagation to probe different spots on the sample. Afterwards the beam is collimated with a large collecting lens and detected by a photodiode. A good alignment of the setup is crucial in order to vary aperture size in a symmetric way around the beam center.

3.3.1 Open aperture z-scan

In an open aperture (OA) experiment one detects transmittance changes while varying the intensity in the sample. The intensity (energy density) is increased by driving the sample closer to the focus. It reaches its maximal value at the focus and then decreases again as

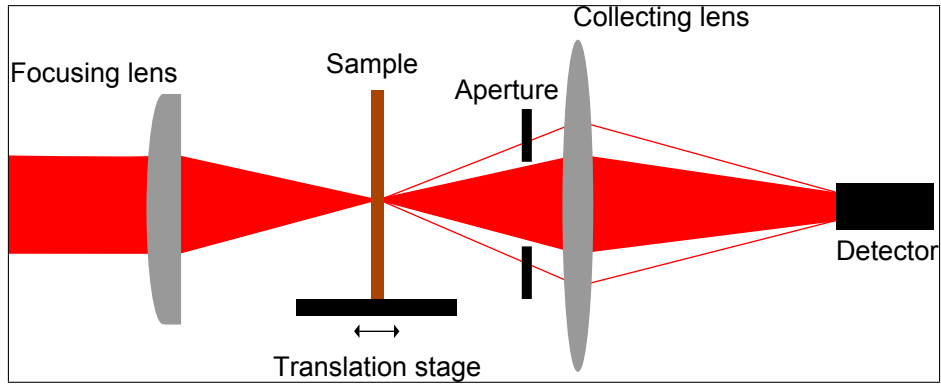


Figure 3.6: Schematic draft of a z-scan setup. The laser beam impinges from the left onto a focusing lens ($f=10$ cm). The beam is focused to a point inside the sample that can be moved with a translation stage. In the far field of the sample, a defined aperture can be placed before light is focused to the detector.

the sample is moved behind the focal plane. In the case that absorption in the sample is intensity-dependent, one can see a drop in transmittance with its minimum exactly in the focus. This behavior is shown in Figure 3.7.

At a certain distance from the focus the nonlinear behavior of the sample vanishes. The transmittance is the normalization to the value of transmission far away from the focus. It is crucial that all light is collected after the lens for every sample position without omitting possibly refracted parts of the excitation beam.

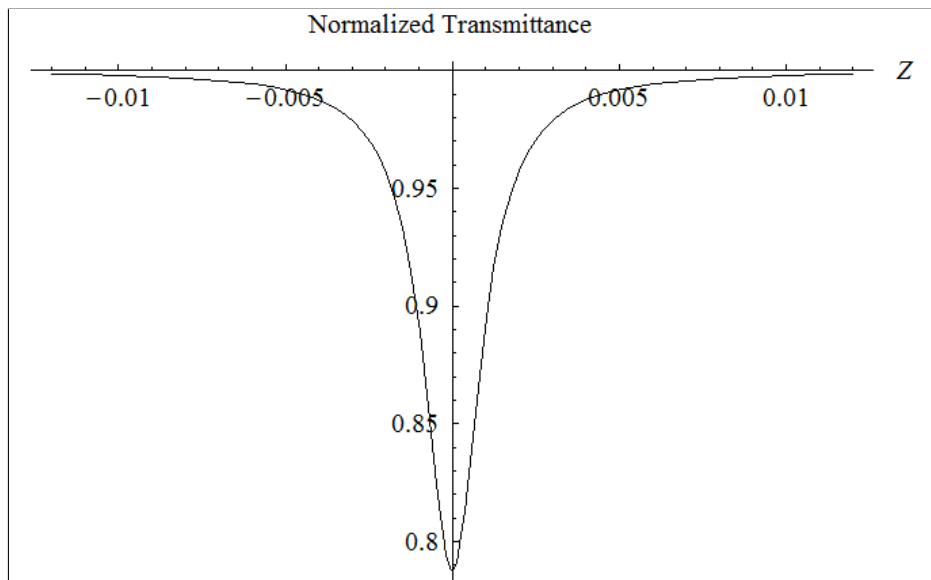


Figure 3.7: Mathematica calculation of Equation 2.88 for a nonlinear absorption behavior in open aperture z-scan. The parameters were chosen arbitrarily to demonstrate the quality of the behavior.

3.3.2 Closed aperture z-scan

In a closed aperture (CA) experiment it is possible to detect changes of intensity-dependent refraction. A modulation of the refractive index takes place in the sample and causes a beam size variation in the far field. This is described as a focusing or defocussing effect symmetrical around the beam center. Both types of refraction can have various physical origins as described in Chapter 2.2. Schemes for defocussing are shown in Figure 3.8 together with the corresponding (simulated) z-scan traces in Figure 3.9(a) and 3.9(b).

When the sample is situated in front of the focus, the transmittance signal is increased

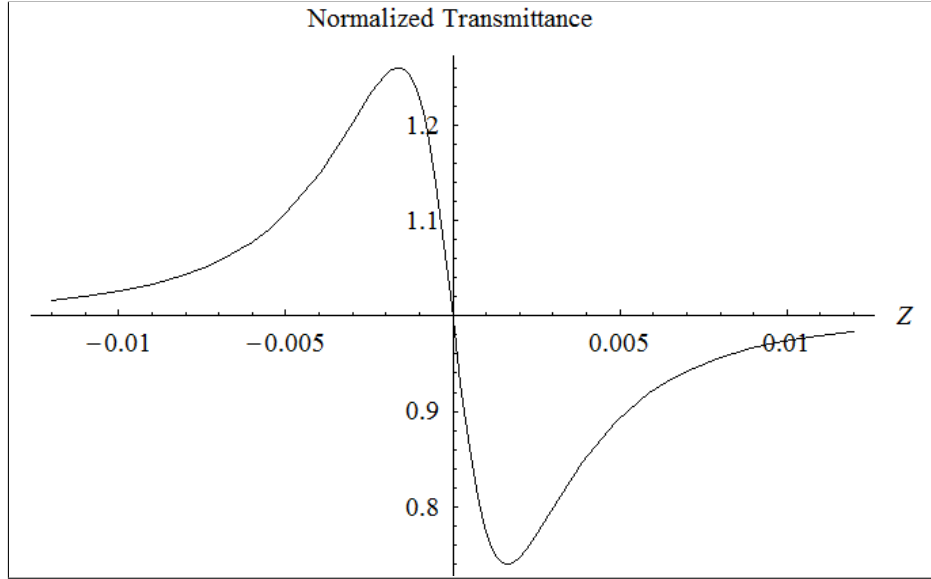


Figure 3.8: Mathematica simulation of Equation 2.76 for a defocussing behavior in closed aperture z-scan experiment.

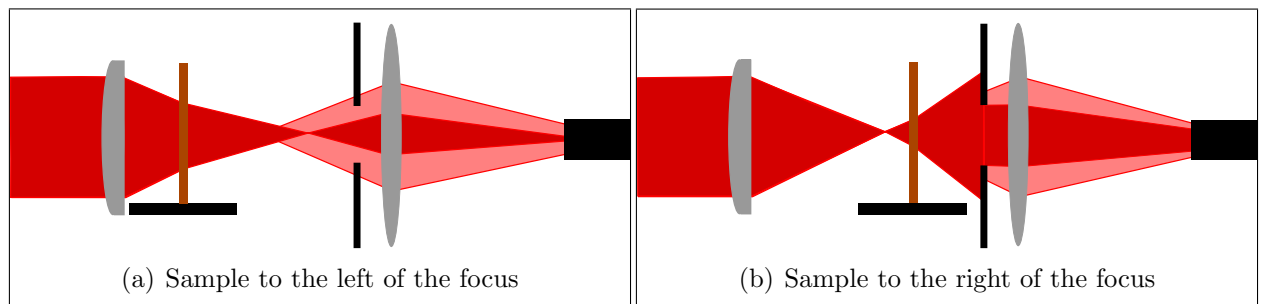


Figure 3.9: Schematic draft of the defocussing effect in a closed aperture z-scan setup as observed for a thermal lens created in the sample.

because a defocussing effect inside the sample moves the focus closer to the aperture. The signal drops for a sample position behind the focus because the defocussing effect broadens the beam size.

The focusing effect is observed in nonlinear Kerr media, see Figure 3.10, 3.11(a) and 3.11(b). Here, one observes a qualitatively opposite behavior compared to the above defocussing. On the left side where the sample is situated in front of the focus the effect causes a

transmittance decrease because the focus is artificially shifted away from the aperture. When the sample is moved to behind the focus, the transmittance increases because more light is refracted to the detector.

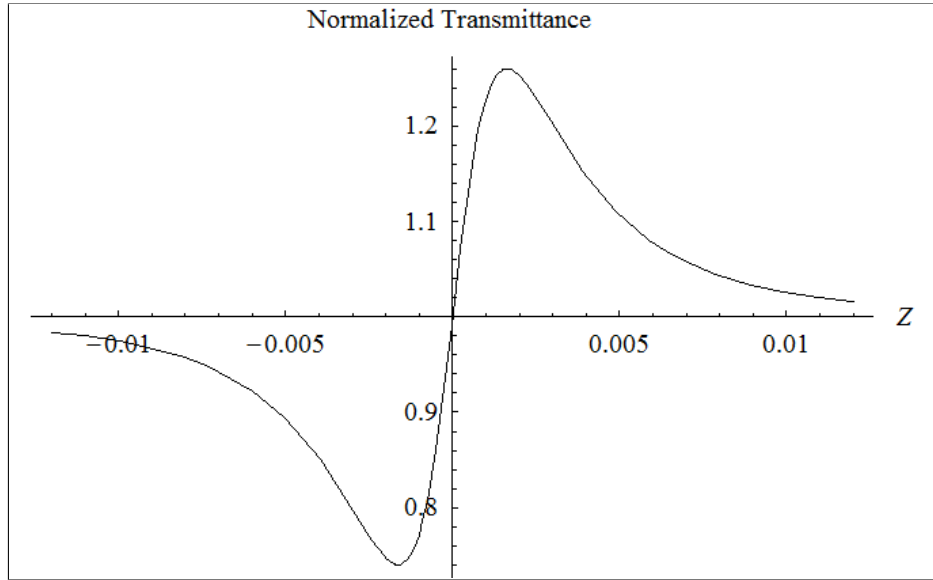


Figure 3.10: Mathematica simulation of Equation 2.76 for a focusing behavior in closed aperture z-scan.

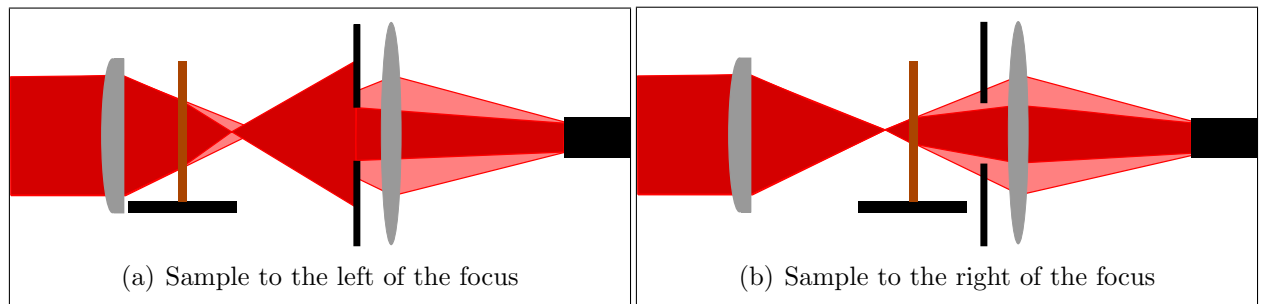


Figure 3.11: Schematic draft of the focusing effect in a closed aperture z-scan setup as observed for a nonlinear Kerr media.

3.4 Photoluminescence detection

3.4.1 On-axis detection of photoluminescence signal

A z-scan experiment is not only useful for transmission measurements as shown in the previous chapter. For fluorescent samples, also the photoluminescence (PL) signal contains important information. In the present case, this PL z-scan provides the additional benefit of distinguishing the signal of the organic from the substrate signal, which can be mixed in transmission measurement. The setup for detection of in collinear photoluminescence detection (i.e. emitted in the direction of laser propagation) is shown in Figure 3.12. Excitation was done using 100 fs pulses of the 800 nm oscillator beam. The exciting beam was chopped at 813 Hz before in-coupling to the z-scan setup. The temporal pulse spacing is 12.5 nanoseconds in case of a 80MHz laser system. This means that internal relaxation has happened before next pulse reaches the sample. Temporal spacing of the pulses is one order of magnitude larger than the sum of vibrational relaxation and S_1 -lifetime. It means that 80MHz repetition rate of the laser can not lead to involvement of triplet excitation. The beam was focused onto the sample, which was mounted on a translation stage. The translation stage was movable by 12 mm to each side of the focus. Behind the sample a collecting lens focused all light from the sample to the detector. On the detection side, the beam was split. The reflected part went through a filter that blocked photoluminescence. The transmitted light of 800 nm wavelength was detected by a photo diode. The transmitted part from the beam splitter was filtered twice in order to exclude the intense excitation beam. The residual photoluminescence was detected by a photomultiplier which was not sensitive to 800 nm. The transmission signal on the photo diode and the photoluminescence signal on the photomultiplier were recorded by lock-in amplifiers. Both lock-in amplifiers were triggered with the chopper frequency.

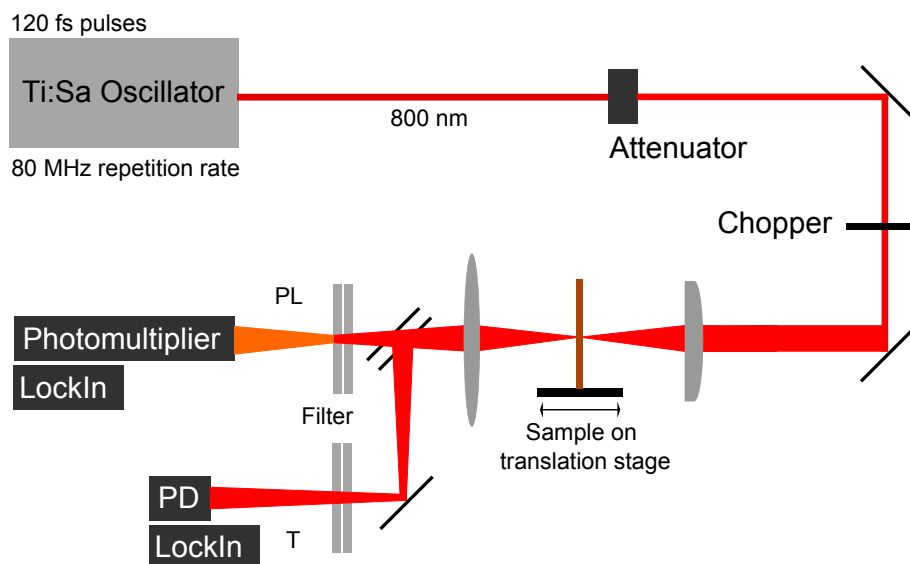


Figure 3.12: Z-scan setup for simultaneous detection of photoluminescence and transmission.

3.4.2 Edge detection of photoluminescence signal

The calibration measurement for the estimation of the TPA coefficient β as well as the z-scan measurements at 400 nm were done with the setup shown in (Figure 3.13). The estimation of the TPA coefficient β was done with a Ti:Sa oscillator. The peak power of the oscillator was already sufficient for two-photon absorption in Alq₃. The second harmonic of the oscillator beam was also used for 400 nm z-scan measurements on neat organic layers. For z-scan measurements on a microcavity, the beam was amplified by a regenerative amplifier which had an output of 1 kHz repetition rate. For linear excitation measurements with 400 nm, the laser pulses were frequency doubled from 800 nm using a second harmonic generating crystal. The average excitation power was measured with a Newport power meter. Part of the emitted photoluminescence from the organic layer was detected on the substrate edge. The wave-guided part of the emission was coupled to an optical fiber and recorded with a USB-spectrometer. The optical fiber was fixed to the translation stage. Driving the stage did not influence the amount of in-coupled light. It was possible to detect spectrally resolved changes of wave-guided photoluminescence and scattered excitation light.

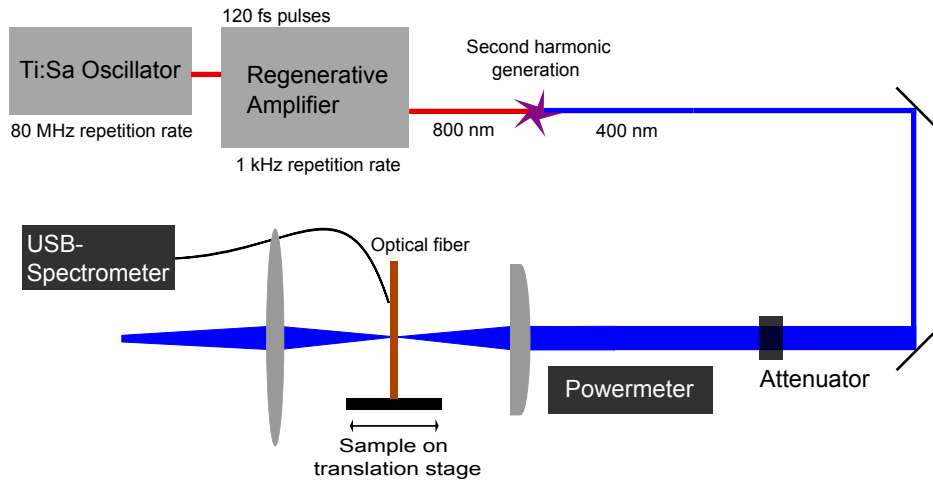


Figure 3.13: Z-scan setup for photoluminescence detection from the sample edge. An optical fiber was placed close to the sample edge and scattered light was detected with a USB spectrometer.

4 Results and discussion

4.1 Input-output measurements in microcavity

Efforts have been made in order to test the organic compound $\text{Alq}_3\text{:DCM}$ in a microcavity concerning two-photon absorption properties. The aim was to use the field enhancement in a microcavity. This field enhancement was expected to promote nonlinear optical effects like two-photon absorption and third harmonic generation. Also one expects a more efficient in-coupling of the excitation beam when transmitting through the low energy side of the DBR transmission. Two different excitation wavelengths were selected to clarify the efficiency of two-photon excitation of DCM (900 nm) and the ability of third harmonic generation in the organic microcavity (1200 nm). With both wavelengths it was not possible to reach the lasing threshold of the organic microcavity. The nature of two-photon absorption was proven by measuring the photoluminescence at different excitation intensities below lasing threshold. The fact that the probability of a two-photon absorption event is much smaller than common linear absorption explains why two-photon pumping is in general less efficient than one-photon pumping. On the other hand, optical losses are reduced while pumping the cavity with low energy photons. It is possible that the latter effect compensates the reduced absorption probability for two-photon excitation.

Figure 4.1 shows a transmission measurement with a white light halogen lamp. One

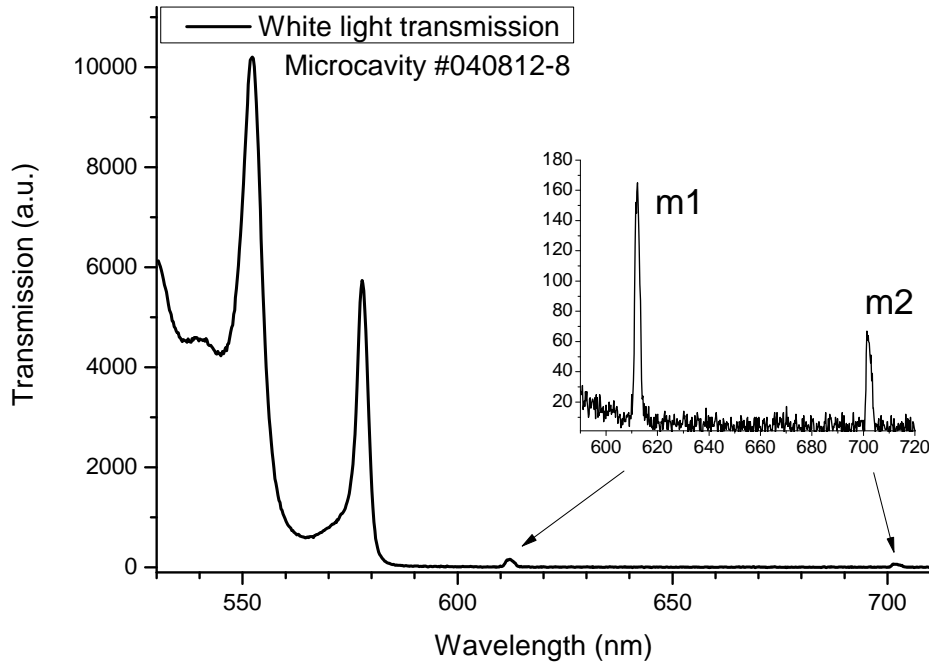


Figure 4.1: White light transmission spectrum of a microcavity. Two modes m1 and m2 are situated in the stopband (inset). The high energy side band of the DBRs is visible from 530 nm to 580 nm.

broad cavity stop band is identified as well as sidebands at the high and low energy ends, respectively. Two modes exist in the cavity stop band as it can be seen from the inset in Figure 4.1. The determination of the input-output slope was done on these two modes (612 nm and 702 nm) for 990 nm excitation. The organic microcavity used in all experiments of this thesis is labeled with the identification number: #040812 – 8 .

4.1.1 Lasing at 495 nm excitation

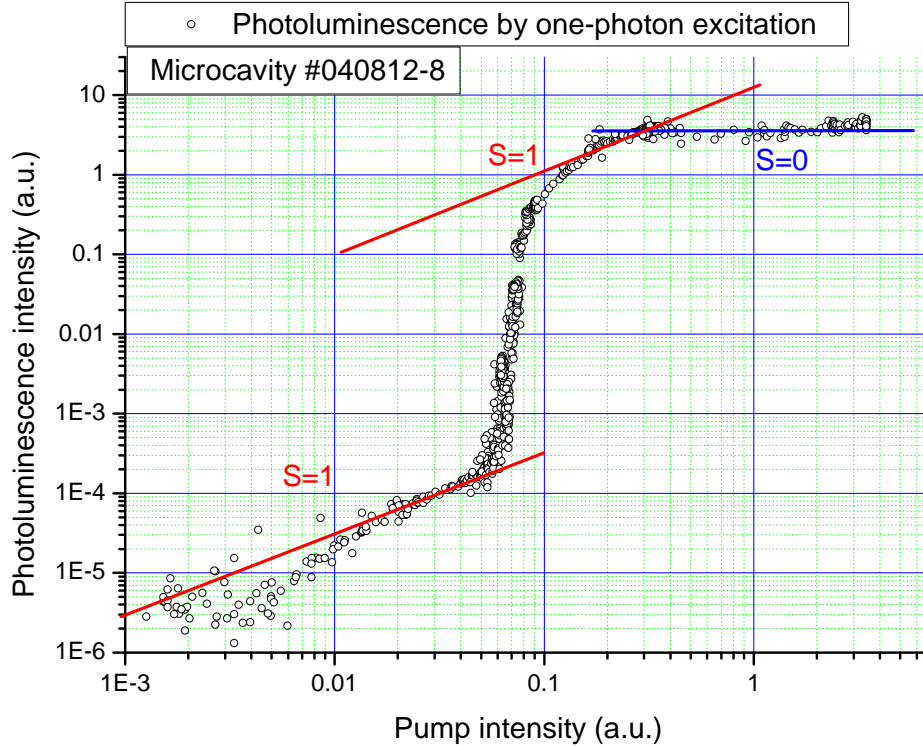


Figure 4.2: Spontaneous emission, lasing and emission saturation under one-photon excitation. The slope in input-output measurement changes from 1 to nonlinear, then to 1 again with increasing intensity. At highest pump level the slope becomes 0.

Figure 4.2 shows a complete input-output measurement. In this measurement the DCM molecules were directly excited at 495 nm. The input intensity stretches over almost 4 orders of magnitude. Yielding output intensities over 7 orders of magnitude. 4 regions of output behavior are identified. Below lasing threshold, the input-output curve shows a slope of 1. At lasing threshold, a nonlinear behavior is observed as the emission undergoes a transition from spontaneous emission to stimulated emission. After lasing is reached there is again a slope of 1. The fourth regime follows after lasing has increased by approximately 1 order of magnitude in output intensity. Here, saturation occurs, which is explained in terms of a mode volume saturation. [Publishing in preparation (R. Brueckner and M. Teich)].

4.1.2 Two-photon optical pumping with 990 nm

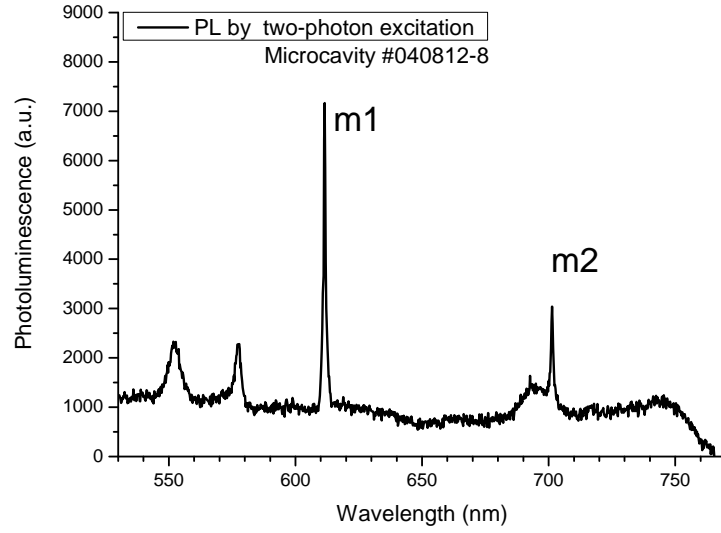


Figure 4.3: Spectrum of the photoluminescence from a two-photon pumped microcavity below lasing threshold. The two cavity modes m1 and m2 are identified for the evaluation of the incident power dependence.

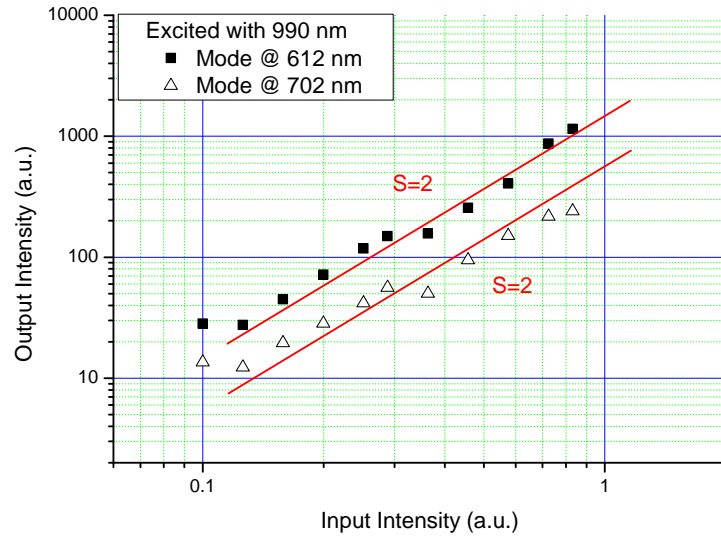


Figure 4.4: Input-output plot of the photoluminescence peak values. The slopes for both cavity modes show quadratic dependence on input intensity below lasing threshold.

A straight forward way to determine the order of an absorption process is measuring the luminescence of a sample as a function of the input intensity. Independent of the process from which luminescence arises one regards the number of exciting photons needed to produce one emitted photon. In case of two-photon absorption the number of excited states is assumed to be proportional to the square of the input intensity:

$$N_{\text{absorbed}} \propto \sigma \cdot I_{\text{input}}^2 \quad (4.1)$$

When measuring the intensity of photoluminescence one expects a quadratic dependence on the input intensity.

$$I_{\text{PL}} \propto I_{\text{input}}^2 \quad (4.2)$$

If the measurement is plotted on a log-log scale, it is possible to directly read out the slope and the order of the absorption process. In a microcavity, one uses the enhanced optical field between the dielectric mirrors in order to increase the effective excitation intensity in the organic active layer. In a measurement, DCM molecules were excited via two-photon absorption by irradiation at 990 nm. The resulting photoluminescence spectrum is shown in Figure 4.3. It exhibits two distinct peaks which represent the two cavity modes. The 702 nm mode is situated on a broad spontaneous emission background. The 612 nm mode is more expressed and narrow. At high energy there are also 2 sideband peaks visible.

In Figure 4.4 the spontaneous emission of the two cavity modes is evaluated as an input-output plot in double logarithmic scale. A clear slope of 2 hints at a two-photon absorption process. The fact itself that photoluminescence is detected indicates that DCM can absorb two photons instantaneously when doped into a Alq₃ matrix and placed inside a microcavity. DCM has no linear absorption at 990 nm.

4.1.3 Third harmonic generation for a wavelength of 1200 nm

By using a larger wavelength, e.g. 1200 nm, there is the chance to generate the third harmonic (THG) of the laser beam inside the sample. The fact that there is no emission

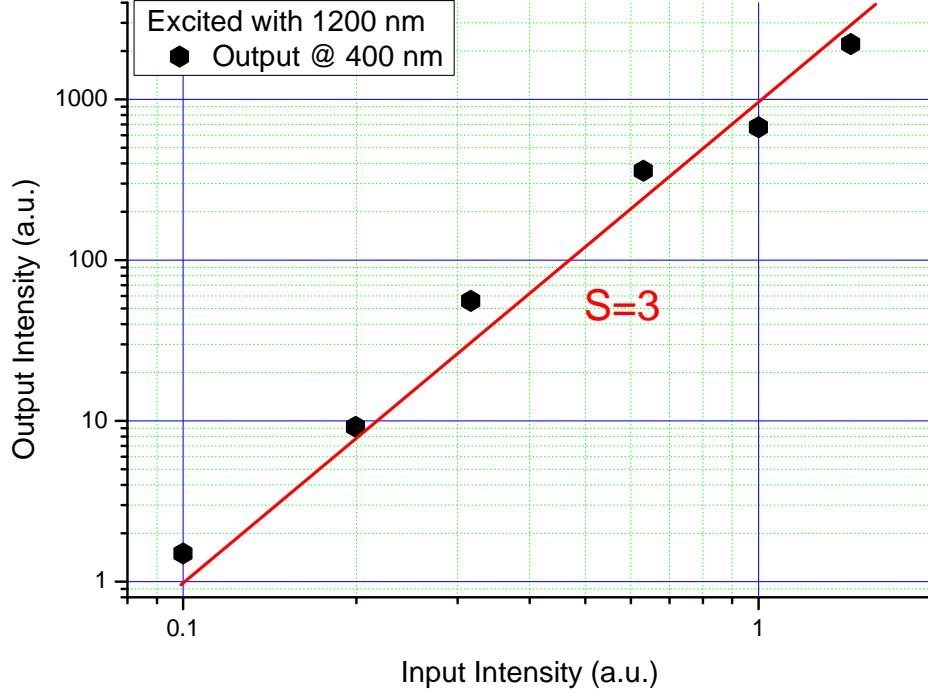


Figure 4.5: Third harmonic generation at 1200 nm excitation in an Alq_3 :DCM organic microcavity. The output intensity at 400 nm shows a cubic dependence on the input intensity.

at 400 nm neither by Alq_3 nor DCM suggests that a frequency mixing process takes place. Blue light coming out of the microcavity was observed already by eye. As one can see in Figure 4.5, THG leads to a slope of 3 in log-log plot for an input-output measurement. The output intensity shows a cubic dependence on the input intensity:

$$I(\lambda = 400\text{nm}) \propto I^3(\lambda = 1200\text{nm}) \quad \text{or} \quad I(3\omega) \propto I^3(\omega). \quad (4.3)$$

This phenomenon is a wave-mixing process which originates from a $\chi^{(3)}$ -contribution to the macroscopic material polarization.

4.2 Z-scan measurements in Alq₃:DCM thin film

4.2.1 Setup characterization

For the analysis of z-scan experiments, it is of crucial importance to have a well defined Gaussian spatial beam profile. Therefore, a beam profile measurement was carried out to clarify whether there are significant irregularities in the beam profile caused by diffraction on the setup components.

The most important part of the beam profile is the region above the $1/e^2$ intensity level which gives most of contribution to the z-scan signal because it contains most of the light (See Chapter 2.4.1). The so called Airy disks influence the z-scan signal because they create an excited area in the sample which is situated beside the intended excitation spot. Possible Airy patterns caused by diffraction do not contribute to a high TPA efficiency in the sample. These are regions where the peak intensity is too low for TPA. Here photon transmit without absorptive interaction when the transition is only reachable by TPA. However, they can lead to a significant intensity loss in the region above the $1/e^2$ intensity level, causing a wrong assumption of the peak intensity which is a sensitive parameter in z-scan analysis. Figure

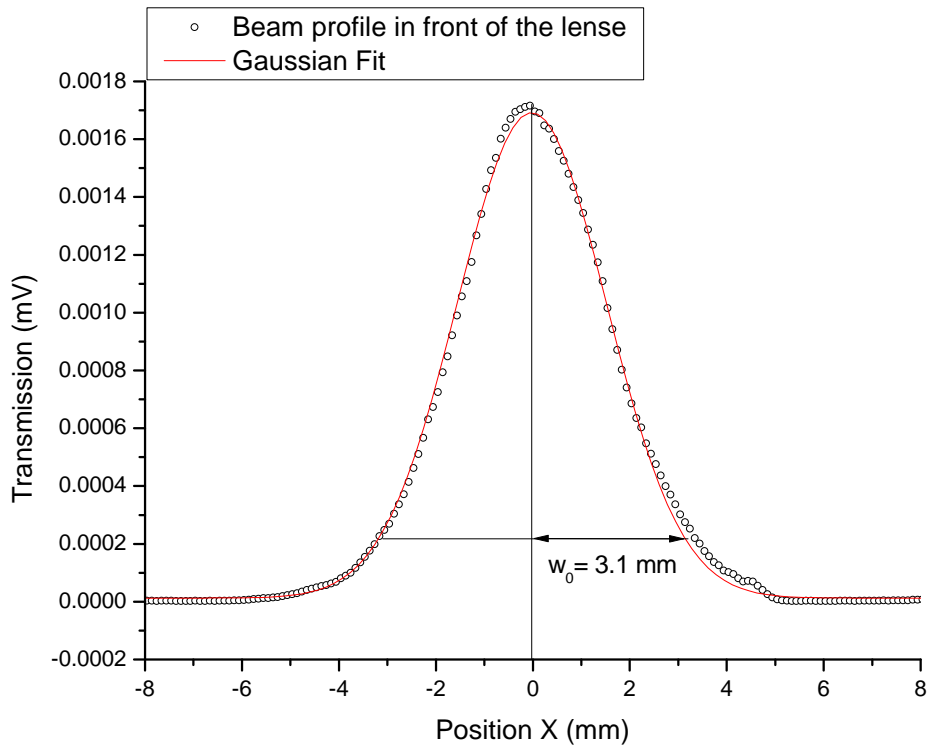


Figure 4.6: Measured beam profile in front of the z-scan lens

4.6 shows the measured beam profile in front of the first lens of the z-scan setup. It was fitted by a Gaussian function and does not introduce significant irregularities. The most important beam parameter is the beam waist radius w_0 . The value of w_0 was extracted after fitting the measurement result yielding a value of 3.1 mm. This, in turn, is used to calculate the of beam waist radius in the focus of the z-scan lens. In order to know the focusing behavior of the z-scan lens, beam profile was measured behind the first lens in the z-scan setup. In Figure 4.7 the measured beam profile is plotted for different distances from the

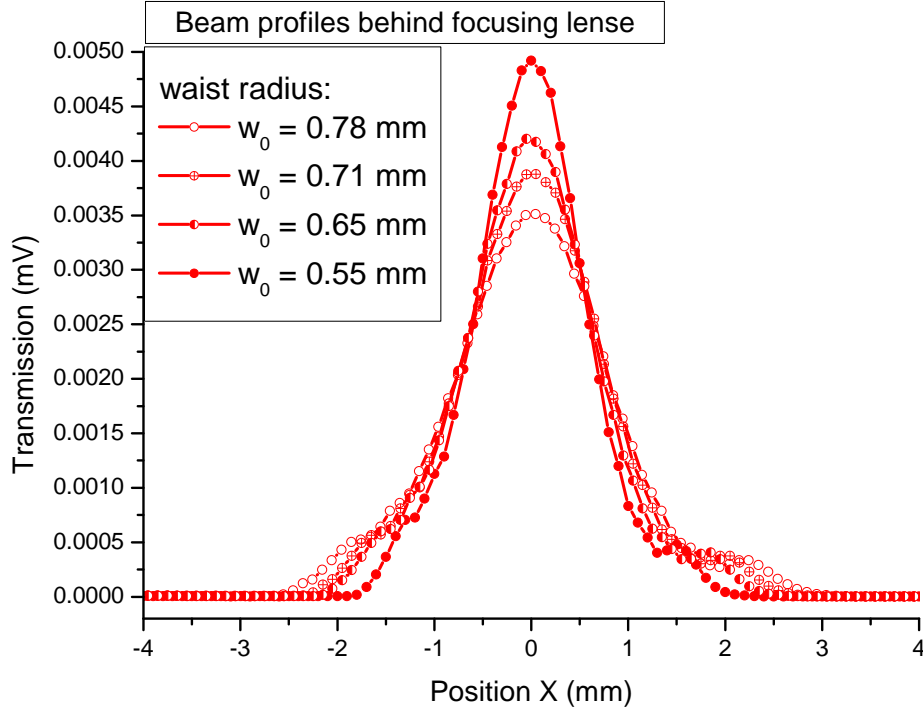


Figure 4.7: Measured beam profile behind the first lens in the z-scan setup. Measurements were carried out at 4 different positions: 0.5 mm, 5.4 mm, 9.2 mm and 16.5 mm away from the first z-scan lens. The beam waist radius w_0 decreases by approaching the focus while peak intensity increases.

lens. Apparently, the beam waist radius becomes more narrow when the beam approaches the focus. As expected, the peak intensity increases while the beam waist radius decreases. Measurements were done at four different positions, yielding a change of the beam waist radius by $\approx 100 \mu\text{m}$. The radius measurement of 0.78 mm was subject to a weak truncation which may be caused by diffraction at setup parts in front of the lens. The small Airy disks become weaker as the beam waist radius approaches 0.55 mm. Pinholes and other diffracting elements can influence the quality of the focused beam. The calculation of the beam waist radius and the Rayleigh length in the focus is done in the following paragraph.

Rayleigh length of the setup

It is important to know the Rayleigh (or diffraction) length of the Gaussian beam in the focus. With the help of this parameter, one can approximate the distance from the focus where a z-scan signal is still present.

In Chapter 2.4.1, Gaussian beam optics was described. One calculates the Rayleigh length in the focus as follows:

$$z'_0 = \frac{\pi \cdot w_0'^2}{\lambda} \quad \text{with} \quad w_0' = \frac{\lambda f}{\pi w_0} \quad (4.4)$$

The waist radius in front of the lens w_0 was taken from the beam profile measurement (Figure 4.6). The waist of the beam in the focus for a focal length of $f = 10 \text{ cm}$ and a wavelength of 800 nm is:

$$w'_0 = 8.2 \mu\text{m}$$

The focal Rayleigh length under the described conditions is thus:

$$z'_0 = 0.264 \text{ mm}$$

The Rayleigh length was calculated for the refractive index of air ($n = 1$). As described in Chapter 3.3 changes of the Gaussian beam profile are detected far away from the sample. The beam waist radius and, with it, the Rayleigh length differ for a different in-coupling of the beam into the setup. Ideally, the beam reaches the first z-scan lens in a collimated way. The refractive index of the sample does not play any role as long as the thin sample condition is fulfilled. This implies that the sample must be much smaller than the Rayleigh length:

$$L \ll z'_0 \tag{4.5}$$

The aim was to measure organic layers of 400 nm to 2 μm thickness, which met this condition. The substrate had a thickness of 1 mm, which was approximately 5 times larger than z'_0 . For large nonlinear phase changes $\Delta\Phi_0 > \pi$ one has to perform z-scan analysis in a different way in order to obtain a good fit of the z-scan trace, as described by Samad [43].

4.2.2 Photoluminescence measurements

400 nm excitation of Alq₃

In this chapter z-scan measurements are presented of Alq₃ and Alq₃:2wt%DCM samples at an excitation wavelength of 400 nm. It was measured the photoluminescence emission of the organic layer was measured by bringing an optical fiber close to the glass edge of the sample. With the help of a USB-Spectrometer, the emitted photoluminescence was spectrally resolved.

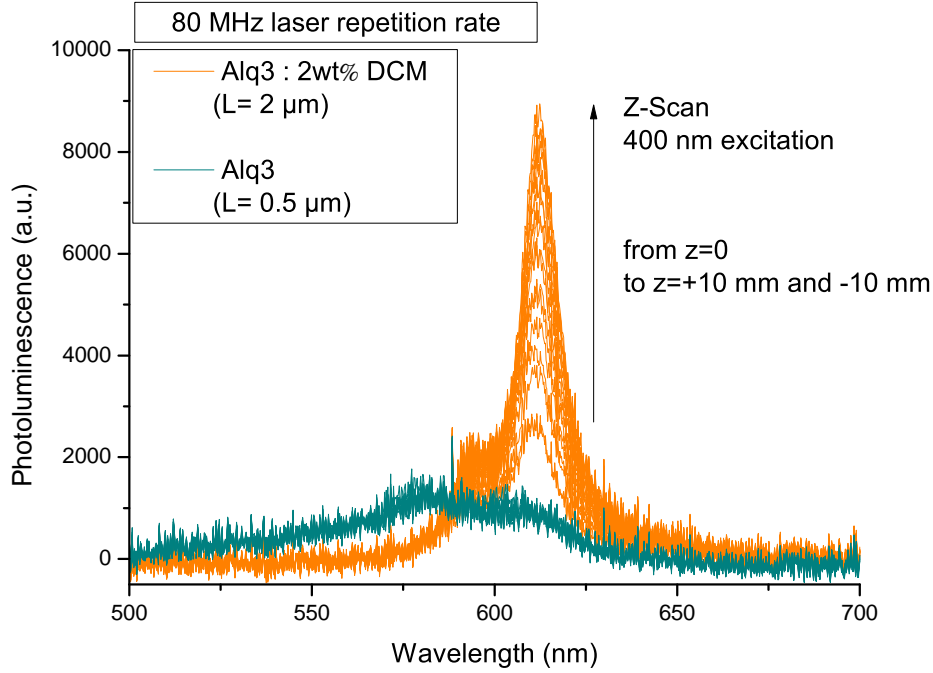


Figure 4.8: Photoluminescence spectra of the edge emission during z-scan for doped and undoped Alq₃. The arrow indicates the development of the saturation effect at 80 MHz laser repetition rate in Alq₃:DCM thin film during z-scan.

As one can see from Figure 4.8, the sample position was varied from -10 mm, going through the focus to +10 mm. A spectrum was taken of every millimeter in z-position. Two different measurements are plotted. The anthracite spectra are recorded from an Alq₃ sample of 500 nm thickness. The orange spectra were measured on Alq₃:2wt%DCM of 2 μm film thickness. As apparent from Figure 4.8, the Alq₃:DCM photoluminescence showed a z-scan signal whereas undoped Alq₃ did not.

In Figure 4.9, the peak values are shown at 612 nm in case of Alq₃:DCM and at 579 nm for Alq₃. One can determine a clear z-scan response of Alq₃:DCM where the signal drop by 72% from low irradiation far away from the focus to intense irradiation in the focus. The undoped Alq₃ showed no significant change in photoluminescence during the z-scan. The drop in photoluminescence of Alq₃:DCM during z-scan is explained by a saturation of the number of excited state DCM molecules for very high intensities at a laser repetition rate of 80 MHz. Assuming an efficient Förster transfer from Alq₃ to DCM one can say that every excitation of Alq₃ is expected to transfer directly to a DCM molecule. There are 50 times less DCM than Alq₃ molecules in the excited area. The laser repetition rate gives a temporal distance of 12.5 ns between two pulses. The Förster transfer can last up to 1 ps.

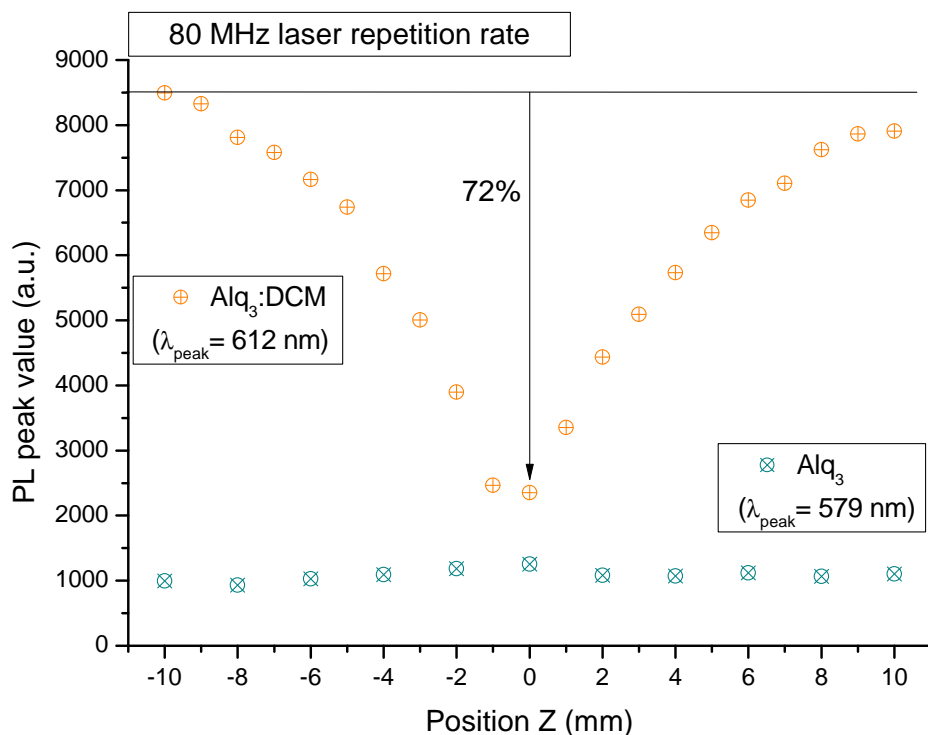


Figure 4.9: Intensity peak values of photoluminescence from Alq₃ and Alq₃:DCM for different z-positions. The saturation effect in Alq₃:DCM thin film becomes manifest in the decrease of PL signal when the sample approaches the focus.

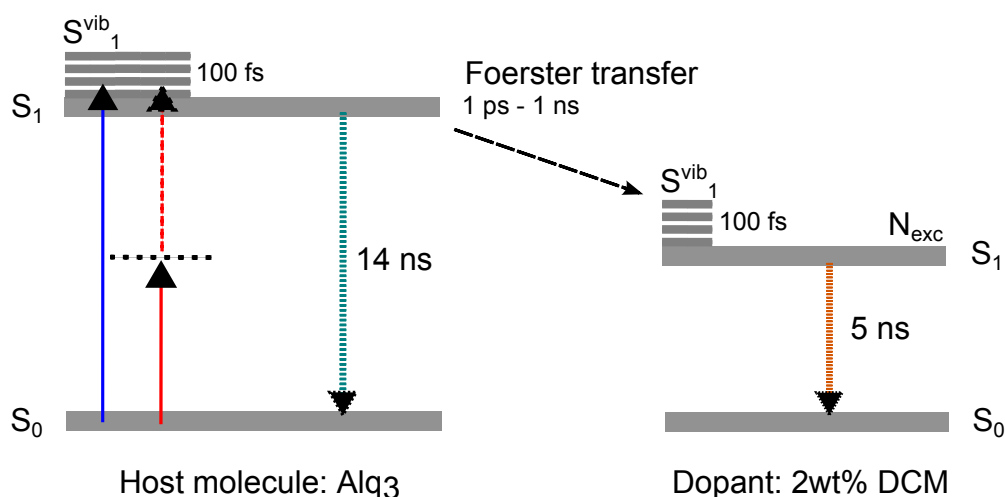


Figure 4.10: Energy level diagram of Alq₃:DCM. Typical relaxation times are shown for both molecules. The excitation wavelength in this experiment was 400 nm. The black dashed line indicates the Förster transfer from Alq₃ to DCM.

For a certain intensity, the saturation of Förster transfer due to the small number of DCM molecules connected with the high laser repetition rate leads to the observed emission saturation. It would be possible to describe this saturation profile for Alq₃:DCM by rate equations [44],[45] combined with the z-scan theory.

This kind of measurement was also done at 1 kHz repetition rate. It showed no saturation effect in Alq₃:DCM within measurement precision. This clearly indicates a dependence of the saturation process on the laser repetition rate.

For a neat layer of Alq₃ without the DCM dopant no significant change is observed in the photoluminescence during z-scan. The average relaxation of Alq₃ molecules from the first excited singlet state S_1 to the ground state S_0 is known to be 14 nanoseconds. The intensity in this experiment is not sufficient to cause any kind of saturation in the emission of a Alq₃ thin film. This shows that Alq₃ itself supports 80 MHz excitation without any limitation in emission due to the spot size or high intensities.

At a wavelength of 400 nm, no excited state absorption (ESA) occurs in Alq₃ for femtosecond pulses. Such a process would cause an increase in PL intensity as the excited state becomes more populated at high intensities. ESA was not expected because temporal pulse width in the experiments was ≈ 120 femtoseconds. As elaborated in Chapter 2.3.3, ESA occurs in organic molecules only for longer pulses (ps, ns).

In order to prove that the measurements in Alq₃:DCM are not only caused by a geometric size effect due to the excitation spot size, the input power dependence was measured in the focus and far away. This approach is similar to z-scan. It tests the linearity of the input power dependence in the focus ($z=0$ mm) and far away from it ($z=10$ mm). Figure 4.11 and 4.12 show the peak values of measured Alq₃:DCM photoluminescence spectra plotted against the incident average power. The slope of the double logarithmic input-output plot for an Alq₃:DCM sample position at $z=0$ mm is smaller than unity. The data were fitted by a linear function with a slope of 0.30 ± 0.02 . This confirms the saturation effect in Alq₃:DCM as observed with z-scan. The slope far away from the focus was found to be linear (0.98 ± 0.06), implying that the intensity is not enough to cause saturation.

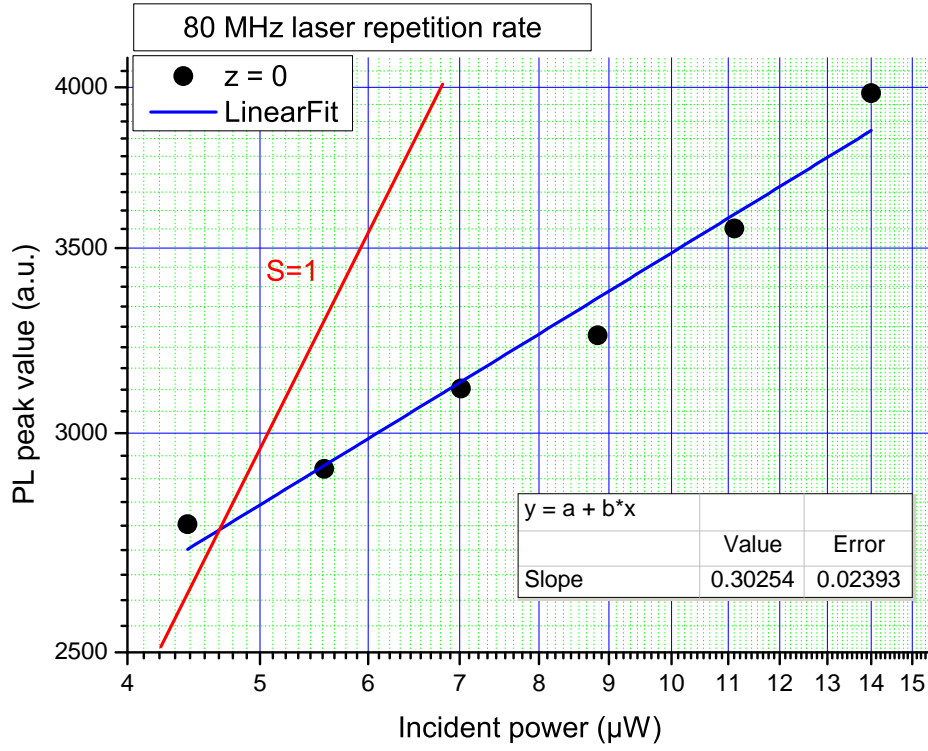


Figure 4.11: Input-output behavior of $\text{AlQ}_3\text{:DCM}$ sample at 400 nm excitation in the focus. Clearly it shows a saturation due to a slope smaller than 1.

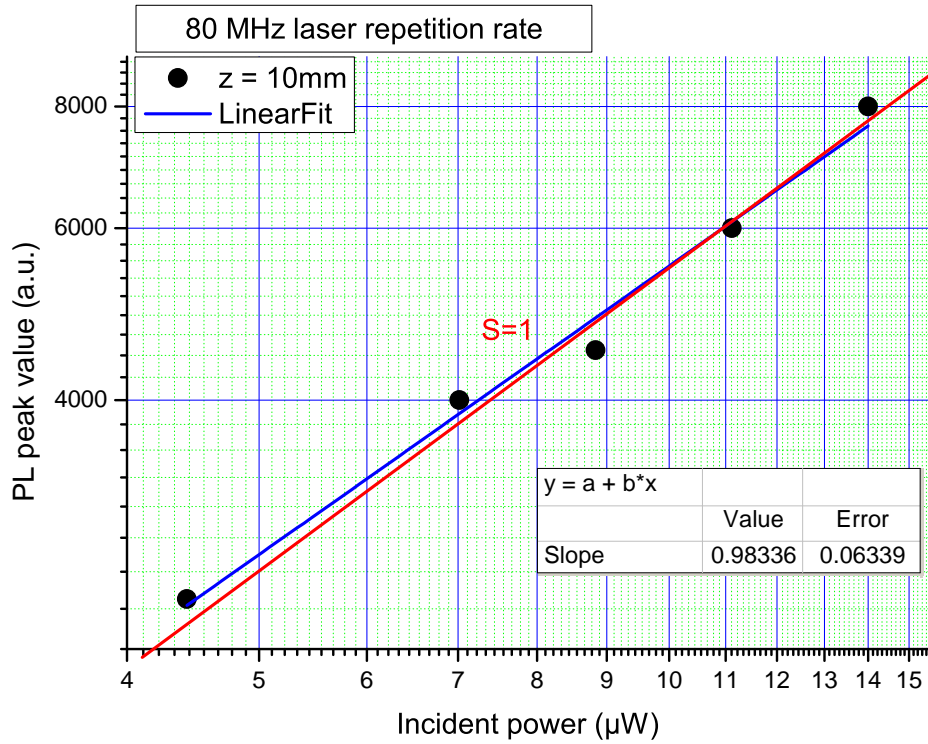


Figure 4.12: Input-output behavior of $\text{AlQ}_3\text{:DCM}$ sample at 400 nm excitation far away from the focus. No saturation effect is present. The measurement shows linear behavior.

800 nm excitation of Alq_3

It was an important concern to verify the two-photon absorption process in Alq_3 with a z-scan measurement. The most reliable parameter to be measured is the amount of emitted photons depending on the incident intensity. If a single absorption process requires two photons then will be visible in a z-scan by measuring photoluminescence. Figure 4.13 shows the z-scan trace of photoluminescence measured in line with beam propagation by a photomultiplier. The measurement was carried out on a $1.6\ \mu\text{m}$ thick organic layer of $\text{Alq}_3\text{:DCM}$ evaporated on a 1 mm thick glass substrate. The incident peak power was varied by using optical density filters. The peak power spread over 1 order of magnitude from 4.3 kW to 43 kW. The main signal response was found in a scanning range of plus ± 4 mm about the focus. A very important and sensitive parameter in z-scan measurements is the beam waist radius in the focus. The beam waist radius is easily extracted from a photoluminescence z-scan because there is no interference with the signal from the substrate, as this does not emit. The most reliable fit was assumed to be at the highest incident peak power. Therefore the beam waist radius was extracted from the 43 kW fit and fixed for all other fitting procedures. The result for the beam waist radius in the focus is $11.28\ \mu\text{m}$. In order to

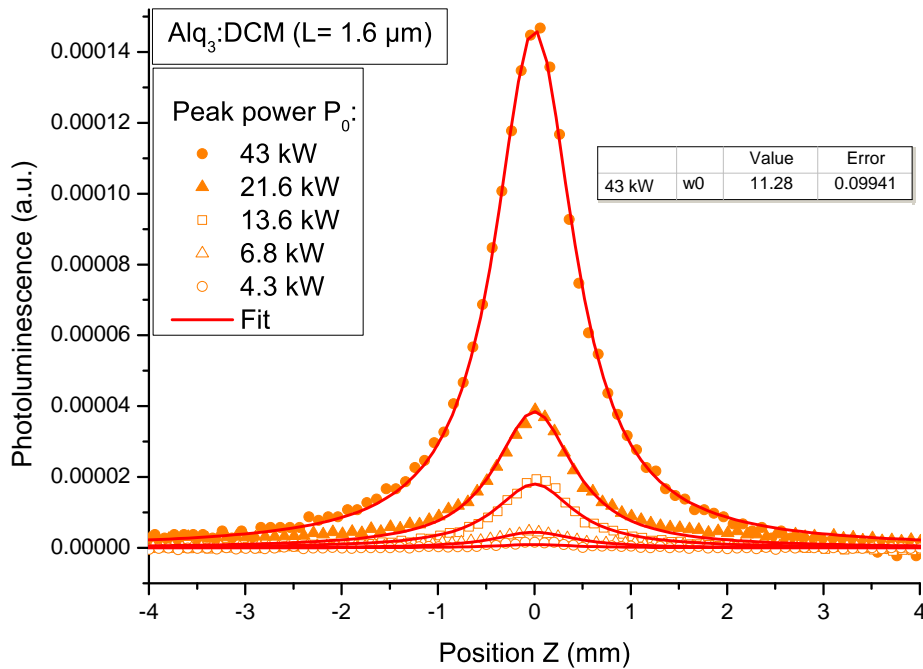


Figure 4.13: Photoluminescence from a $\text{Alq}_3\text{:DCM}$ thin film of $1.6\ \mu\text{m}$ thickness for different peak power values. The measurement was done with the on-axis detection method.

confirm the two-photon nature of the process, one evaluates the measured peak intensity of the photoluminescence in the focus. Figure 4.14 plots the photoluminescence peak intensity in the focus of the z-scan traces, in dependence on the incident peak power of the laser pulses. The measurement results were plotted on a double logarithmic scale and fitted using a linear function. The slope of this input-output analysis is 1.92 ± 0.01 . This is understood as a clear indication for two-photon absorption in the organic $\text{Alq}_3\text{:DCM}$ layer.

The evaluation of z-scan traces in transmission is not easily done here. As one can see from Figure 4.15, there is a significant influence of the glass substrate on the transmission

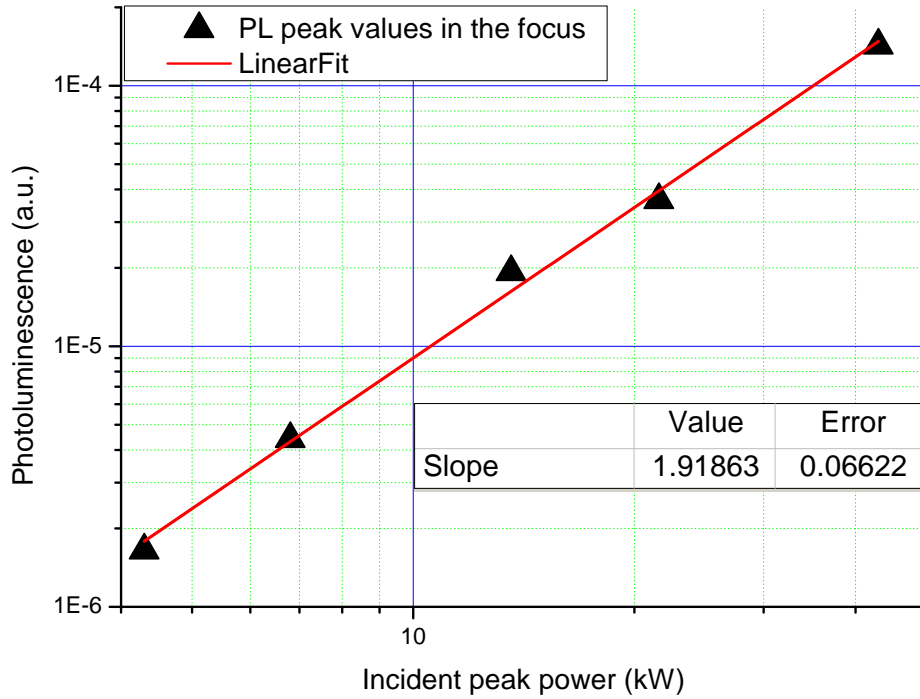


Figure 4.14: Intensity peak values of photoluminescence from Alq₃:DCM sample situated in the focus. The quadratic dependence indicates a two-photon absorption process.

z-scan trace. The transmission was recorded simultaneously to the photoluminescence measurement and normalized to the value of the transmission far away from the focus. The variation of the incident peak power per pulse is the same as in Figure 4.13. Also shown is the z-scan signal of a clean glass substrate without any organic on top. The difference in the normalized transmittance of an organic layer in comparison to the plain glass substrate is immediately visible. With the glass signal serving as a reference, the absorption process in Alq₃:DCM layer was identified. By going to a lower peak power, the normalized transmittance shows a decrease. In common z-scan theory one expects exactly the opposite behavior. The behavior in the present measurement is explained by the glass substrate influence. Glass seems to exhibit a nonlinear behavior at 80 MHz laser repetition rate. The signal depends on the incident peak power. The glass signal increases when approaching the focus. By reducing the incident peak power, the actual transmittance drop caused by the organic layer becomes more visible. Therefore, it is not possible to extract the two-photon absorption coefficient β directly from transmission measurements. The competing signals of substrate and organic layer can not be separated from each other. It is not clear, at which intensity the glass signal disappears completely because the measurement sensitivity was not sufficient to use even lower incident peak powers.

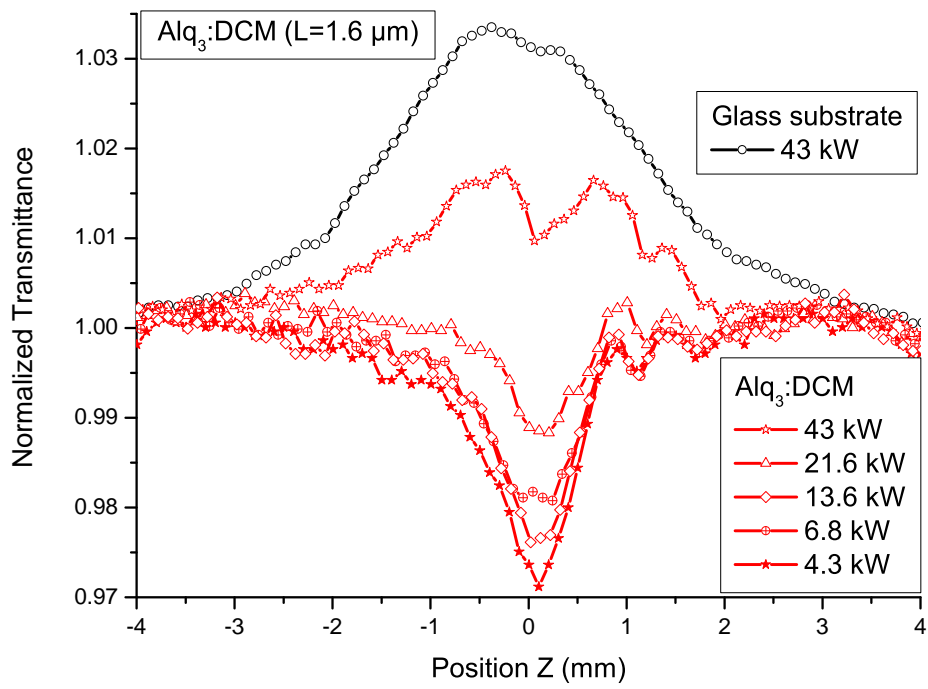


Figure 4.15: Z-scan trace in transmission that was measured simultaneously with the photoluminescence. The substrate signal is shown for comparison with the development of transmission through the complete $\text{Alq}_3\text{:DCM}$ sample, for different peak powers.

4.2.3 Substrate

Open aperture z-scan

In Figure 4.16 z-scan traces are plotted for a common BK7 glass plate which was used as the substrate for the organic layer. The measurements were carried out at 800 nm pulsed excitation in the femtosecond regime with a repetition rate of 80 MHz. A nonlinear response was observed in the substrate. An increasing z-scan trace appeared in the glass at these experimental conditions. The z-scan traces were measured for different incident peak powers varying over one order of magnitude. An important step in the evaluation was to identify

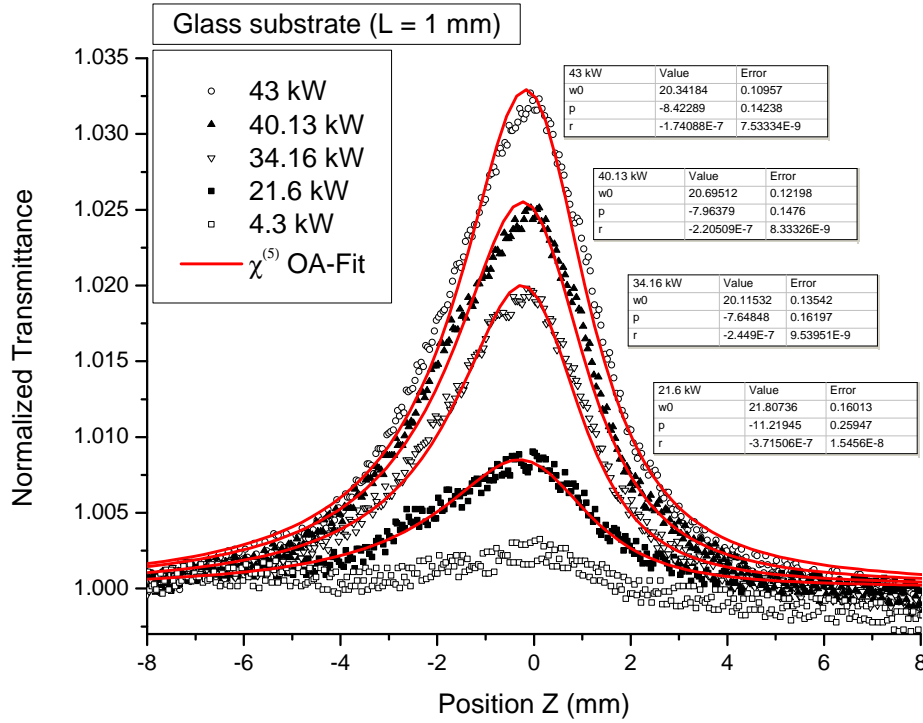


Figure 4.16: Z-scan signal caused by 1 mm glass substrate at 80 MHz laser repetition rate under 800 nm excitation. A $\chi^{(5)}$ -fitting formula was used because cubic dependence of the z-scan peak value in the focus indicates a three-photon process.

the order of the process occurring in the glass. Therefore, the peak values of the signal were evaluated for each incident peak power. The absolute signal difference was taken between $z = -8$ mm and $z = 0$ mm. The plot in Figure 4.17 shows the result on a double logarithmic scale. The linear fit gave a slope of 3. This indicates a cubic dependence of the z-scan signal in glass. Apparently, there is a weak linear absorption of glass at 267 nm, which can be excited by a three-photon process [46]. It is known that wide band gap materials show z-scan traces under femtosecond excitation for intensities of a few GW/cm^2 [47].

The normalized transmittance in Figure 4.16 was fitted for four different peak powers. The OA z-scan traces were fitted with the formula for a $\chi^{(5)}$ - process. The process in glass seems to be a three-photon absorption that saturates during z-scan. As apparent from Figure 4.16 all fitting procedures gave similar results for the beam waist radius w_0 , absorptive parameter p and refractive parameter r . As discussed in Chapter 2.4.3, it is possible to enhance a weak absorption by using high repetition rate laser. Especially for 80 MHz repetition rate, the

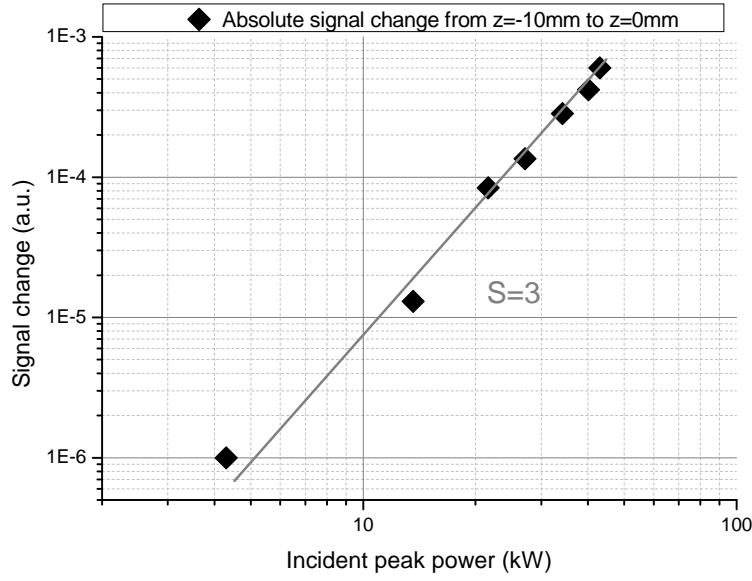


Figure 4.17: Absolute signal change dependent on incident peak power

time between two pulses is much shorter than the heat diffusion time constant of glass. This leads to a cumulative effect because the material does not return to its equilibrium state after each pulse. For a beam waist radius of $11 \mu\text{m}$, the calculated thermal diffusion time with a typical thermal diffusion constant $D = 10^{-3} \text{cm}^2/\text{s}$ for glass is [42]:

$$t_c = \frac{w_0^2}{4D} = 300 \mu\text{s} \quad (4.6)$$

For a 80 MHz pulsed laser system, the time between two pulses (12.5 ns) is much smaller than the characteristic time during which heat diffuses out of the exciting laser spot. The z-scan response is broader than expected from the beam waist calculations in Chapter 4.2.1. Light outside the beam waist radius also contributes to the cumulative absorption because thermal energy flows radially from the center to the excitation spot borders. The beam waist parameters fitted in Figure 4.16 are approximately twice larger than the reliable one extracted from a photoluminescence z-scan (Second part of Chapter 4.2.2).

Closed aperture z-scan

Another hint for thermal enhancement of the z-scan signal is the 43 kW measurement in Figure 4.18. It was measured an OA z-scan trace quite similar in appearance and fitting to the measurement shown in Figure 4.16. A closed aperture measurement is shown in Figure 4.18. The defocussing behavior during z-scan indicates the formation of a thermal lens. The measured peak-valley distance is $\Delta z_{p-v} = 1.59 \text{ mm}$. The Rayleigh length for the fitted beam waist ($w'_0 = 20 \mu\text{m}$) is $z'_0 = 1.57 \text{ mm}$. Assuming a thermally enhanced $\chi^{(5)}$ -process, I used the following factor multiplied to the Rayleigh length in order to obtain the peak-valley distance of the transmittance z-scan trace [42]:

$$z_{p-v} = 1.02 \cdot z_0 \quad (4.7)$$

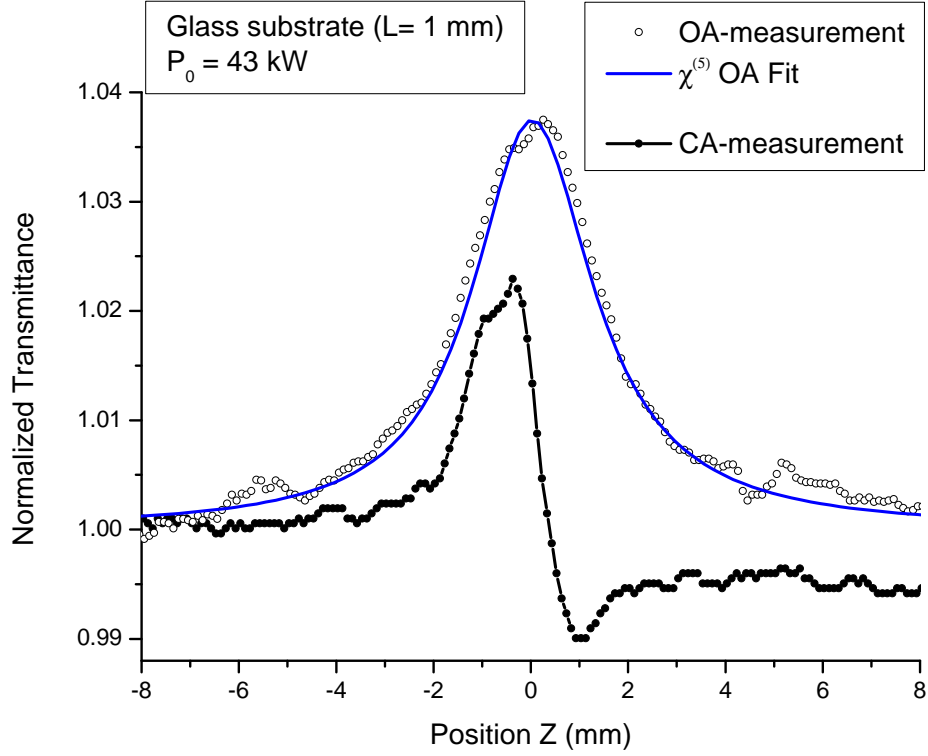


Figure 4.18: Closed aperture z-scan measurement of 1 mm glass substrate. Maximal peak power was used in order to show the formation of a thermal lens.

It fits in good agreement to the extracted parameters.

The fact that glass does not emit light leads to the conclusion that the absorbed energy is released in the form of heat. It makes the evaluation of z-scan more difficult because absorption creates a temperature profile which leads to a thermal lens. Δz_{p-v} is a very sensitive parameter which helps to distinguish between glass and organic signal. It was used together with the sign of closed aperture z-scan trace as the evaluation tool in further measurements.

4.2.4 Transmission measurements

An organic layer of Alq₃:DCM with 1.6 μm thickness was measured in open and closed aperture z-scan. The peak power of the laser pulses was 0.25 kW. At this low peak power the glass signal is expected to be much weaker than the organic component because a $\chi^{(5)}$ -process decreases faster than a $\chi^{(3)}$ -process with decreasing peak power. The transmittance drop at $z=0$ is proportional to I_0^2 for glass and to I_0 for the organic layer. Glass gives a positive transmittance change and organic a negative one, partly compensating each other. At the peak power where this measurement was done glass signal is still not vanished completely. It is possible to estimate a first bottom limit for the β -coefficient and the refractive index change with this measurement.

The refractive index change for a $\chi^{(3)}$ -process is given by [41]:

$$\Delta n = \gamma \cdot I_0 \quad (4.8)$$

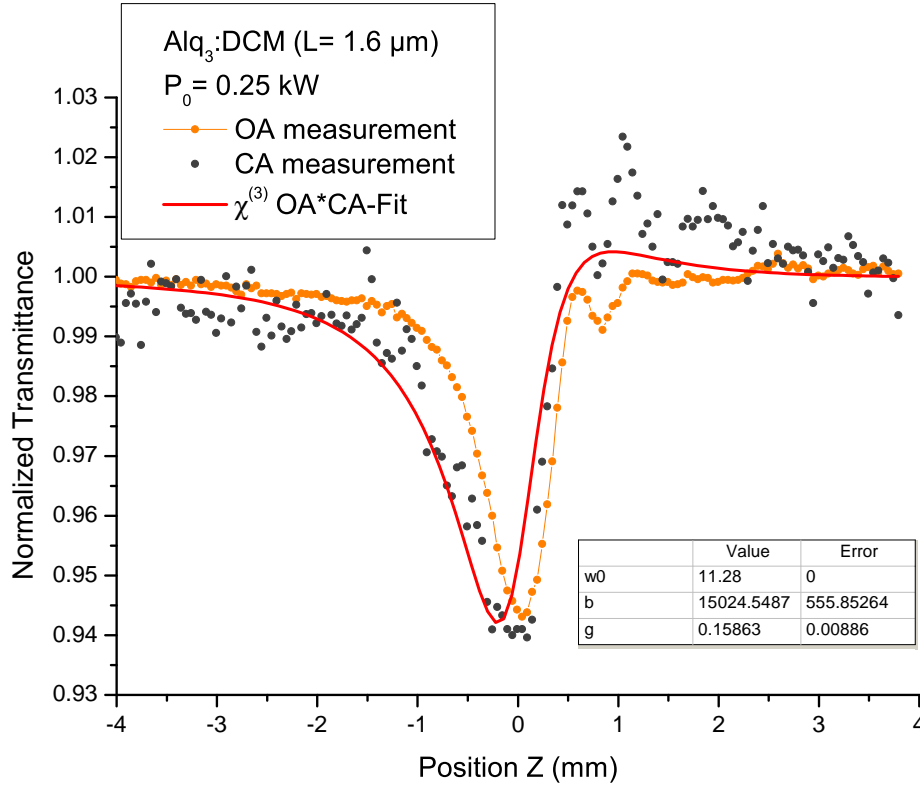


Figure 4.19: Open and closed aperture measurement of $\text{Alq}_3\text{:DCM}$ with 1.6 μm thickness at a peak power of 0.25 kW

The closed aperture measurement in Figure 4.19 was fitted by an OA·CA function which describes the overlaid processes of absorption and refraction. For a reliable fitting procedure the waist radius from PL measurement was used ($w_0 = 11.28 \mu\text{m}$). The refractive parameter is $\gamma = (0.222 \pm 0.006) \text{ cm}^2/\text{GW}$. The two-photon absorption coefficient was found to be:

$$\beta = (12.2 \pm 0.4) \cdot 10^4 \text{ cm/GW} \quad (4.9)$$

The figure of merit for fitting the closed aperture measurement is:

$$\frac{\beta}{2k\gamma} = \frac{\beta \cdot \lambda}{4\pi\gamma} = 0.35 \quad (4.10)$$

The open aperture z-scan traces showed an intrinsic refractive behavior that was not possible to avoid by setup changes. Especially the detector size for the transmission measurement can improve the situation. There is a way to separate the absorptive and refractive part with a symmetrization method described by Yin [48].

Figure 4.20 shows the open aperture measurement as well as its absorptive and refractive component. When the absorptive part is fitted by an OA-function, a larger β -coefficient is extracted compared to the OA*CA fit from above:

$$\beta = (15.4 \pm 0.2) \cdot 10^4 \text{ cm/GW} \quad (4.11)$$

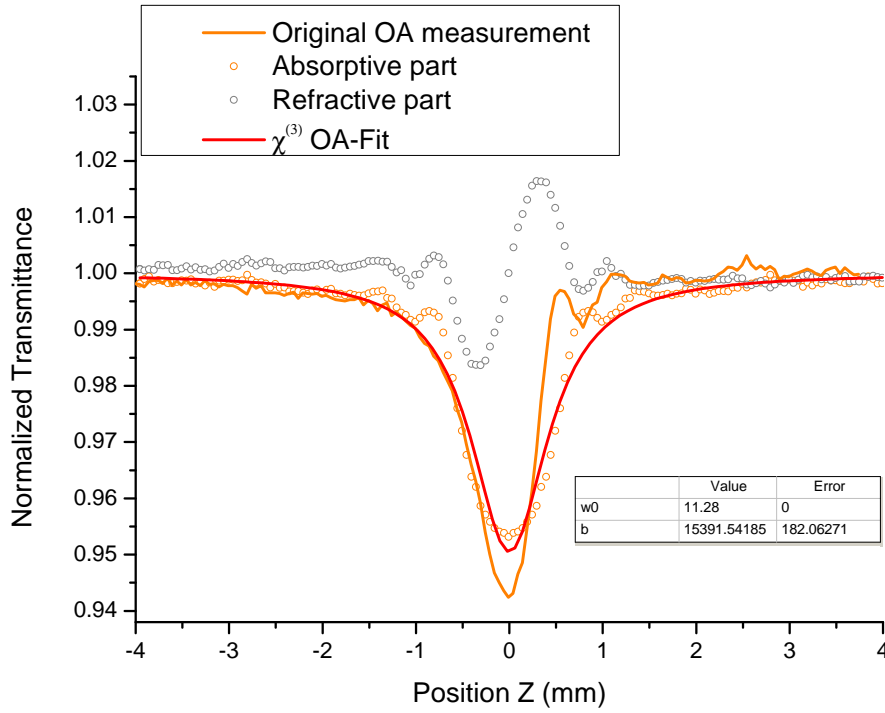


Figure 4.20: Result of the symmetrization method. From the open aperture measurement the intrinsic refractive part was separated from the absorptive one in order to obtain better fitting results for β .

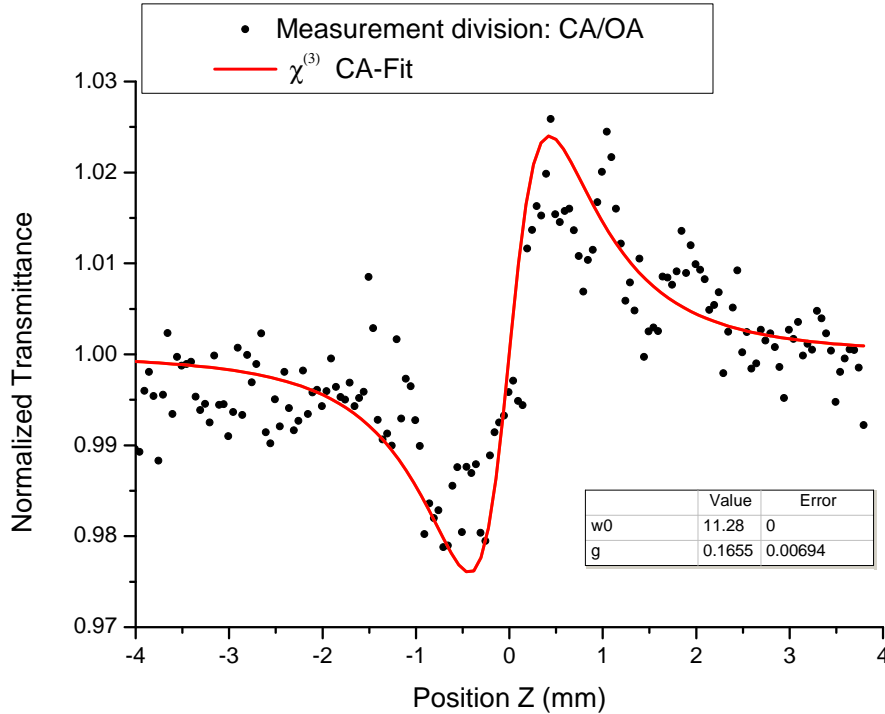


Figure 4.21: Result of the division method. A closed aperture z-scan trace was divided by open aperture z-scan trace. This procedure leads to a more reliable fitting of γ (labeled as g in the plot).

The refractive index change can be extracted reliably by the division method. In Figure 4.20 is plotted the division [41] result of OA and CA measurement from Figure 4.19. The refractive parameter from the division method is:

$$\gamma = (0.166 \pm 0.007) \text{ cm}^2/\text{GW} \quad (4.12)$$

The figure of merit for the separation method is:

$$\frac{\beta}{2k\gamma} = \frac{\beta \cdot \lambda}{4\pi\gamma} = 0.59 \quad (4.13)$$

The most reliable proof that the signal originates from the organic is to check the peak-valley distance for the CA trace. The beam waist radius in this measurement was $11.28 \mu\text{m}$. This gives a Rayleigh length of 0.49 mm . In Figure 4.21 a peak valley distance of $\Delta z_{p-v} = 0.83 \text{ mm}$ was extracted. The ratio of these measurement results is:

$$\frac{\Delta z_{p-v}}{z'_0} = 1.76. \quad (4.14)$$

This demonstrates the correctness of using a $\chi^{(3)}$ -fit (Equation 2.79) and it indicates that the CA z-scan measurement is dominated by the organic signal for very low incident peak powers. The author found one comparable paper, where organic dendrimers were measured under 790 nm femtosecond excitation in chloroform [49]. It was found a γ value being 1 order smaller than the one of this work.

4.2.5 Estimation of the two-photon absorption coefficient

Substrate-organic signal interplay

As shown in Chapter 4.2.3 substrate gave a positive z-scan trace which decreased with decreasing peak intensity. The intensity dependence of this process is cubic which indicates a $\chi^{(5)}$ -process in glass. It was done an on-axis photoluminescence z-scan, which carried out a very efficient TPA of Alq₃ molecules (Chapter 4.2.2). For 800 nm excitation, only TPA by Alq₃ occurs in the Alq₃:DCM film. There was no saturation detected in the photoluminescence for two-photon excitation. The transmittance z-scan trace is expected to be negative because no saturation occurs at 800 nm excitation neither for Alq₃ nor Alq₃:DCM thin films.

Figure 4.22 shows z-scan measurements on a 500 nm thick Alq₃ layer. The full power measurement with 43 kW peak power shows a significant glass signal onset clearly visible as an increasing transmittance between $z = \pm 3$ mm and $z = \pm 1$ mm. Between $z = -1$ mm and $z = +1$ mm the organic negative signal dominates. When going to lower peak powers, the glass still contributes to the z-scan trace. A similar behavior is observed in Alq₃:DCM

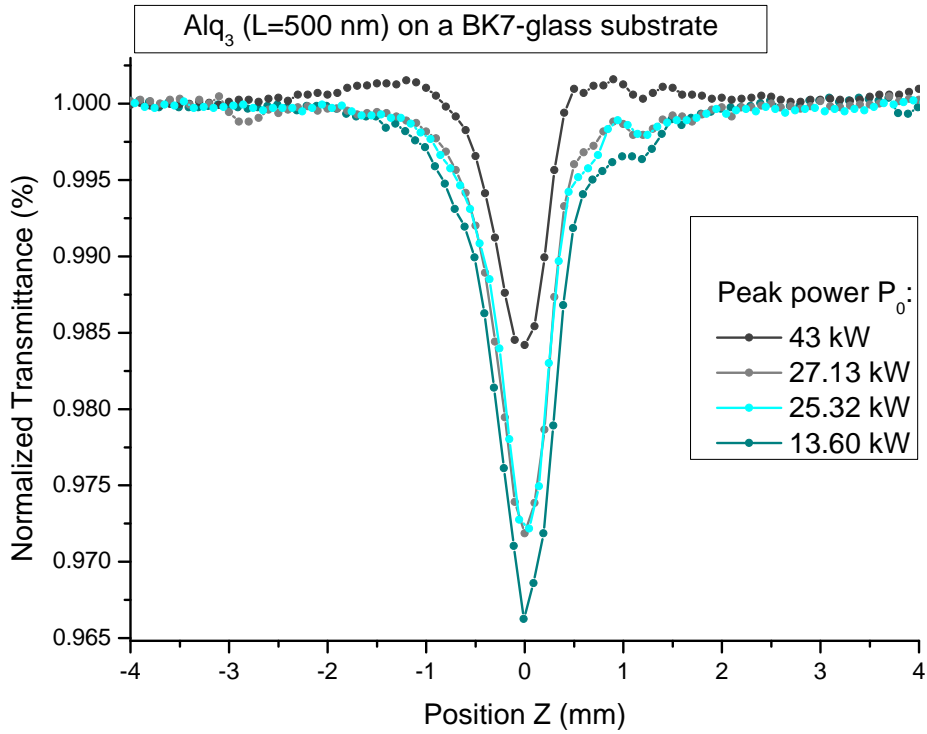


Figure 4.22: Glass-organic signal interplay demonstrated on a Alq₃ sample. By decreasing the incident peak power, the organic signal changes with quadratic and the substrate signal with cubic dependence.

samples as shown in Figure 4.23. For comparison, the original glass signal is plotted without any organic material on the substrate. This measurement spans over 2 orders of magnitude in peak power down to 0.2 kW. It can be seen that 3rd order glass contribution vanishes. The actual drop in transmittance due to TPA in organic layer becomes dominant.

Due to the fact that the precision of the transmission z-scan deteriorates for low peak powers, I had to go a different way to estimate the two-photon absorption cross section of Alq₃.

The experimental parameter β^* should reach a plateau at low peak power. Therefore, the absolute signal change was plotted against the incident peak power for all measurements in Alq_3DCM and Alq_3 sample. The result is shown in Figure 4.26. One can see a similar behavior for both organic layer types at measured high peak powers. Below 10 kW the slope apparently changes and is expected to go to zero. In order to proof a certain plateau value, a calibration measurement for Alq_3DCM was done. It is describe in the following chapter.

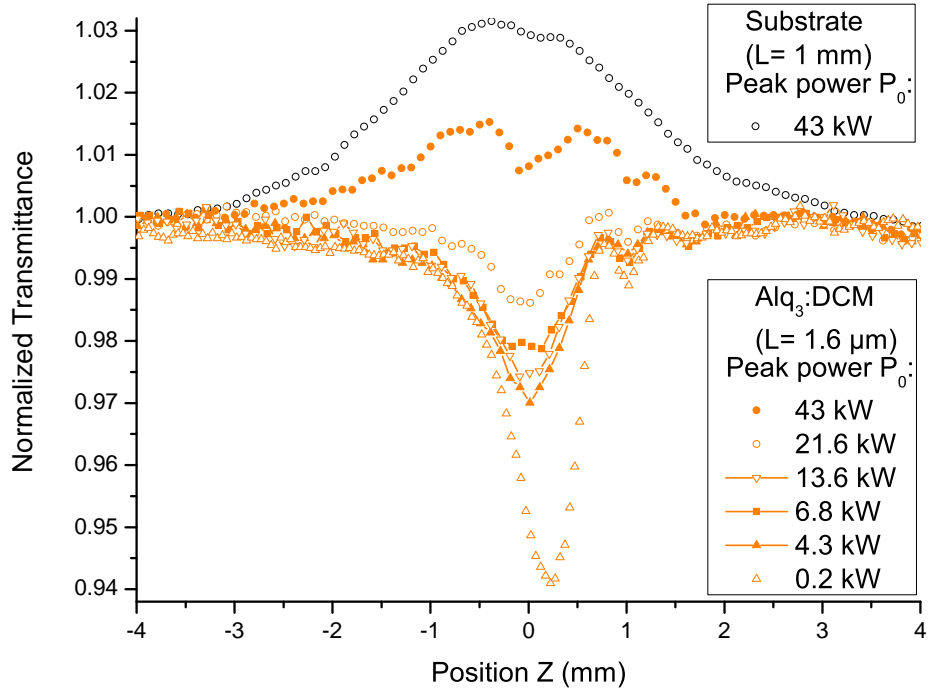


Figure 4.23: Z-scan transmission measurements down to very low peak powers in $\text{Alq}_3\text{:DCM}$ sample. The smallest incident peak power was 0.2 kW.

Direct estimation of the two-photon absorption coefficient

For the estimation of the two-photon absorption coefficient, a simple calibration measurement was done in the setup described in Chapter 3.4.2.

The idea was to balance the number of excited states at 400 nm and 800 nm excitation, respectively. The detection of photoluminescence was done with a USB-spectrometer into which scattered PL light was coupled with an optical fiber. Figure 4.24 shows an example for spectrally resolved scattered light from the substrate edge. A reliable detection of PL light was possible even with two-photon excitation at 800 nm. A small rest of scattered excitation light did not disturb the detection because PL signal was stronger. The measure-

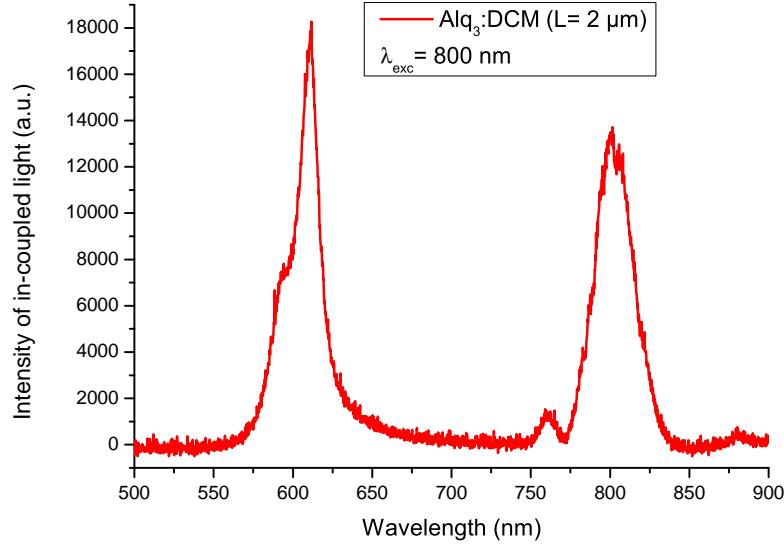


Figure 4.24: Scattered PL and excitation light from the sample edge

ments were carried out in a $2\ \mu\text{m}$ $\text{Alq}_3\text{:DCM}$ sample situated in the focus of the z-scan setup. The beam waist radius in the estimation formula is a very sensitive parameter because it enters quadratically for the excited area. With the help of this experiment, a formula for the two-photon absorption coefficient was derived. The estimated two-photon absorption coefficient is a bottom limit. The formula for the calibration measurement is derived in the following way. The transmittance can be expressed for both excitation regimes (400 nm and 800 nm). The formula for two-photon absorption at 800 nm was taken from Chapter 2.4.2.

$$T_{\text{linear}} = e^{-\alpha^{(400)} L} \quad (4.15)$$

$$T_{\text{non-linear}} = \frac{1}{1 + \beta I_0^{(800)} L} \quad (4.16)$$

The number of excited state is proportional to the beam intensity loss in the sample.

$$\Delta I^{(400)} = \left(1 - e^{-\alpha^{(400)} L}\right) \cdot I_0^{(400)} \quad (4.17)$$

$$\Delta I^{(800)} = \left(1 - \frac{1}{1 + \beta I_0^{(800)} L}\right) \cdot I_0^{(800)} \quad (4.18)$$

Bringing the photoluminescence to the same intensity at 400 nm and 800 nm excitation one sets Equation (4.17) equal to Equation (4.18).

With the substitution $I_0^{(800)} = P_0^{(800)}/(\pi w_0^2)$, solving for β yields:

$$\beta = \frac{\pi w_0^2}{P_0^{(800)} L} \cdot \left[\frac{1}{1 - \frac{P_0^{(400)}}{P_0^{(800)}} (1 - e^{-\alpha^{(400)} L})} - 1 \right] \quad (4.19)$$

The parameters used for the calculation are the linear absorption coefficient of Alq₃ at 400 nm: $\alpha^{(400)} = 4 \cdot 10^4 \text{ cm}^{-1}$ [16], the calculated beam waist radius of the setup: $w_0 = 8.2 \mu\text{m}$ and the Alq₃:DCM thin film thickness: $L = 2 \mu\text{m}$.

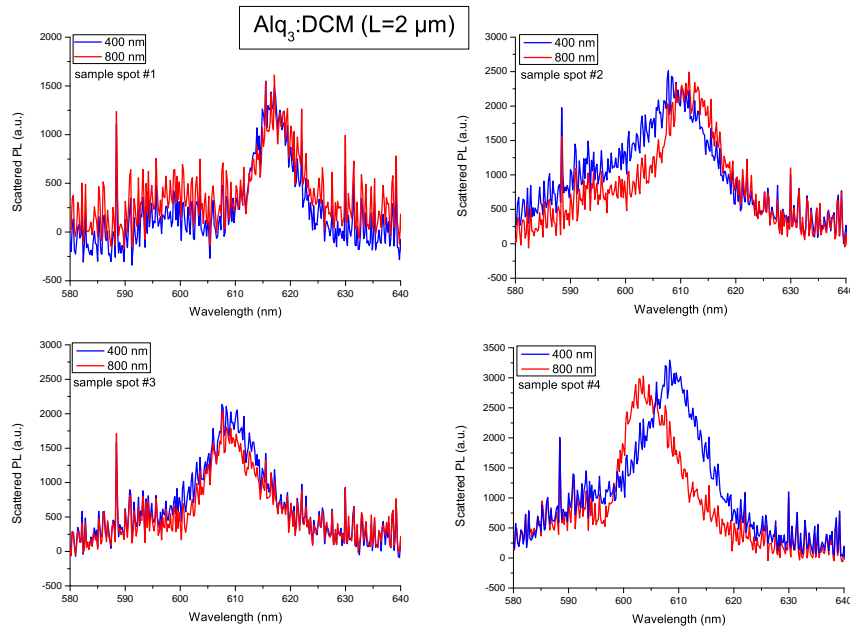


Figure 4.25: Spectra of the photoluminescence from Alq₃:DCM sample for 400 and 800 nm excitation at four different sample spots.

Spot	Average power $P_0^{(400)}$	Average power $P_0^{(800)}$	TPA-coefficient β
#1	14 μW	65 mW	$3.49 \cdot 10^4$ cm/GW
#2	10 μW	47 mW	$4.78 \cdot 10^4$ cm/GW
#3	4 μW	43 mW	$2.28 \cdot 10^4$ cm/GW
#4	12 μW	64 mW	$3.09 \cdot 10^4$ cm/GW

Four measurements were done at different sample spots. They are listed in the table with their measured average power for 400 nm and 800 nm excitation. The two-photon absorption coefficient average value of all 4 measurements is $(3.4 \pm 1.3) \cdot 10^4 \text{ cm/GW}$. The error of estimation is 33%. Plotted in Figure 4.26 is the estimated two-photon absorption coefficient with error bars. It represents a plateau, which is reached, when the glass signal disappears completely in z-scan.

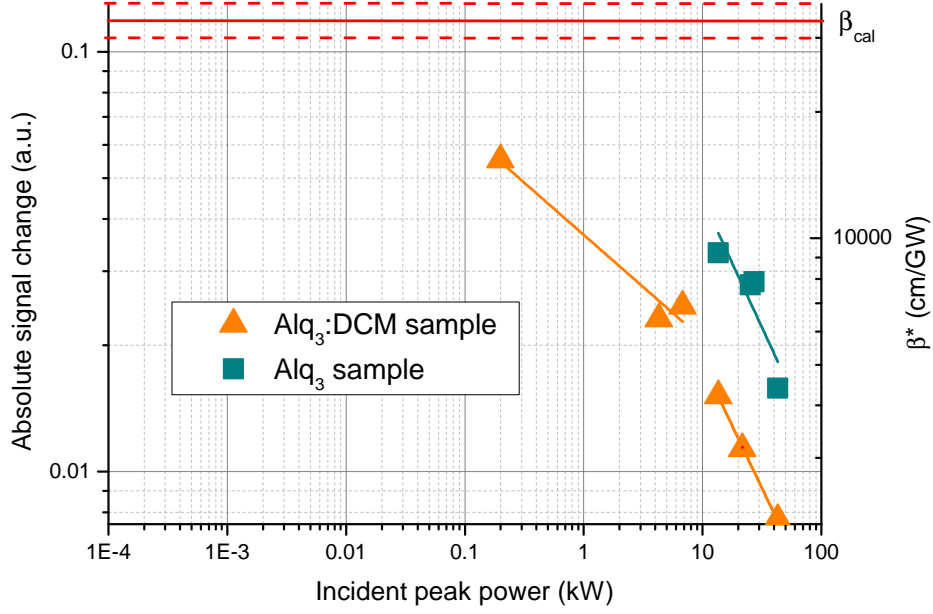


Figure 4.26: β^* for Alq₃ and Alq₃:DCM samples plus calibration result

Koschorreck et al. [50] estimated a molecular density of $5 \cdot 10^{19}$ molecules/cm³ for DCM in a 2wt%-doped thin film of Alq₃DCM. With the molecular density of Alq₃ one can calculate its two-photon absorption cross section. DCM gives a negligible contribution to the absorption at 400 nm. There is a factor of 50 between the Alq₃ and DCM density for 2wt% doping. Hence the molecular density of Alq₃ in a thin layer of Alq₃:DCM is:

$$N_{\text{Alq}_3} = 2.5 \cdot 10^{21} \text{ molecules/cm}^3. \quad (4.20)$$

The formula for the calculation of TPA cross-section is:

$$\sigma_{\text{Alq}_3} = \frac{\hbar\omega\beta}{N_{\text{Alq}_3}} \quad (4.21)$$

With an energy of 1.55 eV per photon, one obtains an two-photon absorption cross section of ($1\text{GM} = 10^{-50}\text{cm}^4\text{sphoton}^{-1}\text{molecule}^{-1}$):

$$\underline{\underline{\sigma_{\text{Alq}_3} = (3 \pm 1) \cdot 10^{-5} \text{GM}.}} \quad (4.22)$$

No sources were found by the author where the two-photon absorption coefficient of Alq₃ was measured in a solid thin film or even in solution. The fact that organic chromophores in general show such high TPA ability is remarkable. Even Alq₃ seems to have a high TPA cross section. The TPA cross section for Alq₃ molecules in a thin film is 2 orders smaller than that for DCM molecules in solution [29]. As DCM is known as a very good two-photon absorber (Chapter 2.3.1) one can say that Alq₃ already possesses an appreciable TPA efficiency for a conjugated chromophore.

5 Conclusion and outlook

This diploma work investigates the nonlinear optical properties of Alq₃ and DCM molecules. The theoretical part of this work treats the relevant theoretical basics for the understanding of the measurements that were done. It also explains optical limiting mechanisms that have to be kept in mind when doing z-scan and interpreting its that data. Relevant considerations about the molecular structure connected with higher order optical response of π -conjugated systems are explained. The characteristic lifetimes of the excitation levels in organic molecules are discussed and correlated to different time scales for pulsed excitation. The morphology in a thin film of evaporated organic molecules is an interesting aspect to consider because the two-photon absorption process is very sensitive to morphological changes like humidity-induced crystallization of Alq₃ and the aggregation of DCM molecules.

Several ways were gone in order to extract information about two-photon absorption in Alq₃:DCM thin films. The detection of emission was very helpful to identify possible saturation processes and their origin. It was proven that DCM molecules separated in an Alq₃ thin film are able to absorb very efficiently two photons instantaneously, when placed in a microcavity, where the optical field is enhanced many times.

With one-photon excitation, two kinds of saturation processes were observed. A thin film of Alq₃:DCM placed in a microcavity was investigated concerning two-photon absorption of DCM. Under one-photon excitation, it showed a saturation of the laser emission from directly excited DCM molecules due to mode volume saturation.

Another kind of emission saturation with increasing excitation intensity was found in a thin film of Alq₃:DCM evaporated on a glass substrate. For femtosecond excitation with 80 MHz repetition rate, it is possible to saturate the emission of DCM in a Alq₃:DCM thin film when Alq₃ is excited with a wavelength of 400 nm. The reason for this observation was the high repetition rate of 80 MHz and the limited number of DCM molecules in the 2wt%-doped thin film.

Z-scan transmission measurements were carried out in order to extract the two-photon absorption coefficient and to calculate the two-photon absorption cross section for Alq₃ in Alq₃:DCM thin films. For the transmission measurements the substrate caused problems because of three photon absorption taking place in the BK7 glass. The z-scan signal showed a saturation of this process manifesting itself in a positive z-scan trace that overlapped the expected negative z-scan trace of organic two-photon absorption. An estimation of the two-photon absorption coefficient of Alq₃ was done with a calibration measurement where the emission was brought to the same intensity by 400 nm and 800 nm excitation. The two-photon absorption cross section of Alq₃ molecules in evaporated thin films was found to be $\sigma_{\text{Alq}_3} = (3 \pm 1) \cdot 10^{-5} \text{ GM}$.

($1\text{GM} = 10^{-50} \text{cm}^4 \text{sphoton}^{-1} \text{molecule}^{-1}$)

The nonlinear refractive index for a cubic nonlinearity in Alq₃:DCM thin films on glass was

estimated by a low power measurement to be $\gamma = (0.20 \pm 0.01) \text{ cm}^2/\text{GW}$.

The z-scan technique is suitable measuring the two-photon absorption of organic molecules. Especially the closed aperture z-scan technique is a very elegant way to determine the sign of an intensity dependent refractive process. The problem of the substrate influence to the z-scan trace will always be a critical concern. To the best of my knowledge, there are no publications, where organic thin films were measured using z-scan on any kind of substrate. Mostly, organic materials are investigated in solution, where one can scale much better the ratio of organic to the surrounding glass cell.

As shown in the Appendix, z-scan can be used for morphological investigations of organic thin films because two-photon absorption is very sensitive to any changes in the film structure. With this technique, optical inhomogeneities at singular sample spots are clearly revealed.

It was intended to investigate microcavities with z-scan. In the Appendix, a way is shown how to obtain access to information about the active organic layer inside the cavity. In order to interpret the data, one must make much more assumptions because of the multi-layered structure and absorption which is not only caused by the organic. Nevertheless, it will be a very interesting topic to pursue because it can give an insight into the influence of the pump spot size and simultaneously increasing intensity on the spontaneous emission from a microcavity and on its lasing behavior.

6 Appendix

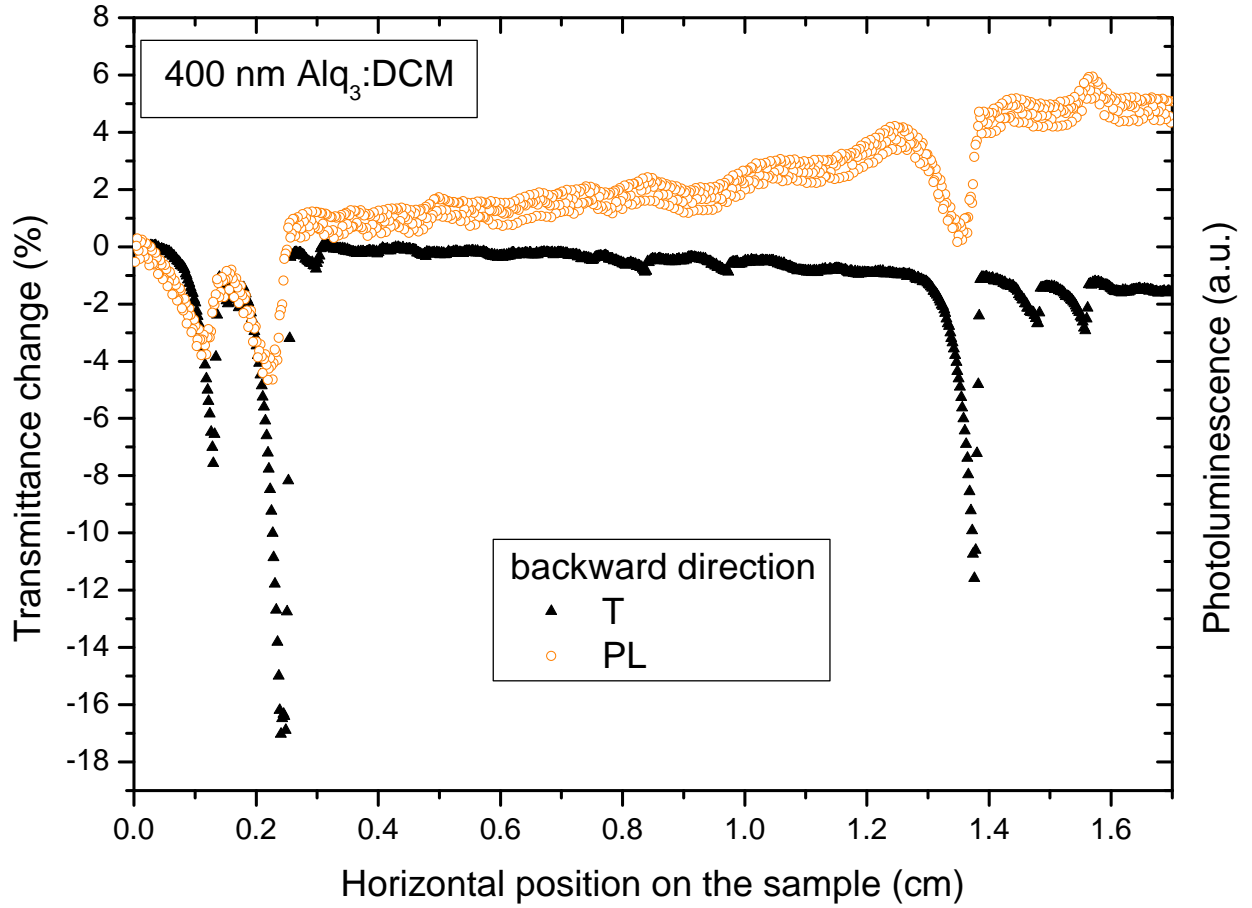


Figure 6.1: Surface scan of a Alq₃:DCM thin film ($L = 400\text{nm}$) placed at the focus of the z-scan setup under 800 nm excitation with a laser peak power of 43 kW (80 MHz laser repetition rate). The plot shows the normalized transmittance change and the on-axis photoluminescence along an horizontal line from the left to the right side of the sample.

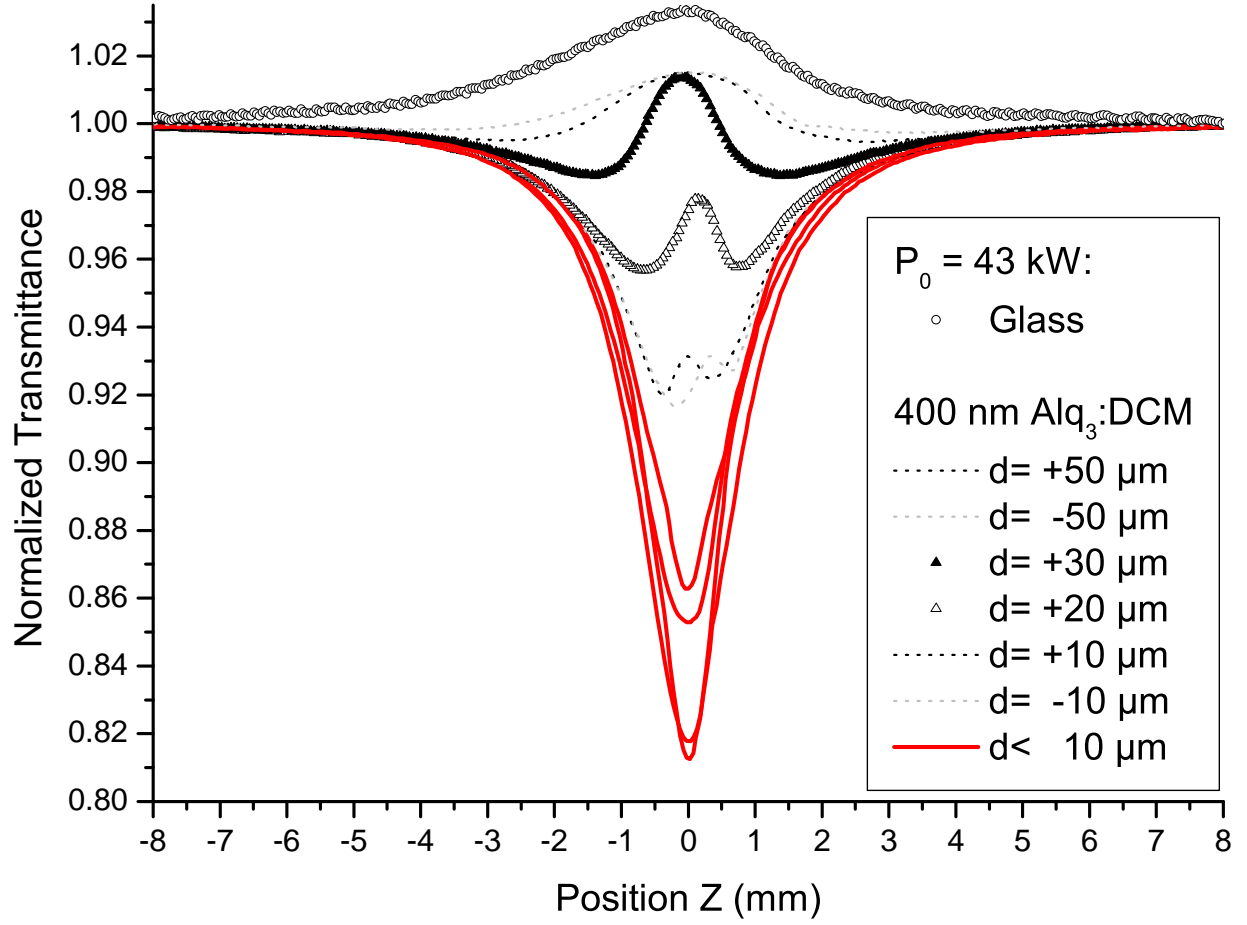


Figure 6.2: Transmittance z-scan of Alq₃:DCM thin film ($L = 400\text{nm}$) at 800 nm excitation with a laser peak power of 43 kW (80 MHz laser repetition rate). Z-scan was performed in a distance d from the maximal signal drop to the left and to the right side along an horizontal line on the sample.

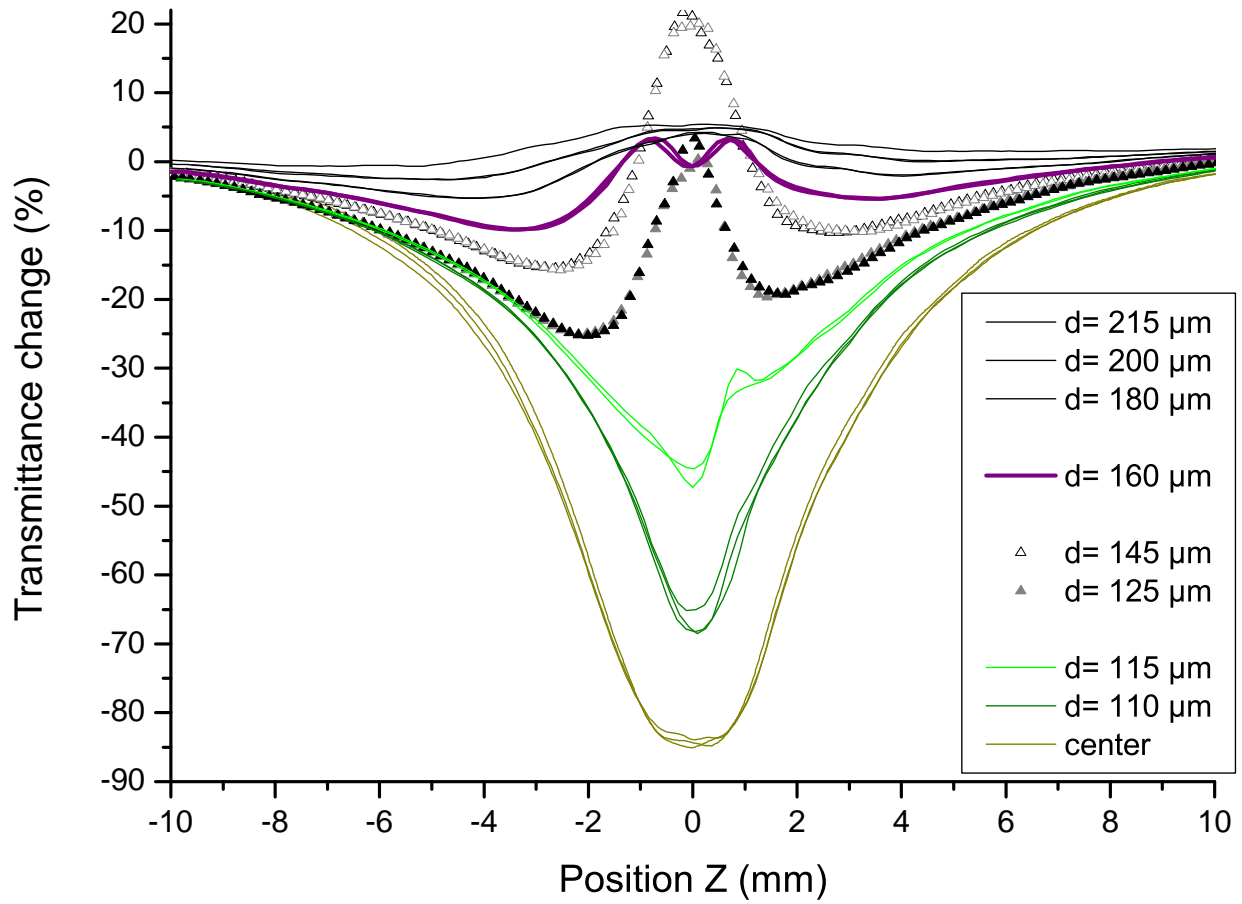


Figure 6.3: Transmittance z-scan of Alq₃:DCM in a microcavity at 800 nm excitation with a laser peak power of 43 kW (80 MHz laser repetition rate). Z-scan was performed in a distance d from the maximal signal drop to the right side along an horizontal line on the sample.

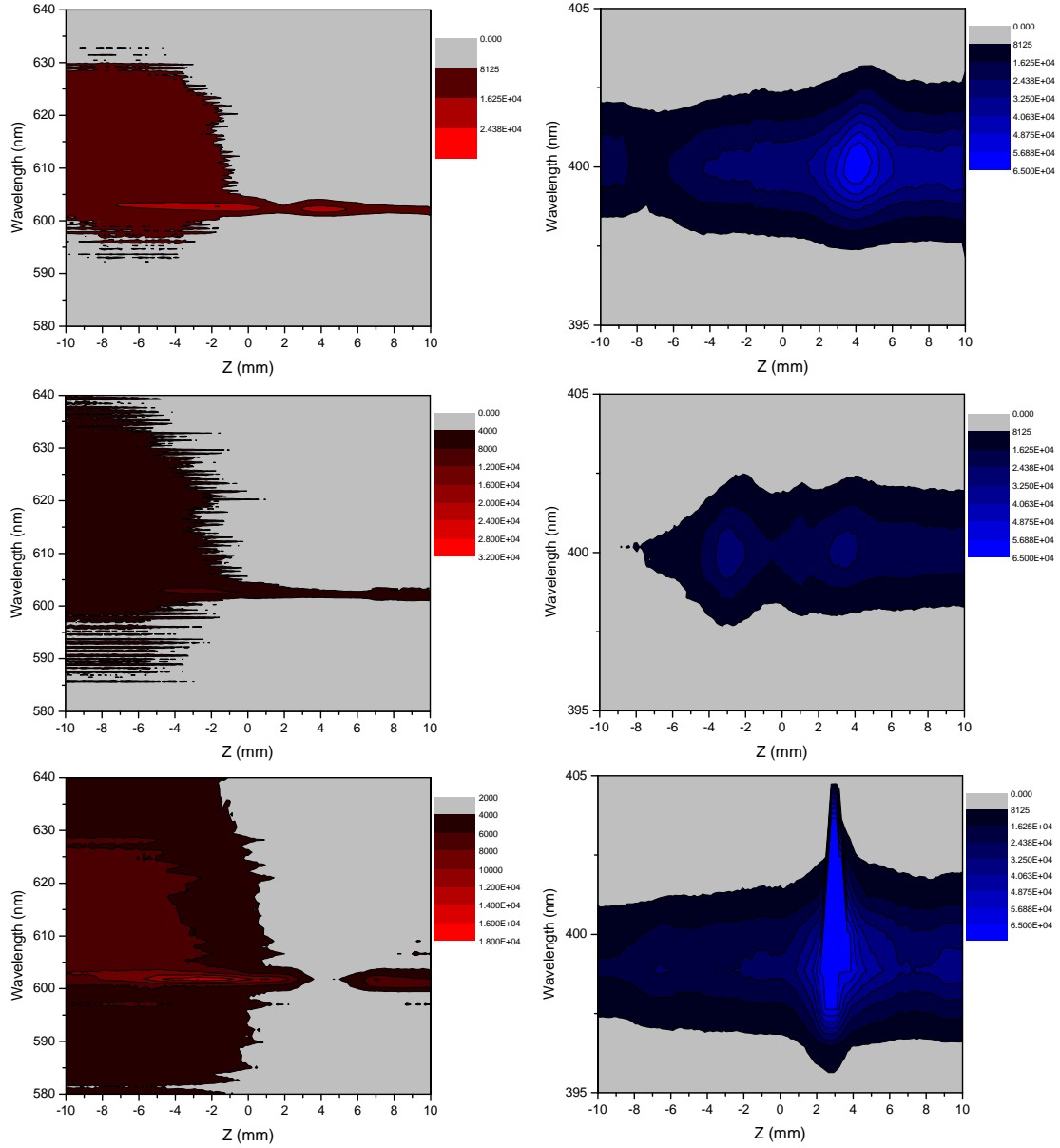


Figure 6.4: Z-scan detecting photoluminescence from the sample edge of Alq₃:DCM in a microcavity at 400 nm excitation with a laser average power of 19.3 μ W (1 kHz laser repetition rate). The left part shows the spectral behavior of scattered spontaneous emission of each scan, whereas the right part is the spectral behavior of scattered excitation light.

Bibliography

- [1] J. D. Bhawalkar, G. S. He, and P. N. Prasad. Nonlinear multiphoton processes in organic and polymeric materials. Reports on Progress in Physics, 59:1041–1070, 1996.
- [2] Wolfgang Demtroeder. Elektrizitaet und Optik. Number 2. Springer, Berlin ; Heidelberg, 3rd edition, 2009.
- [3] Goeppert-Mayer. Ann. Phys., Lpz, 9:273, 1931.
- [4] L. W. Tutt and T. F. Boggess. A review of optical limiting mechanisms and devices using organics, fullerenes, semiconductors and other materials. Progress in Quantum Electronics, 17:299–338, 1993.
- [5] C.R. Guiliano and L.D. Hess. IEEE Journal of Quantum Electronics, 3:358, 1967.
- [6] Robert W. Boyd. Nonlinear optics. Academic Press, Amsterdam, 2. ed. edition, 2006.
- [7] B. S. WHERRETT. J. Opt. Sot. Am., 67, 1984.
- [8] D. C. HUTCHINGS and E. W. VAN STRYLAND. J. Opt. Sot. Am. B., 9:2065, 1992.
- [9] A. E. KAPLAN. Radiophys. Quantum Electron., 12:692, 1969.
- [10] Richard L. Sutherland. Handbook of nonlinear optics, volume 2. ed., rev. and expanded. Dekker, New York ; Basel, 2003.
- [11] D. SINCLAIR and LAMER. Chem. Rev., 44:245, 1949.
- [12] G. MIE. Ann. d Phys., 25:377, 1908.
- [13] S. Bakic. Time integrated detection of femtosecond laser pulses scattered by small droplets. Applied Optics, 47:523–530, 2008.
- [14] B. J. Coe. Combining very large quadratic and cubic nonlinear optical responses in extended, tris-chelate metallochromophores with six pi-conjugated pyridinium substituents. Journal of the American Chemical Society, 132:3496–3513, 2010.
- [15] D. Z. Garbuzov. Photoluminescence efficiency and absorption of aluminum-tris-quinolate (alq(3)) thin films. Chemical Physics Letters, 249:433–437, 1996.
- [16] A. Aziz and K. L. Narasimhan. Optical absorption in alq. Synthetic Metals, 114:133–137, 2000.
- [17] P. E. BURROWS. J. Appl. Phys., 79:10, 1996.
- [18] G. Baldacchini. Optical spectroscopy of tris(8-hydroxyquinoline) aluminium thin films. Philosophical Magazine B-Physics of Condensed Matter Statistical Mechanics Electronic Optical and Magnetic Properties, 82:669–680, 2002.

-
- [19] A. CURIONI. Chem. Phys. Lett., 294:263, 1998.
- [20] P.W. Anderson. Phys. Rev., 149:109, 1958.
- [21] H. Fritzsche. J. Non-Cryst.Solids, 6:49, 1971.
- [22] A. Mukherjee. 2-photon pumped up-converted lasing in dye-doped polymer waveguides. Applied Physics Letters, 62:3423–3425, 1993.
- [23] J. Jakabovic. Properties of 4-dicyanomethylene-2-methyl-6-(p-dimethyl-aminostyryl)-4h-pyran-doped alq layers as optically pumped lasers. Applied Physics Letters, 83:1295–1297, 2003.
- [24] Y. F. Zhou. Theoretical investigation on two-photon absorption properties of (dicyanomethylene)-pyran derivatives. Journal of Molecular Structure-Theochem, 545:61–65, 2001.
- [25] P. Shao. Two-photon absorption properties of two (dicyanomethylene)-pyran derivatives. Optical Materials, 29:337–341, 2006.
- [26] V. A. Svetlichnyi. Experimental study of nonlinear absorption in polymethine dye solutions by the z-scan method. Quantum Electronics, 36:51–55, 2006.
- [27] C. R. Moylan. (dicyanomethylene)pyran derivatives with c-2v symmetry: An unusual class of nonlinear optical chromophores. Journal of the American Chemical Society, 118:12950–12955, 1996.
- [28] Y. Q. Xia. Ultrafast nonlinear optical properties of dye-doped pmma discs irradiated by 40 fs laser pulses. Optics and Laser Technology, 41:700–704, 2009.
- [29] S. S. Chunosova. Measurement of the two-photon absorption cross sections of dicyanomethylene-pyrans by the z-scan method. Quantum Electronics, 35:415–418, 2005.
- [30] G. S. He and L. S. Tan. Multiphoton absorbing materials: Molecular designs, characterizations, and applications. Chemical Reviews, 108:1245–1330, 2008.
- [31] B. N. Jagatap. J. Opt. Soc. Am. B, 26:73:19, 2002.
- [32] H. S. Nalwa. Organic materials for 3rd-order nonlinear optics. Advanced Materials, 5:341–358, 1993.
- [33] C. R. Moylan. (dicyanomethylene)pyran derivatives with c-2v symmetry: An unusual class of nonlinear optical chromophores. Journal of the American Chemical Society, 118:12950–12955, 1996.
- [34] J. Swiatkiewicz. Opt. Commun., 135:157, 1998.
- [35] G. S. He. Phys. Chem. A, 4805:104, 2000.
- [36] V. G. Kozlov and V. Bulovic. Temperature independent performance of organic semiconductor lasers. Applied Physics Letters, 71:2575–2577, 1997.

- [37] V. G. Kozlov and G. Parthasarathy. Structures for organic diode lasers and optical properties of organic semiconductors under intense optical and electrical excitations. Ieee Journal of Quantum Electronics, 36:18–26, 2000.
- [38] V. G. Kozlov and V. Bulovic. Study of lasing action based on forster energy transfer in optically pumped organic semiconductor thin films. Journal of Applied Physics, 84:4096–4108, 1998.
- [39] H. Aziz, Z. Popovic, S. Xie, A. M. Hor, N. X. Hu, C. Tripp, and G. Xu. Humidity-induced crystallization of tris (8-hydroxyquinoline) aluminum layers in organic light-emitting devices. Applied Physics Letters, 72:756–758, 1998.
- [40] Dieter Meschede. Optik, Licht und Laser. Vieweg + Teubner, 3rd edition, 2008.
- [41] M. Sheikbahae and Said. Sensitive measurement of optical nonlinearities using a single beam. Ieee Journal of Quantum Electronics, 26:760–769, 1990.
- [42] M. Falconieri. Thermo-optical effects in z-scan measurements using high-repetition-rate lasers. Journal of Optics a-Pure and Applied Optics, 1:662–667, 1999.
- [43] R. E. Samad and N. D. Vieira. Analytical description of z-scan on-axis intensity based on the huygens-fresnel principle. Journal of the Optical Society of America B-Optical Physics, 15:2742–2747, 1998.
- [44] H. Yokoyama. Rate equation analysis of microcavity lasers. JAP, 66:4801–4805, 1989.
- [45] H. Yokoyama. Controlling spontaneous emission and threshold-less laser oscillation with optical microcavities. OQE, 24:245–272, 1992.
- [46] Alexander Horn. Zeitaufgeloeste Analyse der Wechselwirkung von ultrakurz gepulster Laserstrahlung mit Dielektrika. PhD thesis, Rheinisch-Westfalischen Technischen Hochschule Aachen, 2003.
- [47] Heping Li Jun Mi Jun He, Yingli Qu and Wei Ji. Three-photon absorption in zno and zns crystals. OPTICS EXPRESS, 13:9235–9247, 2005.
- [48] M. Yin. Determination of nonlinear absorption and refraction by single z-scan method. Applied Physics B-Lasers and Optics, 70:587–591, 2000.
- [49] O. Varnavski. Large nonlinear refraction and higher order nonlinear optical effects in a novel organic dendrimer. Journal of Physical Chemistry B, 104:179–188, 2000.
- [50] M. Koschorreck and R. Gehlhaar. Dynamics of a high-q vertical-cavity organic laser. Applied Physics Letters, 87, 2005.

Danksagung

Ich möchte mich bei Herrn Prof. Leo dafür bedanken, dass er mir die Möglichkeit gegeben hat in der spex-Gruppe zu arbeiten und meine Diplomarbeit über ein spannendes Thema im Bereich der Laserphysik anzufertigen. Ich bekam die Chance mit einem äußerst modernen Lasersystem zu arbeiten und auf eigenständige Weise experimentelle Fertigkeiten zu erwerben. Ein weiterer Dank geht an meinen Betreuer Markas Sudzius, der viel Vertrauen in meine selbständige Arbeitsweise hat und mir die Freiheit lies, neue Ideen auszuprobieren. Dadurch war es mir möglich Selbstbewußtsein in der experimentellen Arbeit im Laserlabor zu entwickeln und wertvolle Erfahrungen zu sammeln.

Darüber hinaus möchte ich ganz besonders Susanne Hintschich danken, dass ich vor über zwei Jahren in der spex-Arbeitsgruppe als SHK anfangen durfte und mir der Weg zur Wahl der Laserphysik als Arbeitsgebiet offen stand. Ihre Hilfe bei den letzten Korrekturen meiner Diplomarbeit war unerlässlich wichtig und wertvoll. Auch Vadim Lyssenko, Ellen Siebert-Henze und Robert Brückner sei gedankt für die hilfreichen Diskussionen und Anregungen, die sie mir gaben.

Schöne Erinnerungen behalte ich an die Weihnachtsfeiern des Instituts und an die Wanderungen des IAPP sowie mit der OLaser-Gruppe von Hartmut Fröb. Ich hatte das Glück einen sehr angenehmen Arbeitsplatz in einem ruhigen Büro zu bekommen, in dem ich mich Dank meiner Zimmergenossen und einem sonnigen Balkon während meiner Arbeit sehr wohl gefühlt habe.

Außerhalb des IAPP gilt mein ganz besonderer Dank meinen Eltern und Großeltern für die Unterstützung und die Privilegien in meinem Leben. Zu guter Letzt danke ich meiner lieben Dorit für die Kraft, die sie mir gibt.

Abschlussklärung

Hiermit erkläre ich, dass ich die von mir am heutigen Tage dem Prüfungsausschuss der Fachrichtung Physik der Technische Universität Dresden eingereichte Diplomarbeit ohne unzulässige Hilfe Dritter und ohne die Benutzung anderer als der angegebenen Hilfsmittel selbständig angefertigt habe. Die aus fremden Quellen direkt oder indirekt übernommenen Gedanken sind als solche kenntlich gemacht. Die Arbeit wurde bisher in gleicher oder ähnlicher Form keiner anderen Prüfungsbehörde vorgelegt, weder im In- noch im Ausland.

Dresden, den 30. November 2010

Martin Teich